SAPIENZA
UNIVERSITÀ DI ROMA

Statistical Mechanics of Hamiltonian Systems with Bounded Kinetic Terms

an Insight into Negative Temperature

Scuola di Dottorato "Vito Volterra"

Dottorato di Ricerca in Fisica – XXXII Ciclo

Candidate

Marco Baldovin

ID number 1494560

Thesis Advisor

Prof. Angelo Vulpiani

A.Y. 2018-2019

Statistical Mechanics of Hamiltonian Systems with Bounded Kinetic Terms
Ph.D. thesis. Sapienza – University of Rome

This thesis has been typeset by LaTeX and the Sapthesis class.

Author's email: marco.baldovin@roma1.infn.it

Abstract

Some physical systems are characterized by regimes in which entropy is a decreasing function of the internal energy, meaning that they can achieve "negative absolute temperature". Such states have been experimentally realized in various contexts, from two-dimensional hydrodynamics to nuclear spins and Bose condensates, and many important theoretical results are available. The usage of negative values of the temperature, however, is not universally accepted, and during the last years a stimulating debate about the possibility to include this formalism in the framework of Statistical Mechanics has been attracting the attention of many authors.

Motivated by the open questions on this topic, in the present Thesis we study a class of Hamiltonian systems characterized by bounded kinetic terms; these models achieve negative temperature in their high-energy regimes, therefore they provide a preferential tool for the analytical and numerical investigation of such states.

First we characterize the equilibrium properties of these models. We discuss the possibility to achieve thermalization between systems at negative temperature, the consequent validity of a Zeroth Principle of Thermodynamics also for these states, and the non-trivial case of long-range interactions, inducing inequivalence between statistical ensembles. Then, aiming at a consistent generalization of Einstein relation and Langevin formalism to cases with negative temperature, we address the problem of Brownian motion of slow particles characterized by bounded kinetic terms, coupled to suitable thermal baths. Classical topics of out-of-equilibrium Statistical Mechanics, such as response theory and Fourier transport, are also considered for this particular class of Hamiltonian systems.

The aim of this project is to show that negative temperatures give a consistent description of the statistical properties of the chosen class of mechanical models; moreover, the introduction of this formalism is shown to be a necessary condition for the extension of usual results of Statistical Mechanics to these systems. This systematic study is expected to provide a useful analogy for more realistic physical models, and a deeper understanding of the fundamental aspects of negative temperature.

Acknowledgments

None of the results discussed in this Thesis could have been achieved without the wise guidance and friendly collaboration of my Ph.D. advisor, Prof. A. Vulpiani, whom I warmly and gratefully thank. The present work is mostly based on ideas originally conceived by him: during the last three years I tried to develop them, to the best of my possibilities, under his supervision.
During this period I had the opportunity to work with outstanding researchers. I am especially grateful to A. Puglisi and F. Cecconi, whose suggestions, teaching and continuous support have been of invaluable help to me. I also acknowledge many useful discussions and a fruitful collaboration with M. Cencini, A. Sarracino, S. Iubini, A. Prados and F. Miceli, among the others.
I owe a particular word of thank to L. Cerino. His work on Hamiltonian systems with bounded kinetic energy has been the starting point for all the results presented here. Moreover, he taught me the basic notions of everyday research when I was preparing my M.S. thesis: I am extremely grateful for all his tips and suggestions, which I continuously employ in my working activity.
Discussing with other Ph.D. students from the same research area has been among the most enriching and stimulating experiences during the last years. Long and vivid conversations with L. Caprini, F. Borra and A. Plati are thankfully acknowledged, as well as their precious friendship.
Finally, I want to thank all the Ph.D. students who transited through the Pi-room during these years, where we shared hopes, frustrations, laughs, and a lot of coffee: Giulia, Nazanin, Sara, Jonathan, Francesco, Diego, Ilaria, Mariano, Ludovica, Paolo, Federica, Giulia, Antonio, Gianmarco, Luca, just to mention a few. This work owes something to each of them.

Contents

Introduction

Since the pioneering work of Boltzmann, Gibbs, Maxwell and the other founders, who had the great intuition to make use of the tools of probability theory to explain the thermodynamic properties of gaseous systems, Statistical Mechanics has developed in many directions. Methods originally introduced in the context of kinetic theory, and successfully employed to the theoretical description of empirically known laws of Thermodynamics, are now applied to a variety of physical systems with very different properties, in fields ranging from Quantum Mechanics to Astrophysics.

Of course, the extension of the known results of Statistical Mechanics to new classes of systems is rarely straightforward; the price to pay is often represented by the generalization of existing techniques and formalisms to cases with new properties and issues. It is well known, for instance, that the study of quantum systems can be only carried out if the symmetry properties of fermions and bosons are taken into account; the theory of glasses deals, by definition, with systems for which no ergodicity property holds; models characterized by long-range interactions (as those encountered in Astrophysics), or by a relatively small number of degrees of freedom, usually display non-additive thermodynamic potentials, resulting in the failure of ensemble equivalence.

Among the others, Statistical Mechanics has been also applied to systems admitting so-called "negative absolute temperature" states, i.e. equilibrium states in which an increase of the internal energy corresponds to a decrease of the entropy [156]. This situation typically occurs when the phase-space volume accessible to the system is bounded. Examples of models with these properties are represented by vortices in two-dimensional domains [144], nuclear spins [152] and Bose condensates in optical lattices [159]. On the other hand, it is easy to understand that usual matter, characterized by kinetic energy contributions which are quadratic in the momenta, cannot be found in such states.

Although the idea of negative temperature was formulated (to the best of our knowledge) already 70 years ago [144], and despite many evidences presented, in the last decades, to substantiate the validity of the concept, a long-lasting debate on the possibility of extending the dominion of Statistical Mechanics to these states is still going on. In recent years, the discussion has been reinvigorated by the publication of new experimental results; some authors suggest that the emergence of negative temperature is just a drawback of the usual definition of entropy, and it could be "solved" by adopting a different convention which leads to only positive values of temperature [18, 82]; others claim that these states should be regarded as out-of-equilibrium states, for which no temperature can be defined [161, 177].

The aim of this Thesis is to investigate the statistical properties of a class of

Hamiltonian systems with bounded kinetic terms, which admit negative temperature states. We reconsider several classical results of Statistical Mechanics in the light of the possibility of negative temperature, with the purpose to show that no severe contradictions emerge; instead, the introduction of this formalism reveals necessary in order to get a consistent thermostatistical description of such systems.

In Chapter 1 we will briefly review some results about negative temperature; a synthetic report of the main positions, among the community, about the possibility of extending Statistical Mechanics to such states allows us to explain the motivation of this thesis.

Chapter 2 is devoted to the study of negative temperature at equilibrium. After some general considerations on the Hamiltonian systems in which such states can be observed, we introduce a particular class of models with bounded kinetic terms, whose properties will be analyzed in different contexts. Through the study of thermalization between a large system and a small "thermometer", we show the validity of the Zeroth Principle of Thermodynamics also at negative temperature. We also study a non-trivial case with long-range interactions and ensemble inequivalence. Some of the results of this Chapter are presented in Refs. [10] and [135].

In Chapter 3 we consider the possibility to derive a Langevin-type equation for systems with general forms of the kinetic energy, comparing our derivation with numerical simulations. We consider in particular a case in which the thermal bath is represented by a Hamiltonian system moving much faster than the considered degree of freedom, and a case where this role is played by a large number of Ising spins evolving trough a Glauber dynamics. Such results also hold at negative temperature. These problems are discussed in Refs. [12] and [15].

In Chapter 4 we present some attempts to study classical problems of non-equilibrium Statistical Mechanics in systems with negative temperatures as those described in Chapter 2. We focus on response theory and Fourier transport. Some of the results presented here are discussed in Ref. [135], others are part of a work (in preparation) in joint collaboration with S. Iubini.

Chapter 5 is dedicated to a discussion on the computational and technical aspects of the work presented in this Thesis. We discuss some of the algorithms used for simulations and data analysis. Particular attention is devoted to a procedure to extrapolate a Langevin equation from time series of data; the power (and the limits) of this method are illustrated through two examples of its application to actual research problems. Such cases are discussed in Refs. [9] and [13].

Chapter 1

Background and motivation

Far from being mere mathematical curiosities, equilibrium states at negative absolute temperature (NAT) can be observed in many important physical systems, characterized by a bound on the available phase space. Several experimental evidences seem to suggest that NATs have to be taken into account in order to properly describe equilibrium properties of such systems. Nonetheless, in recent years a stimulating debate, still ongoing, on the nature of negative temperatures has attracted the attention of the Statistical Physics community.

In this Chapter we briefly review some important examples in which NAT states naturally appear. We also discuss the main points of the debate on negative-temperature states, aiming at showing the rich variety of opinions among the community. The work contained in this Thesis is then presented as an answer to some of the raised questions.

1.1 Examples of systems allowing negative temperature

Classical physical systems that are investigated by Statistical Mechanics can be usually described by Hamiltonians of the form

$$\mathcal{H}(\mathbf{p},\mathbf{q}) = \sum_i \frac{p_i^2}{2m_i} + \mathcal{U}(\mathbf{q}) \tag{1.1}$$

where $(\mathbf{p},\mathbf{q})$ are the canonical coordinates. They give a quite accurate description of ordinary matter, which is encountered in everyday life, as gases and liquids. It is well known (and it will be discussed in some detail in Section 2.1) that the microcanonical entropy, for such kind of systems, is a non-decreasing function of the energy. From the thermodynamic relation

$$T^{-1} = \frac{\partial S}{\partial E} \tag{1.2}$$

one concludes that temperature is always non-negative for these systems, and this is the reason why negative temperature states are rarely discussed in textbooks.

A completely different scenario emerges when the methods of Statistical Mechanics are applied to models with generalized Hamiltonians (classical or quantum) that do not include the standard quadratic kinetic terms in Eq. (1.1): in this case

the number of available states can be a decreasing function of the energy, and the absolute temperature defined by Eq. (1.2) can assume negative values.

1.1.1 Point vortices in two dimensions

To the best of our knowledge, the concept of negative absolute temperature was originally introduced by Lars Onsager in his famous work on the statistical hydrodynamics of inviscid fluids in two dimensions [144]. It was already well known, from the work of Kirchhoff, Ruth and Lin [119], that the motion of vortices in two dimensions, in absence of viscosity, could be described by the following Hamilton equations:

$$\begin{cases} k_i \dot{x_i} = \partial_{y_i} \mathcal{H} \\ k_i \dot{y_i} = -\partial_{x_i} \mathcal{H} \,, \end{cases} \tag{1.3}$$

where k_i is the vorticity (positive or negative) of the i-th vortex, while x_i and y_i are their spatial coordinates. The Hamiltonian is defined as

$$\mathcal{H} = -\frac{1}{2\pi} \sum_{i>j} k_i k_j \log r_{ij} \,, \tag{1.4}$$

being $r_{ij} = \sqrt{(x_i - x_j)^2 + (y_i - y_j)^2}$ the Euclidean distance. In this system the conjugate variables describing each degree of freedom are the corresponding spatial coordinates on the x and y directions. The energy of the system ranges form $-\infty$, when a pair of vortices with opposite signs coincide, to $+\infty$, when vortices with the same vorticity occupy the same position.

The above description still holds when the dynamics is constrained inside a closed spatial domain $\mathcal{A}$, with the only difference that additional terms must be added to the Hamiltonian in order to take into account the image forces arising between the particles and the boundaries. This corresponds to replacing $-\log r_{ij}/2\pi$ with $G(r_{ij})$, where $G(z)$ is the Green function of the Laplacian operator in the dominion $\mathcal{A}$. Onsager noted that in this case the phase-space of the system (which coincides with the configuration space $\mathcal{A}^N$, where N is the number of considered vortices) is bounded. As a consequence, the following inequality holds:

$$\int_{-\infty}^{E} dE' \; \omega(E') \leq \mu(\mathcal{A})^N \quad \forall E \in \mathbb{R} \,, \tag{1.5}$$

where μ is the usual Lebesgue measure and $\omega(E)$ is the density of states

$$\omega(E) = \int_{\mathcal{A}^N} \prod_j dx_j dy_j \; \delta(E - \mathcal{H}(\mathbf{x}, \mathbf{y})) \,. \tag{1.6}$$

Since $\omega(E)$ is always positive, Eq. (1.5) states that it cannot be a non-decreasing function of E. In particular, it can be shown that, after an initial regime in which $\omega'(E) > 0$, there is a maximum at some finite energy E_m, after which $\omega(E)$ is always decreasing. We can define the microcanonical entropy of the system as

$$S(E) = k_B \log \omega(E) \,, \tag{1.7}$$

so that the (inverse) temperature associated to this model reads

$$\beta = \frac{1}{k_B}\partial_E S(E) = \frac{\omega'(E)}{\omega(E)}\,. \tag{1.8}$$

Since $\omega(E)$ changes the sign of its slope for $E > E_m$, it is clear that the above quantity needs to be negative in that regime. The value of E_m can be deduced by imposing upper and lower bounds for the wave numbers of the fluid [181].

Further investigations on the same model showed that it is possible to derive a canonical distribution for a small portion of the system even at negative temperature; in the same context, an attempt to solve the BBGKY hierarchy for the distribution of the vorticity was discussed, using the Vlasov approximation [138]. Similar studies were done in the context of guiding-center plasma, that can be modeled with the same equations of point vortices in two-dimensional hydrodynamics [175, 176].

In the 70's, early numerical simulations of Eq. (1.3) supported the picture that negative temperature would signal the emergence of a new ordered phase at high energies [138]. Nowadays modern computational tools allow for much more extensive simulations of the vortices dynamics, and the underlying physical mechanisms can be efficiently observed and studied [198, 197]. As predicted by Onsager, in the $\beta < 0$ regime, negative and positive vortices separate into two large clusters. The energetic cost of the negative-temperature configuration is very high, since each pair of vortices with equal sign, at small distance, gives a positive contribution to the total energy of the system. Let us notice that energy tends to be transferred from small-scale structures (wandering pairs of opposite-sign vortices) to a large-scale configuration (two clusters containing almost all vortices). This mechanism is somehow opposite to what usually happens in three-dimensional turbulence, where energy is carried from large to small spatial scales: this phenomenon is therefore called "inverse energy cascade".

In more recent years, the above theory has been adopted and studied in the context of quantum superfluids [174, 76, 190]. In particular it has been shown by numerical simulations that isolated Bose-Einstein condensates, under suitable conditions, relax towards the ordered phase at negative temperature described by Onsager. The mechanism behind the formation of large clusters of equal sign vortices is the so-called "evaporative heating". From time to time, pairs of opposite-sign vortices happen to melt together and disappear, while their energy is transferred to the other vortices through the produced sound waves. During such process the energy of the system is conserved, but the entropy of the vortices decreases, due to the disappearing of a pair [174].

Experimental evidences of inverse energy cascade and of hydrodynamics states at negative temperature have been reported in two very recent works [66, 97]. The two research groups have realized, independently of each other and using different methodologies, experimental setups that allow for the observation of vortices in superfluid Bose-Einstein condensates. In both cases, steady large-scale clusters of vortices with equal sign are observed, certifying the validity of Onsager's interpretation in the context of quantum superfluids.

1.1.2 Systems of nuclear spins

Just one year after the work by Onsager, the concept of negative absolute temperature was also introduced in a completely different context. At that time, novel investigation techniques based on magnetic resonance allowed physicists to characterize the nuclear magnetization of crystals subjected to strong external fields. Purcell, Pound and Ramsey, in particular, conduced a series of experiments on crystals of lithium fluoride (LiF).

First, they observed that the thermal equilibration between the nuclear spins and the crystal lattice occurred in some minutes, while the spin-spin relaxation process had typical relaxation times of 10^{-5} seconds [150]. Such time-scale separation allowed them to define a "spin temperature" characterizing the thermal state of the nuclear spins only, intended as a thermally isolated system: this possibility was already discussed in Ref. [38]. Then, in a famous experiment, Purcell and Pound were able to reverse adiabatically the magnetization of a small LiF crystal, initially at equilibrium in a strong external field. After this operation, the nuclear spins stayed for several seconds in a condition of internal equilibrium at high energy, such that the magnetization of the crystal was opposite to the external field [152]. From the point of view of Statistical Mechanics, the realized equilibrium state could be described by a negative value of the (spin) temperature, as stressed by the authors.

Also in this case, as for the two-dimensional vortices studied by Onsager, the possibility to achieve negative absolute temperature is related to the finiteness of the phase-space. This concept was clarified by Ramsey in a pioneering work on negative temperatures, see Ref. [156], which is (to the best of our knowledge) the first systematic attempt to generalize the bases of Statistical Mechanics to negative-temperature cases. In this paper Ramsey enumerates the essential requirements for negative temperature:

1. the elements of the considered system must be in thermal equilibrium;
2. the possible energy of the allowed states of the system must be bounded;
3. the system must be thermally isolated from all other systems which do not satisfy conditions (1) and (2).

Actually condition (2) holds only for discrete systems, as the nuclear spins studied by Ramsey. We will come back to this point in Chapter 2. Ramsey also stresses that in order to consider negative temperature, Kelvin-Planck formulation of the Second Law of Thermodynamics needs to be modified in the following way:

> It is impossible to construct an engine that will operate in a closed cycle and produce no effect other than (1) the extraction of heat from a positive temperature reservoir with the performance of an equivalent amount of work or (2) the rejection of heat into a negative-temperature reservoir with the corresponding work being done on the engine.

All the alternative formulations do not need to be modified.

A rigorous analysis on the concept of spin temperature was then performed by Abragam and Proctor [1]; by reviewing the corpus of experimental results available

at that time, the authors showed that the introduction of such notion not only is justified under suitable conditions, but it also brings to novel predictions when the intensity of the external field is comparable with that of the spin-spin interactions. In this sense its introduction is necessary to have a coherent description of the system on mesoscopic time scales.

In the experiments by Purcell and Pound recalled above, a negative temperature state was signaled by the fact that the spin magnetization and the external field had opposite signs. In more recent years, it was possible to prove the emergence of negative temperature also by looking at the ferromagnetic/antiferromagnetic ordering of the spins [142]. In the case of silver (see Ref. [78]) the Hamiltonian of nuclear spins $\{\mathbf{I}_j\}$ assumes the form

$$\mathcal{H} = -\sum_{\langle ij \rangle} J_{ij} \mathbf{I}_i \mathbf{I}_j + \mathcal{H}_{dip} - \hbar \mathbf{B} \cdot \sum_i \gamma_i \mathbf{I}_i \tag{1.9}$$

where the first term is the dominating spin-spin energy, due to the nearest-neighbors interactions, which depends on a positive coupling constant J_{ij} [163]. The energy related to the remaining spin-spin interactions $\mathcal{H}_{dip}$ is smaller by a factor 3. Finally, the last term accounts for the Zeeman effect when the crystal is subjected to an external field $\mathbf{B}$ (here γ_i is the gyromagnetic ratio). In Ref. [78] the authors showed that it is possible to realize an equilibrium state, in the sense discussed above, such that the order of the spins is ferromagnetic even if the coupling is antiferromagnetic, a clear hint of the NAT state reached by the system.

Quite recently, the consistency of an equilibrium description through spin temperature (positive or negative) has been tested through optical magnetometry techniques, measuring the polarization of a system of spins as a function of the external field and comparing it to the theoretical predictions [193].

1.1.3 Cold atoms in optical lattices

In the last decades there has been an increasing interest in quantum systems of so-called "cold atoms" trapped by optical lattices. It is well known from quantum mechanics that atoms lightened by a coherent beam of photons will emit them back in random directions; this process results in an average increase of momentum by h/λ along the light beam direction, where h is the Planck constant and λ the wavelength of the incident beam [6]. A kind of viscous friction can be induced on atoms by using counterpropagating lasers whose frequency is resonant with the lowest side of the absorption spectrum; in this case each atom will scatter only photons propagating in the direction opposite to its velocity (the others having too small frequency to be absorbed, due to Doppler effect). The net effect is a damping force that decelerate the particles, resulting in a cooling of the gas [47].

Among the several studies that can be performed on the "cold" atoms prepared with this technique, a very active branch of research is represented by experiments with optical lattices, i.e. grids of laser beams able to confine cold atoms exploiting Stark effect [95]. Such setup can be used to induce a thermalization of cold atoms at negative temperature, due to the peculiar band structure of the system: it can be shown that the number of available states in the "valence" band is, for suitable choices of the parameters, a decreasing function of the energy [139]. Of course, to

prevent leaks of atoms (and energy), which would spoil the negative-temperature equilibrium, one has to check carefully that the tunneling effect between the "valence" and the "conduction" band has a negligible rate.

The Bose-Hubbard (quantum) Hamiltonian provides a simple quantitative model for bosonic atoms in optical lattices [68]:

$$H = -J \sum_{\langle i,j \rangle} (b_i^\dagger b_j + b_j^\dagger b_i) + \sum_i \epsilon_i \hat{n}_i + \frac{1}{2} U \sum_i \hat{n}_i (\hat{n}_i - 1) \tag{1.10}$$

where b_i and $b_i^\dagger$ are the annihilation and creation operators for bosonic atoms at lattice site i, satisfying the boson commutation relation $[b_i, b_j^\dagger] = \delta_{i,j}$, while $\hat{n}_i = b_i^\dagger b_i$ counts the number of such atoms. The first sum in Eq. 1.10 is extended to couples of first-neighbor sites only, so that parameter J determines the hopping between adjacent spots; U accounts for the repulsive force between atoms in the same site and ϵ_i is a site-dependent energy offset. Such constants can be tuned by varying the parameters of the optical lattice, an operation that can be performed with high precision [95, 158]. A typical case is that of a quadratic confining potential, i.e.

$$\epsilon_i = V_0 \mathbf{r}_i^2 \tag{1.11}$$

where $\mathbf{r}$ is the spatial position of the i-th site. The model described by Eqs. (1.10) and (1.11) admits negative temperature if U and V_0 are negative: with such choice of the parameters, states at higher energy are characterized by smaller entropy. It can be shown that thermalization at negative temperature can be expected in this case, due to the symmetry relating the case $U < 0$, $V_0 < 0$ to a corresponding model with $U > 0$, $V_0 > 0$ [157].

Let us notice an important qualitative difference between this physical system and those discussed in the previous paragraphs (Onsager vortices, spins systems): the present model does not allow for positive-temperature states, due to the negative sign of the quadratic potential [139]. The scenario is somehow opposite to that of ordinary matter with quadratic kinetic terms, briefly mentioned at the beginning of this Section (we will discuss it in more detail in the next Chapter).

From an experimental point of view, realizing a system which only admits negative temperature states is a non-trivial task, since cold atoms have to be initially prepared in a $T > 0$ state. Following a strategy initially proposed by Mosk [139], in Ref. [158] a possible method is illustrated, based on the following steps:

1. prepare the system in a positive temperature state, with external parameters $J \neq 0$, $U > 0$, $V_0 > 0$;
2. suddenly increase the intensity of the optical lattice, so that J drops to zero and atoms cannot change their site anymore;
3. slowly reverse the external and interaction potentials: $U \to -U$, $V_0 \to -V_0$;
4. switch J back to its initial value.

The above procedure has been realized in a famous experiment, whose results are presented in Ref. [23]. In that context it has been possible to observe the momentum

distribution of the cold atoms at the end of the process, and it has been verified that it corresponded to the one expected for a negative-temperature equilibrium state [157].

1.1.4 The DNLS equation

One of the most widely used models in non-linear physics is the so-called Discretized Non-Linear Schrödinger (DNLS) equation. In one of its possible formulations, it reads:

$$i\dot{z}_j = \left(\Lambda|z_j|^2 + \xi_j\right) z_j - \frac{z_{j-1} + z_{j+1}}{2} \tag{1.12}$$

where $\{z_j\}$ are complex variables, while Λ and $\{\xi_j\}$ are constant parameters. The above expression can be obtained by discretizing the Schrödinger equation for a quantum particle in presence of a suitable external potential, whence its name. This model is of particular interest because of its ability to develop discrete breathers, i.e. stable, localized excitations characterized by periodic oscillations; this non-trivial behavior is due to the combined effect of the discrete form of Eq. 1.12 and of nonlinear terms, which oppose to the decay of the breathers [34, 60].

First introduced in biophysical contexts, this equation is a prototype for the lattice dynamics in presence of nonlinear interactions, and it is able to describe localization effects in a wide range of physical situations [103]. A large field of application for the DNLS equation is nonlinear optics: it is well known, for example, that such model can be used to describe the emergence of solitons for light propagating in optical waveguides [55].

The DNLS equation can also be employed to describe the dynamics of Bose-Einstein condensates (BEC) in one-dimensional optical lattices, as argued by Trombettoni and Smerzi [184]. The relation between the DNLS equation and the Bose-Hubbard model, Eq. (1.10), is detailed in Ref. [60]. The argument is based on the fact that when the limit $J/U \gg 1$ is considered, in which the hopping process dominates over the interactions, it is reasonable to assume that the ground-state configuration of the Bose-Hubbard model can be approximated by a product of on-site states; with a suitable ansatz on its form, a time-dependent variational principle can be applied to determine a (classical) effective mean-field Hamiltonian for the complex order parameter $z_j = \langle b_j \rangle$:

$$\mathcal{H} = \sum_j \left(\frac{U}{2}|z_j|^4 + \epsilon_j |z_j|^2 \right) - \frac{J}{2} \sum_j (z_j^* z_{j+1} + z_{j+1}^* z_j) \,. \tag{1.13}$$

The order parameters satisfy the Poisson brackets $\{z_j^*, z_k\} = i\delta_{j,k}/\hbar$, and they provide a proper set of canonical coordinates. The corresponding equation of motion is given by Eq. (1.12), where $\lambda = U/J$, $\xi_j = \epsilon_j/J$ and time has been rescaled as $\tau = Jt/\hbar$. The dynamics is characterized by two first integrals, namely the total energy and the norm $\mathcal{A} = \sum_j |z_j|^2$.

Trombettoni and Smerzi analyze the evolution of Gaussian wave-packets subjected to the DNLS dynamics, showing that, depending on the initial parameters of the packet, both static and mobile breathers can emerge. Such localized states can be induced on BECs trapped in optical lattices exploiting the dissipation of atoms at the boundaries, as discussed in Ref. [120].

In 1999 Rasmussen *et al.* [159] discussed the statistical properties of the DNLS. A grand-canonical approach, in which $\mathcal{A}$ plays the role of the total number of particles, allows to characterize the (a, h) parameter space, where $a = \mathcal{A}/N$ is an average excitation norm and $h = \mathcal{H}/N$ is the energy density: for each couple (a, h), the corresponding inverse temperature β can be calculated. With this approach one shows that there exists a region of the parameter space such that $\beta < 0$. In successive papers, it has been shown that such $\beta < 0$ states are actually metastable, and that the system will eventually reach, after astronomical times, an equilibrium state in which a background state at $\beta = 0$ and a delta-shaped excitation including all the remaining energy are superimposed [167, 87].

The negative-temperature states in BECs have been extensively studied by using numerical simulations [87]. The system evolves toward a state with a finite density of breathers. Very slow coarsening processes are observed, which are expected to lead the system to its final configuration described above. The metastable nature of such intermediate states, in which the system appears "frozen" for extremely long times, has been recently investigated through suitable stochastic models [92].

The DNLS equation has been also used as a prototypical model to study negative-temperature states out of equilibrium [90, 88]. In particular, it has been shown that a DNSL chain at contact with a heat reservoir at positive temperature and to a pure dissipative bath reaches long-lasting states showing that the typical features of the $\beta < 0$ regime [93]. This phenomenon has still to be completely understood from a theoretical point of view, and poses interesting questions about the role of negative-temperature states in non-equilibrium Statistical Mechanics.

1.2 The dispute about negative temperature

The concept of negative temperature, since its introduction in the seminal papers by Onsager, Purcell, Pound and Ramsey, has always inspired debates about the right way, if any, of extending classical results of Statistical Mechanics to negative temperature cases. The reformulation of the Kelvin-Planck version of the Second Principle discussed in Section 1.1.2, and the bound on Carnot efficiency, see Section 1.2.2 below, are examples of typical controversial points.

In recent years a stimulating debate about the nature of negative temperature states, and their proper statistical description, has interested a considerable part of the Statistical Mechanics community [178]. Some authors argued that the use of negative temperature could be avoided by adopting a different definition of entropy (the so-called "volume entropy" already discussed by Gibbs in its classical treatise on Statistical Mechanics [70]), which has in turn interesting mechanical properties [18, 52, 36]. Other people investigated the conceptual problems that are found in extending the theory of thermodynamic cycles to systems allowing negative temperature [161, 37]. Finally, it has also been argued that negative temperature states should be always considered as out of equilibrium, so that no temperature, neither negative nor positive, can be defined to describe their thermal condition [177]. Such proposals, on the other hand, have been criticized by those who believe that negative temperatures can be safely included in the Statistical Mechanics theory, with small adaptations, and that their usage reveals useful or even necessary [62, 41, 179,

2].

A detailed report on the discussion is out of the scope of this introductory chapter: in the following we will only outline a brief summary of it, which can be useful to understand the motivation of the research presented in this Thesis.

1.2.1 Two definitions of entropy

Let us consider a generic physical system, described by some Hamiltonian $\mathcal{H}(\mathbf{X}; \{A_i\})$, where $\mathbf{X}$ is the vector of the canonical coordinates, living in a $2N$-dimensional space, and the variables $A_i, i = 1, ..., n$, with $n \ll N$, represent some tunable parameters of the system (volume, external magnetic field...). We suppose that $\mathcal{H}$ is bounded from below, so that we can define the phase-space volume confined by the hypersurface at constant energy E:

$$\Gamma(E; \{A_i\}) = \int_{\mathcal{H}(\mathbf{X};\{A_i\})<E} d\mathbf{X}\,. \tag{1.14}$$

The density of states $\omega(E; \{A_i\})$ is nothing but its derivative with respect to the energy,

$$\omega(E; \{A_i\}) = \frac{\partial \Gamma}{\partial E}. \tag{1.15}$$

The usual definition of entropy in Statistical Mechanics, commonly attributed to Boltzmann (and engraved on its tombstone), reads

$$S_B(E; \{A_i\}) = k_B \ln \omega(E; \{A_i\})\,, \tag{1.16}$$

where k_B is the Boltzmann constant. Even if Eq. (1.16) is actually due to Planck [132], the wording "Boltzmann entropy" is usually adopted, and we will conform to this tradition. S_B is clearly a (logarithmic) counter of the number of states available to the system in the microcanonical ensemble, at fixed energy E. As pointed out in Ref. [52], for dimensional consistency Eq. (1.16) needs to be rewritten as

$$S_B(E; \{A_i\}) = k_B \ln[\epsilon\, \omega(E; \{A_i\})]\,, \tag{1.17}$$

where ϵ is a constant which has physical dimensions of an energy. Of course the presence of ϵ is irrelevant when considering the derivatives of S_B, i.e. the physically measurable quantities). The corresponding inverse temperature,

$$\beta_B = \frac{1}{k_B T_B} = \frac{1}{k_B} \frac{\partial S_B}{\partial E} \tag{1.18}$$

has the following, fundamental property [85]: when two systems $\mathcal{S}_1$ and $\mathcal{S}_2$ are brought in (weak) thermal contact, once equilibrium is reached, β_B is the same for both systems. As a consequence, T_B is the proper temperature one has to consider in deriving the canonical distribution from a microcanonical description [100, 41].

In his classical treatise on Statistical Mechanics [70], Gibbs discusses an alternative definition of entropy, sometimes called "volume entropy":

$$S_G(E) = k_B \ln[\Gamma(E)]\,. \tag{1.19}$$

This form of the entropy and the corresponding temperature,

$$T_G = \frac{1}{S'_G(E)}\,, \tag{1.20}$$

have indeed remarkable properties.

1. *Exact validity of thermodynamic relations.*

   First Law of Thermodynamics expresses energy conservation as

   $$dE = dW + \delta Q\,, \tag{1.21}$$

   i.e. it states that the amount of energy dE acquired by the system during an infinitesimal transformation is given by the sum of the work dW done on the system and of the heat δQ absorbed during such transformation. By definition, the macroscopic work done on the system can be written as

   $$dW = \sum_i \left\langle \frac{\partial \mathcal{H}}{\partial A_i} \right\rangle dA_i \tag{1.22}$$

   where $\langle\cdot\rangle$, under the assumption of ergodicity, is an average on the micro-canonical ensemble. Second Principle assures, on the other hand, that a state function S, the thermodynamic entropy, exists such that

   $$\delta Q = T dS \tag{1.23}$$

   for reversible transformations. Thermodynamic consistency requires therefore that relations

   $$\frac{1}{T} = \frac{\partial S}{\partial E} \tag{1.24}$$

   and

   $$T\frac{\partial S}{\partial A_i} = -\left\langle \frac{\partial \mathcal{H}}{\partial A_i} \right\rangle \tag{1.25}$$

   hold. It can be shown [36] that the above equations are verified exactly (i.e., also for a finite number of particles) only if S is a function of $\Gamma(E)$. Definition (1.19) can then be deduced from the particular case of ideal gas.

2. *Adiabatic invariance*

   Suppose that parameters $\{A_i\}$ vary in time, and that such transformation has a typical time τ; since $\mathcal{H}$ is now time-dependent, E is no more a conserved quantity. A function $I(E(t); \{A_i(t)\})$ is called adiabatic invariant, in the mechanical sense, if its evolution tends to a constant behavior in the limit $\tau \to \infty$. As discussed in Ref. [52], an adiabatic process in the mechanical sense (very slow variation of the parameters $\{A_i\}$) is also adiabatic in the thermodynamic sense (no exchange of heat between the system and the environment) if and only if

   $$\frac{dE}{dt} = \sum_i \left\langle \frac{\partial \mathcal{H}}{\partial A_i} \right\rangle \frac{dA_i}{d_t}\,, \tag{1.26}$$

i.e. if the whole energy variation can be associated to some form of external work done on the system. But this is only true if S is constant along the transformation, i.e. if S is an adiabatic invariant in the mechanical sense. As a consequence, to recover an exact analogue between Mechanics and Thermodynamics, the mechanical definition of entropy must be an adiabatic invariant. It can be proved that S_G possesses such property [102, 35]. This is exactly true also for finite systems.

3. *Equipartition theorem*

   A well-known result of Statistical Mechanics states that

$$\left\langle x_i \frac{\partial \mathcal{H}}{\partial x_i} \right\rangle = k_B T \,, \tag{1.27}$$

   where x_i is any canonical coordinate. For quadratic Hamiltonians Eq. (1.27) implies that energy is equally distributed, on average, among the different degrees of freedom (Equipartition theorem). In deriving such result (see e.g. Ref. [85]) one actually makes use of Gibbs' definition of entropy: Eq. (1.27) is thus exactly verified only if one considers $T = T_G$.

4. *Helmholtz theorem*

   A fundamental property of thermodynamic entropy, expressed by Eq. (1.23), states that dS is an exact differential, i.e. that T^{-1} is an integrating factor for δQ. Helmholtz was able to identify a mechanical analogue of S for one-dimensional *monocyclic* systems, i.e. Hamiltonian models in which each energy E corresponds to only one possible closed trajectory, of the form

$$\mathcal{H}_H(p, q; V) = p^2/2m + \phi(q; V) \tag{1.28}$$

   where (p, q) are the canonical coordinates, m is the mass of the particle and ϕ an external potential depending on the parameter V. The corresponding "entropy" S_H is indeed the one-dimensional version of S_G, depending only on the phase-space area enclosed by the trajectory at energy E [36]. As discussed in Ref. [64], chapter IX, the Helmholtz theorem had an important role in the early development of Statistical Mechanics, being one of the starting points for Boltzmann's project of deriving Thermodynamics from classical Mechanics. A generalization of Helmholtz theorem to many degrees of freedom, which makes use of S_G, is given in Ref. [36].

Based on the above observations, Berdichevsky, Kunin and Hussain in 1991 proposed to substitute the usual definition of entropy with S_G [18]. An immediate consequence of this choice is that S_G is a monotonically non-decreasing function of the energy, so that T_G cannot be negative, by definition. In this way the authors intended to solve Onsager's "paradox" of negative temperature in vortex motion (see Section 1.1.1). The same proposal was put forward by Dunkel and Hilbert in 2014, on the basis of thermodynamic consistency [52], and taken up by following works [82, 79, 36].

In the above mentioned papers many examples were considered in which S_B fails to describe systems with a small number of degrees of freedom N. However, it has

been pointed out that the examined properties of S_G can be appreciated only in the case of systems with a small number of degrees of freedom, of limited interest for Statistical Mechanics [179], since, as soon as $N \gg 1$, for all systems with quadratic kinetic energy S_B and S_G provide indistinguishable results [85]. Critics of Gibbs' definition of entropy often argue that the choice between S_B and S_G should be based on the analysis of systems in which the two descriptions give considerably different results also in the thermodynamic limit, as the ones discussed in the first part of this Chapter. Some authors stress that S_G is unable to catch the indisputable qualitative differences between the positive and negative T_B regimes, such as the high-energy order emergence in systems of Onsager vortices [137], cold atoms [169] or nuclear spins [62, 2]. Indeed, as pointed out in Ref. [192], S_G is a constant function of the energy, in the thermodynamic limit, for all states corresponding to $T_B < 0$, so that T_G is infinite for all such states; moreover, this limit behavior is reached exponentially fast in N, where N is the number of particle, so that the S_G description is only useful, for such systems, when just a few particles are considered. A striking example of this failure of S_G is discussed in Ref. [25], in which a phase transition at high energy can be only predicted by relying on S_B.

Other authors remark that T_G violates the Zeroth Principle of Thermodynamics. Using T_G, one can indeed exhibit examples in which heat flows from hotter to colder systems, also in the thermodynamic limit [169, 62]. Authors of Ref. [79], however, reply that in the microcanonical ensemble the "right" state variable is the energy, and therefore one should not wonder if temperature is unable to determine the direction of heat flux once two initially isolated systems are put into contact.

Finally, critics of Gibbs' definition of entropy stress that S_G is unphysical in the following sense: it is a function of a phase-space volume region which includes states that the system is not allowed to visit, because of energy conservation [169]. As a consequence, it is impossible to measure T_G in an experiment or in a molecular dynamics simulation using its definition, even assuming ergodicity; to deduce T_G one can rely on the equipartition theorem, which, as discussed before, is based on S_G. However, the hypotheses of such theorem are typically not verified for systems which admit negative T_B, so that in those cases T_G is not a physical observable [41]. On the other hand, the "Boltzmann" temperature T_B can be always deduced from the fluctuations of proper observables [41, 164].

1.2.2 Thermodynamic cycles and efficiency larger than 1

One of the most challenging points when one tries to extend usual Thermodynamics to cases with negative temperature is represented by thermodynamic cycles. The possibility to design a thermodynamic engine operating between two temperatures T_1 and T_2 with $T_2 < T_1 < 0$, or even $T_2 < 0 < T_1$, would imply efficiencies larger than one in modulus; for this reason, several works have been devoted to the study of this topic.

In his famous paper on negative absolute temperatures [156], Ramsey mentions that Carnot cycles can be designed for spins systems subjected to an external field $\mathbf{B}$ (such as that described by Eq. (1.9)). $\mathbf{B}$ can be continuously varied, at a very slow rate, so that the system can be considered in thermal equilibrium at any time: such external parameter plays the role assumed by the volume in the case of ideal

gases. In principle, we can perform reversible transformations at fixed temperature, positive or negative, as well as adiabatic transformations in which the system does not exchange heat with the environment. It is therefore possible, as in the well-known case of ideal gases, to perform Carnot cycles.

Let us first consider the case in which the temperatures of the two reservoirs have the same sign. The efficiency of a Carnot cycle is defined as

$$\eta = 1 - \frac{Q_2}{Q_1} = 1 - \frac{T_2}{T_1} \tag{1.29}$$

where Q_1 is the heat absorbed at temperature T_1 and Q_2 is that released at temperature T_2 (we are assuming that T_1 is hotter than T_2, i.e. we are either in the $0 < T_2 < T_1$ or in the $T_2 < T_1 < 0$ case). As argued by Ramsey, the fact that for $T_2 < T_1 < 0$ the efficiency can be negative, and even less than -1, means that work must be done on the system in order to maintain the cycle: this behavior is opposite to the positive-temperature case, in which the absorbed heat is converted into work by the engine. The whole scenario is consistent with the "generalized" version of the Kelvin-Planck formulation of the second principle, enunciated by Ramsey itself (see Sec. 1.1.2), stating that at negative temperature the complete transformation of work into heat (and not the reverse) is forbidden. In a later paper by Landsberg a precise correspondence is established between heat pumps at negative temperatures and heat engines at positive ones [110].

The above considerations can appear counterintuitive at a first sight, but they reveal to be completely consistent and lead to no paradoxes. The case in which T_1 and T_2 have different signs is a bit more complicated. Ramsey notes that, for systems of nuclear spins, no way is known to operate adiabatic transformations between temperatures of opposite signs, since the experimental techniques that are usually employed to achieve negative values of β rely on a non-quasistatic inversion of the external magnetic field. However it is not clear, a priori, whether an adiabatic transformation between positive and negative temperature would be forbidden in any system, or in spin systems only [187].

An attempt to answer the question is due to Schöpf [170]: after a systematic theoretical analysis of the possible thermodynamic cycles, only based on the First and Second Principles of Thermodynamics, he concludes that any adiabatic transformation linking states at negative and positive temperature would result in some inconsistencies. His proof is a reductio ad absurdum based on the careful analysis of the possible shape of the transformations in the state-variable space. In a subsequent work [188] it has been shown that one of the proofs is incomplete, and that the Third Law of Thermodynamics has also to be assumed. A proof for the case with bounded energy is given in Ref. [183]. Under reasonable hypotheses, it is shown that if one considers a thin enough region around the $\beta = 0$ surface, in the state-variables space, entropy is constant, and maximal, at $\beta = 0$. An immediate consequence is that such surface cannot be crossed by an isoentropic transformation.

Even if quasi-static Carnot cycles between temperatures with opposite signs are forbidden, their non-quasistatic versions can be still operated. A systematic discussion can be found in Ref. [111]. The efficiency of such engines, according to Eq. (1.29), is larger than one. This result could appear paradoxical. However, one should keep in mind that Eq. (1.29) is derived under the assumption that heat is

absorbed by the system at temperature T_1 and released at temperature T_2, which is not possible if they have opposite signs. In that case (see Ref. [37]) heat is absorbed at both temperatures and completely converted into work (or, for a heat pump, released to both reservoirs), so that the efficiency

$$\eta = \frac{W}{Q} \tag{1.30}$$

is actually always equal to 1.

Of course, the above result does not provide a way to convert heat into work: as correctly pointed out, e.g., in Ref. [177], the amount of work that is necessary to realize a negative-temperature bath largely exceeds the one that can be obtained in this way. Experimental realizations of such cycles have been performed in quantum systems [7].

1.2.3 NAT states as non-equilibrium states

The possibility of realizing thermodynamic cycles with efficiency larger than 1, discussed in the previous Section, is one of the main source of skepticism and concern about negative temperature. Some authors, even among those who recognize the validity of the "Boltzmann" entropy S_B, question that one can speak about equilibrium when referring to systems at negative temperature; basically, such authors claim that the only proper equilibrium states are those corresponding to points on the branch of $S(E)$ with positive slope [177, 30].

An argument which is often used against the legitimacy of negative temperature states is their *instability*; with this term some authors mean that once coupled to the external environment, any system $\mathcal{H}$ initially at negative temperature is doomed to release energy until it reaches some positive value of T [161]. This behavior is due to the fact that the global system composed by $\mathcal{H}$ and the environment does not admit $T < 0$ (assuming that the environment is made of ordinary matter: see the discussion in Sec. 2.1.1). This observation is completely correct (see also Section 2.3 and Ref. [26]), however one should also recall that in all experimental studies about negative temperature states the relaxation times of the considered systems are much smaller than the typical time-scales on which heat is exchanged with the surrounding environment; it is then generally argued that for time interval small enough the system can be considered as isolated [150, 139].

It has also been noted that, at least in systems interacting with external fields and with negligible internal interactions, the negative-temperature description can be avoided by suitable modifications of the thermodynamic formalism [30]. In particular, if one explicitly describes the external field as an additional work term, which does not participate in the internal energy of the system, negative temperatures do not appear. Such conclusions are similar to those discussed in Ref. [1], where it is established that the introduction of a (possibly negative) "spin temperature" does not lead to novel predictions in the case of high external field. However, in the same paper it is also shown that when the external field is of the same order of the internal interactions, the concept of spin temperature has to be taken into account in order to make sensible predictions; it is not clear whether the formalism suggested in Ref. [30] can be also extended to such cases, predicting, for example,

the emergence of ferromagnetic order in presence of antiferromagnetic couplings, which has been experimentally observed [78].

Finally, other authors argue that since negative temperature states are not spontaneously present in nature, and they can only be prepared trough sudden transformations which are not quasi-static, they should be always considered as out-of-equilibrium states for which no temperature can be defined. This interpretation is consistent and preserves, of course, the original Kelvin-Planck formulation of Second Principle [177]. However, the introduction of NATs, with the consequent slight modifications of the known formulations of Thermodynamics, allows a simple and efficient descriptions of several interesting phenomena in modern physics: unless unpleasant byproducts are found (e.g. deep contradictions or paradoxes), opposition to the use of NATs seems questionable.

1.3 Motivation

The long-lasting debate on the concept of negative temperature, briefly reported in the previous Section, has raised several interesting questions which need to be addressed. As it is clear from the above discussion, the experimental realization of NAT states is often a challenging task; however, considerable insight into the conceptual aspects of negative temperature can be obtained through the study of simple theoretical models, whose statistical properties can be studied either analytically or numerically. Such line of research can give a valuable contribution to the debate on a conceptual level, since the results are easily reproducible and hardly questionable, and their interpretation is usually straightforward.

In the next Chapter we will introduce and discuss a class of Hamiltonian models, characterized by a kinetic energy term with a bounded, non-quadratic form. The thermodynamic behavior of such systems can be studied numerically and, in some cases, also analytically. In this Thesis we will mainly deal with these models. As discussed in the following, if one adopts the Boltzmann's definition of entropy (1.16) and the corresponding temperature, such systems can achieve negative temperature states.

Using the mentioned class of models we will be able to address the study of important topics of Thermodynamics and Statistical Mechanics such as Zeroth Law and thermometry, ensemble (in)equivalence, fluctuation/dissipation relations, response theory, Fourier transport. As we will see, in all the mentioned contexts, both in and out of equilibrium, the introduction of negative temperature will be not only useful, but also necessary in order to achieve a consistent thermostatistical description of the presented results.

In Ref. [79] the authors state that Ising models are bad benchmarks for establishing the conceptual validity of a given thermostatistical description, since in nature it does not exist any evidence of Hamiltonians bounded from above; Ising-like systems are, in the words of the authors, *ad-hoc* truncations of more fundamental Hamiltonians which are not bounded from above, and therefore it is not advisable to consider them when trying to address fundamental questions. We are aware that the same critique can be addressed to the class of models analyzed in this Thesis. Let us stress, however, that our aim here is not to demonstrate that the Boltz-

mann's entropy (1.16) is a better choice than the Gibbs' one (1.19) for the models with unbounded spectrum, usually studied by classical Thermodynamics. On the contrary, we aim at showing that the use of S_B allows for an extension of the realm of Statistical Mechanics to systems with bounded Hamiltonians: the consequent introduction of negative temperature does not lead to any paradox nor contradiction, and offers, in our opinion, a coherent thermostatistical picture. We hope to convince the reader that such systems can be actually studied in the framework of Statistical Mechanics, and to shed some light on the physical meaning of negative temperature in the different problems that are considered in this Thesis.

Chapter 2

Systems with bounded phase spaces: equilibrium properties

In this Chapter we discuss some aspects of negative temperature equilibrium states, by investigating the statistical properties of Hamiltonian systems living in bounded phase-spaces.

First, we sketch some general considerations about the conditions for the emergence of NAT in separable Hamiltonian systems. This preliminary analysis allows us to introduce a class of simple mechanical models that will be used to illustrate the main ideas discussed in this Thesis. Next, we introduce the possibility to define and use a thermometer able to measure also negative temperature, thus revealing the connection between the statistical and the thermodynamic definitions of temperature even in this regime. Finally, we study the equilibrium features of a system with long-range interactions, which violates ensemble equivalence; it is shown, analytically and numerically, that such non-trivial metastable condition can be reached also in a NAT regime.

2.1 General conditions for negative temperature

As already mentioned in Sec. 1.1, mechanical systems whose energy quadratically depends on the Hamiltonian coordinates cannot display negative-temperature equilibrium distributions; therefore, in order to model and study these thermodynamic states, we need to focus our attention on a wider class of mechanical systems. We will consider Hamiltonian models of the form:

$$\mathcal{H}(\mathbf{p},\mathbf{q}) = \sum_{i=1}^{N} k_i(p_i) + \mathcal{U}(\mathbf{q}) \tag{2.1}$$

where (q_i, p_i), $i = 1, ..., N$ are pairs of canonical coordinates, while $k_i(p)$ and $\mathcal{U}(\mathbf{q})$ are smooth functions of their arguments. $\mathbf{X} = (\mathbf{q}, \mathbf{p})$ is therefore a point of a suitable $2N$-dimensional space Ω. The Hamilton equations that rule the evolution of this system read

$$\dot{q}_i = \frac{\partial k_i}{\partial p_i} \qquad \dot{p}_i = -\frac{\partial \mathcal{U}}{\partial q_i}\,. \tag{2.2}$$

In the following we will refer to q_i as the "position" and to p_i as the "momentum" of the i-th degree of freedom, extending the terminology of the Newtonian case to these generalized mechanical systems. The Hamiltonian terms depending on the momenta can thus be interpreted as generalized kinetic energies and, consistently, we require that their functional forms $k_i(p)$ satisfy the following conditions:

- $k_i(p) = k_i(-p) \quad \forall i, \quad$ i.e. all k_i are even functions of their argument;
- $k_i'(p) \geq 0$ if $p \geq 0$;
- $k_i(0) = 0$.

From a physical point of view, the first requirement means that the energy of the system does not change under time-reversal transform $t \to -t, \mathbf{q}_i \to \mathbf{q}_i, \mathbf{p}_i \to -\mathbf{p}_i$; the second one is equivalent to asking that the velocity $\dot{q}_i$ has the same sign of the corresponding momentum p_i (even if, in general, they are not proportional); the third one has no consequences on the dynamics, and it only states that the energy of a system of non-interacting particles at rest is equal to zero, in analogy with the Newtonian case.

Let us remark that in Eq. (2.1) we did not consider terms depending on more than one momentum coordinate p_i, nor terms that couple positions and momenta. In the following we will only deal with Hamiltonian systems of this kind, but it should be stressed that negative temperatures can be found in models with more general properties, e.g. the DNLS equation mentioned in Section 1.1.4: indeed, it can be shown that the DNLS can be written in a classical Hamiltonian form, in which positions and momenta are coupled [88].

Let us define the phase-space volume delimited by the hypersurface at constant energy E as

$$\Gamma(E) = \int_{\mathcal{H}(\mathbf{X})<E} d\mathbf{X}\,; \tag{2.3}$$

where the synthetic notation $d\mathbf{X} \equiv dp_1 ... dp_N\, dq_1 ... dq_N$ has been adopted. In the following we will assume, without lack of generality, that $\Gamma(E)$ is a well-defined quantity $\forall E \geq 0$ and that it vanishes at $E = 0$. We will also assume that no integrals of motion other than the total energy are present in the dynamics, so that the microcanonical state of the system is completely specified by E and by the parameters of the Hamiltonian. The density of states is thus defined as

$$\omega(E) = \partial_E \Gamma(E) = \int_\Omega d\mathbf{X} \delta(\mathcal{H}(\mathbf{X}) - E) \tag{2.4}$$

and the microcanonical entropy reads

$$S(E) = \ln \omega(E)\,. \tag{2.5}$$

Here and in the following we consider units such that the Boltzmann constant is unitary, $k_B = 1$.

Inverse temperature β is given by

$$\beta = \partial_E S(E)\,; \tag{2.6}$$

as already discussed, $\beta(E)$ assumes negative values if and only if $\omega(E)$ is, locally, a decreasing function of E.

2.1.1 Role of the interacting potential

If an Hamiltonian system of non-interacting particles

$$\mathcal{H}_0(\mathbf{p}) = \sum_i k_i(p_i) \tag{2.7}$$

is characterized by a non-decreasing entropy $S(E)$ and some of the $k_i(p)$ have no upper bound, adding an interacting potential will not introduce negative temperature. In order to understand that, we consider the density of states at energy E of

$$\mathcal{H}(\mathbf{X}) = \mathcal{H}_0(\mathbf{p}) + \mathcal{U}(\mathbf{q})\,. \tag{2.8}$$

Such quantity can be written as

$$\begin{aligned}\omega(E) &= \int_\Omega d\mathbf{X}\,\delta(\mathcal{H}(\mathbf{X}) - E) \\ &= \int_\Omega d\mathbf{X} \int_0^{\min(E,U_{max})} du\,\delta(u - \mathcal{U}(\mathbf{q}))\delta(\mathcal{H}_0(\mathbf{p}) + u - E) \\ &= \int_0^{\min(E,U_{max})} du\,\omega_q(u)\omega_p(E-u)\end{aligned} \tag{2.9}$$

where U_{max} is the maximal energetic contribution associated to the q_i, possibly infinite, and ω_q, ω_p can be seen as the contributions to the density of states due to the positions and momenta, respectively. Let us note that in the above calculation we made implicit use of the hypothesis that $\mathcal{H}_0(\mathbf{p})$ is unbounded.

If we consider some value of the energy $E' > E$, the following inequality holds:

$$\begin{aligned}\omega(E) &= \int_0^{\min(E,U_{max})} du\,\omega_q(u)\omega_p(E-u) \leq \\ &\leq \int_0^{\min(E',U_{max})} du\,\omega_q(u)\omega_p(E'-u) = \omega(E')\,,\end{aligned} \tag{2.10}$$

since the integrand is positive and $\omega_p(E)$ is non-decreasing by hypothesis. As a consequence, system $\mathcal{H}(\mathbf{X})$ only admits positive temperatures.

The above argument can be repeated in a quite similar way if we want to add degrees of freedom to an unbounded Hamiltonian which cannot reach negative temperatures. It can be easily shown that there is no way to induce negative temperature states by coupling it with some other Hamiltonian system. This simple observation will be better discussed in Section 2.3.

As an immediate (and important) example, we can consider the case of quadratic kinetic energy. First, we recall that the phase space volume of the ideal gas

$$\mathcal{H}_0(\mathbf{X}) = \sum_i \frac{p_i^2}{2m_i} \tag{2.11}$$

confined in a box of length L is given by

$$V(E) = \frac{(2\pi)^{N/2} L^N}{\Gamma(1+N/2)} E^{N/2} \tag{2.12}$$

where the formula for the volume of an N-dimensional sphere with radius $\sqrt{2E}$ has been used (here Γ represents the Euler Gamma-function, and $N = Dn$ where D is the number of spatial dimensions and n the number of particles). As a consequence, the density of states verifies

$$\omega(E) \propto E^{\frac{N}{2}-1}\,, \tag{2.13}$$

i.e. it is an increasing function of the total energy as soon as $N > 2$. In the light of the above, we can also state that, no matter what kind of interacting potential is considered, an Hamiltonian system with quadratic kinetic energy terms will never admit negative temperature at equilibrium. Furthermore, coupling it to a different Hamiltonian system will never lead to a negative temperature equilibrium state.

2.1.2 Momentum distribution

The following simple argument allows to deduce the momentum distribution of a single particle (see also Ref. [41]). Let us consider the Hamiltonian model defined by Eq. (2.1). The microcanonical probability density function (p.d.f.) for the j-th momentum is given by

$$\begin{aligned}\rho_j(p|E) &= \frac{1}{\omega(E)}\int_\Omega d\mathbf{X}\,\delta(\mathcal{H}(\mathbf{X})-E)\delta(p-p_j)\\ &= \frac{1}{\omega(E)}\int_{\widetilde{\Omega}} d\widetilde{\mathbf{X}}\,\delta\left(\widetilde{\mathcal{H}}(\widetilde{\mathbf{X}})+k_j(p)-E\right)\\ &= \widetilde{\omega}(E-k_j(p))/\omega(E)\\ &= \exp\left[\widetilde{S}(E-k_j(p))-S(E)\right]\end{aligned} \tag{2.14}$$

where

$$\widetilde{\mathbf{X}} = (q_1,...,q_N,p_1,...,p_{j-1},p_{j+1},...,p_N) \tag{2.15}$$

is the generic point of the reduced phase-space $\widetilde{\Omega}$ obtained by excluding the coordinate p_j, and

$$\widetilde{\mathcal{H}}(\widetilde{\mathbf{X}}) = \mathcal{H}(\mathbf{X}) - k_j(p_j) \tag{2.16}$$

is the part of Hamiltonian (2.1) which does not depend on p_j. The corresponding quantities $\widetilde{\omega}$ and $\widetilde{S}$ are defined accordingly.

We can now expand Eq. (2.14) assuming that $k_j(p)$ is much smaller than the total energy: this expansion is always legitimate if $k_j(p)$ is bounded from above by some constant k_{max} and $E \gg k_{max}$. We get

$$\begin{aligned}\rho_j(p|E) &\simeq \exp\left[\widetilde{S}(E) - \frac{d\widetilde{S}(E)}{dE}k_j(p) - S(E)\right]\\ &\propto \exp\left[-\beta k_j(p)\right]\end{aligned} \tag{2.17}$$

(assuming $d\widetilde{S}/dE \simeq dS/dE \equiv \beta$ in the thermodynamic limit).

Let us notice that this expression *does not* exclude the possibility that Hamiltonian systems with unbounded energy assume negative temperature at equilibrium: it is sufficient for the domain of the corresponding coordinates to be bounded, so that the normalization of the p.d.f. is well-defined.

Let us also stress that in the above derivation we assumed that the energy of the system was much larger than those related to the momenta of the single particles. Of course this assumption is reasonable in the thermodynamic limit, when one considers a set of identical particles. Still, some – quite pathological – cases (see Section 2.1.4) violate such assumption, and the above result cannot be stated in a more general form.

2.1.3 Bounded energy: an unnecessary condition for NAT

In his fundamental paper about the Statistical Mechanics of negative temperatures [156], Ramsey states that an upper bound on the energy of the system is a necessary condition for observing negative temperature equilibrium states. The statement is correct in the context of the paper, since only the case of quantum systems with discrete degrees of freedom is examined (as it is natural for the study of nuclear spin systems). On the other hand, if one is interested in the statistical properties of systems described by continuous coordinates, the condition of a bound on the total energy is not needed anymore: as observed by Machlup [126], the only requirement is the existence of the average energy $\langle \mathcal{H} \rangle$ in the canonical ensemble at infinite temperature, i.e. negative temperature states can be observed if

$$\langle \mathcal{H} \rangle_{\beta=0} = \int dE\, e^{-\beta E} \omega(E) E \Big|_{\beta=0} = \int dE\, \omega(E) E < \infty\,, \tag{2.18}$$

even if E is unbounded.

From the microcanonical point of view, we know for sure that systems with unbounded energy living in bounded phase spaces verify

$$\lim_{E\to\infty} \Gamma(E) = \Gamma_{max} < \infty \tag{2.19}$$

so that $\omega(E)$, by continuity, has to be a decreasing function of its argument for some energy interval. This is therefore a sufficient condition for negative temperature states. As an example, we can consider the following Hamiltonian:

$$\mathcal{H}(\mathbf{X}) = \sum_{i=0}^{N} \tan^2(p_i) + \sum_{i=0}^{N-1} \tan^2\left(\frac{q_{i+1} - q_i}{2}\right). \tag{2.20}$$

with $p_i, q_i \in (-\pi/2, \pi/2)$: the total energy can assume arbitrarily large values, but, due to the bound on the phase space, $\Gamma_{max} = \pi^{2N}$, and NAT states can actually appear.

2.1.4 Bounded phase space

In the light of the above discussion, one could expect that a bounded phase-space is a necessary condition for NAT states in the microcanonical description. Strictly speaking, this guess is false. In principle, one could imagine a model with $\omega(E)$ slowly decreasing such that $\Gamma(E) = \int_0^E \omega(E')dE' \to \infty$, e.g. $\omega(E) \propto E^{-\alpha}$ with $0 < \alpha \leq 1$.

Let us consider, for instance, the particular case of a Hamiltonian characterized by N bounded degrees of freedom and a single particle with quadratic kinetic energy, labeled with the subscript 1, i.e.

$$\mathcal{H}(\mathbf{X}) = \frac{p_1^2}{2} + \mathcal{H}_0(\mathbf{X}_0) \tag{2.21}$$

where the condition $\mathcal{H}_0(\mathbf{X}_0) \leq E_0$ holds. Here $\mathbf{X}_0$ is the vector including all canonical coordinates except p_1.

Let us compute $\Gamma(E)$ in the case $E > E_0$:

$$\begin{aligned}\Gamma(E) &= \int_{\mathcal{H}(\mathbf{X})<E} dp_1\, d\mathbf{X}_0 \\ &= \int_0^{E_0} dE' \int_{\mathcal{H}(\mathbf{X})<E} dp_1\, d\mathbf{X}_0 \delta(\mathcal{H}_0(\mathbf{X}) - E') \\ &= \int_0^{E_0} dE' \int_{\Omega_0} d\mathbf{X}_0 \delta(\mathcal{H}_0(\mathbf{X}_0) - E') \int_{-\tilde{p}(E-E')}^{\tilde{p}(E-E')} dp_1\,.\end{aligned} \tag{2.22}$$

In the last expression, Ω_0 is the (bounded) dominion where $\mathbf{X}_0$ is defined, while $\tilde{p}(E) = \sqrt{2E}$ is the (positive) single-particle momentum corresponding to an energy E for kinetic terms with the usual quadratic shape. We have therefore

$$\Gamma(E) = 2\sqrt{2} \int_0^{E_0} dE' \sqrt{E - E'} \omega_0(E')\,, \tag{2.23}$$

where

$$\omega_0(E') = \int_{\Omega_0} d\mathbf{X}_0 \delta(\mathcal{H}_0(\mathbf{X}_0) - E')\,. \tag{2.24}$$

Taking the derivative of Eq. (2.23) w.r.t. E one gets the density of states

$$\omega(E) = \frac{d\Gamma}{dE} = \sqrt{2} \int_0^{E_0} dE' \frac{\omega_0(E')}{\sqrt{E - E'}}\,, \tag{2.25}$$

which, in the limit $E \gg E_0$, is proportional to $E^{-1/2}$: it is a decreasing function of the energy and, as a consequence, the system can achieve negative temperature.

Let us note, however, that in this particular setting the energy of the system is almost completely stored in the quadratic kinetic term, which is a quite peculiar situation (not very meaningful from the point of view of Statistical Physics).

2.2 Systems with bounded kinetic terms: a useful class of models

One of the aims of the present Thesis is to show, through the study of suitable Hamiltonian systems, that the introduction of NAT does not lead to any form of paradox, and that it provides a useful tool for the statistical descriptions of systems with bounded phase spaces. To this end, we will focus on Hamiltonian systems that satisfy the following conditions:

1. The phase space accessible to the system is bounded; we have shown (see Section 2.1.4) that it is possible to build mechanical models which admit NAT even if the total accessible phase space is infinite, but such cases seem to be quite peculiar and cannot be considered, in our opinion, paradigmatic of the statistical behavior occurring on real physical systems.

2. The Hamiltonian can be splitted into the sum of a kinetic and a potential contribution. This, of course, is not a requirement to achieve NAT (important physical examples such as the DNLS equation are not included in this category); however, due to the simple argument discussed in Sec. 2.1.2, in these systems temperature can be easily measured by looking at the momentum distribution.

3. The kinetic terms are bounded from above: even if this requirement is not strictly necessary to achieve NAT states (as shown in Sec. 2.1.3), we stress that the choice of unbounded kinetic terms may lead to considerable technical difficulties in numerical simulations. The main reason is that if $k(p)$ reaches infinite values in a finite domain for p, $\dot{q} = k'(p)$ can assume arbitrarily high values in such domain, making very difficult to control the precision of numerical simulations of the dynamics.

4. We also choose to consider periodic boundary conditions on the domain of the $\{p_i\}$ (in other words, we consider momenta living on a torus). In this way we are sure that the dynamics of the system is always well-defined, i.e. the dynamics never leads the system out of the domain in which it is defined. Another way to reach the same goal would have been that of choosing $k(p)$ in such a way that $k'(p) \to \infty$ at the boundaries; again, this choice leads to instability on the numerical simulations, whose outcomes would be difficult to control.

2.2.1 The model

In the light of the above discussion, we restrict ourself to the class of mechanical models whose Hamiltonians have the form

$$\mathcal{H}(\mathbf{p}, \mathbf{q}) = \sum_{i=1}^{N} [1 - \cos p_i] + \mathcal{U}(\mathbf{q}) \tag{2.26}$$

where both positions and momenta live on the torus $[-\pi/2, \pi/2)$ with periodic boundary conditions, i.e. they are angular variables. This class of Hamiltonian systems has been introduced in Ref. [41], and the form of the kinetic energy is quite similar to that experimentally observed in a celebrated work about systems of cold atoms [23], discussed in Section 1.1.3. A system with this form of the kinetic energy is also briefly discussed in Ref. [82].

The proposed form of the kinetic energy is of course artificial, meaning that it does not reproduce any known dynamics of real particles; nevertheless, the study of this simple model can improve the understanding of general mechanisms that also hold for more realistic systems allowing NAT states. Let us also notice that:

- the volume of the phase-space accessible by the system is bounded;
- the total kinetic energy is always positive and it is bounded from above by the value $2N$;
- for small values of the total energy, the kinetic terms can be approximated by $p_i^2/2$, i.e. we recover the usual expression of the kinetic energy for particles with unitary masses;
- the velocity of the i-th particle, $\dot{q}_i = \sin p_i$, is also bounded in this model, and it has the same sign of the momentum (even if it is not a monotonic function of the latter).

In some cases it will be useful to consider some dependence of the single-particle dynamics on generalized "masses". In particular, the possibility to tune such masses can be used to produce an effective time-scale separation on the evolutions of different oscillators (see Section 3.2). To impose additivity of both kinetic energy and momentum of particles with the same velocity, it can be shown that kinetic terms have to be written in the following way:

$$\mathcal{H} = \sum_i m_i c^2 \left[1 - \cos(p_i/m_i c)\right] + \mathcal{U}(\mathbf{q}) \tag{2.27}$$

where c is a constant with the physical dimensions of a velocity (in the following we put $c = 1$) and the constants $\{m_i\}$ play the role of generalized masses. This topic will be discussed in some detail in Section 3.1.

2.2.2 Measuring β

In the following we will often deal with numerical simulations of Hamiltonian systems of the form (2.26); since the measure of the inverse temperature β is a crucial point in all considered cases, we briefly examine here the proper ways for determining it from the dynamics. Technical aspects about the integration algorithms are discussed in Chapter 5.

In Hamiltonian systems with the usual kinetic energy $\sum_i p_i^2/2m$ one would exploit the equipartition theorem [125, 85] and measure $T = 1/\beta$ as the (temporal) average $\langle p_i^2/m \rangle$ – assuming that the ergodic hypothesis holds. Of course in this case the form of the physical observable to study has to be different, since the kinetic energy is not quadratic.

One could be tempted to measure $\langle p \sin(p/m) \rangle$, as suggested by the equipartition theorem, which asserts that

$$\langle x_i \frac{\partial \mathcal{H}}{\partial x_j} \rangle = \delta_{ij} T \tag{2.28}$$

where x_i and x_j are generic canonical variables. As already discussed in Section 1.2, the temperature appearing in Eq. (2.28) is the so-called "Gibbs temperature", whose physical meaning is quite different from T_B, the Boltzmann temperature, and which can never assume negative values. Since T_B and T_G are related (see Ref. [82]), computing T_B as a function of T_G could still appear as a feasible option; however, as discussed in Ref. [41], in this case the hypotheses of the equipartition theorem

are not fulfilled and not even T_G can be measured in this way. Indeed, the usual derivation of Eq. (2.28) is based on the fact that the l.h.s. of Eq. (2.28) can be written as

$$\frac{1}{\omega(E)}\frac{\partial}{\partial E}\left[\int_{\mathcal{H}<E} d\mathbf{p}d\mathbf{q}\frac{\partial}{\partial x_j}[x_i(\mathcal{H}-E)] - \delta_{ij}\int_{\mathcal{H}<E} d\mathbf{p}d\mathbf{q}\frac{\partial}{\partial x_j}(\mathcal{H}-E)\right] \tag{2.29}$$

where the first term is assumed to vanish, due to the fundamental theorem of calculus. However, this is only true if the boundary of the integration domain coincides with the closed curve $\mathcal{H} = E$: if, instead, the phase space is bounded, the domain $\mathcal{H} < E$ can be also delimited by the boundary of the phase space itself, and nothing can be said about the considered term.

Even if the Equipartition theorem does not hold, it can be proved that there exists a mechanical observable whose ensemble average gives the microcanonical (inverse) temperature, assuming that ergodic hypothesis holds [164, 165]:

$$\beta = \langle \nabla \cdot \left(\frac{\nabla \mathcal{H}}{||\nabla \mathcal{H}||^2}\right)\rangle \,. \tag{2.30}$$

The above result is very important from a conceptual point of view, but of course it can be difficult to apply it to the study of systems with many degrees of freedom. A much easier way is to study the form of the single-particle momentum distribution, and to infer β through a numerical fit on the functional form

$$\rho(p_j) = \mathcal{N} \exp\left[\beta m_j \cos(p_j/m_j)\right] \tag{2.31}$$

where $\mathcal{N}$ is the normalization constant. In Fig. 2.1(A) we show some histograms of the momenta of single particles, in molecular dynamics simulations of model (2.26) with $m_j = 1\ \forall j$ and

$$\mathcal{U}(\mathbf{q}) = K\sum_{i=0}^{N}\left[1-\cos(q_i - q_{i+1})\right]\,, \qquad q_0 \equiv q_{N+1} \equiv 0\,, \tag{2.32}$$

for different values of the total energy E. The value of β is inferred from a fit on the p.d.f. with the functional form (2.31). In Fig. 2.1(B) we plot the inferred values of β as a function of the specific energy $\varepsilon = E/N$: the analytical relation

$$\varepsilon(\beta) = 1 - \frac{I_1(\beta)}{I_0(\beta)} + K\left[1 - \frac{I_1(\beta K)}{I_0(\beta K)}\right]\,, \tag{2.33}$$

which is derived in Appendix 2.A is nicely reproduced. Here $I_n(x)$ is the n-th modified Bessel function of the first kind. Let us stress that, here and in the following, the particular choice for the value of K (or other parameters appearing in the potential term) is not crucial to the possibility of observing the discussed phenomenology.

At small energies the system reduces to a chain of harmonic oscillators, and the momentum p.d.f. is similar to a Gaussian profile, centered in zero. This condition corresponds to positive-temperature states. When the energy exceeds a certain threshold, the volume of the phase-space region that can be accessed by the system

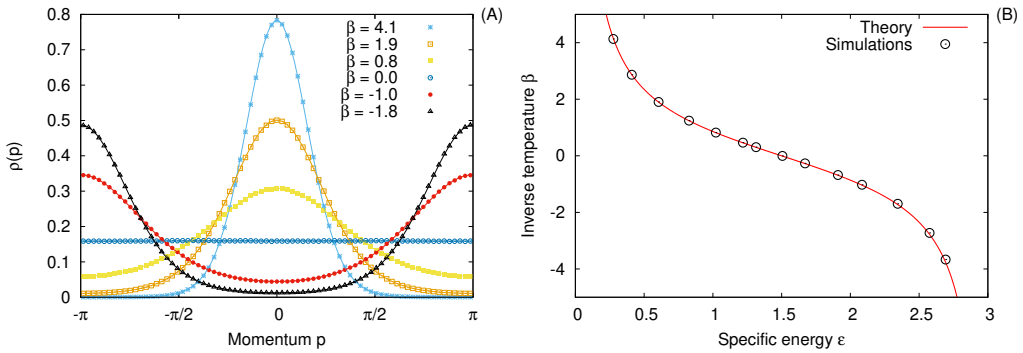

Figure 2.1. Measuring β from the momentum p.d.f.. Panel (A): histograms of the single-particle momentum distribution (points), for different values of the total energy of the system; solid lines are best fits for the functional form (2.31), from which we compute the values of β reported in the legend. The profiles are obtained by averaging over all particles. Panel (B): caloric curve $\beta(\varepsilon)$ inferred from simulations (circles) compared to the analytical relation (2.33). Here $K = 0.5$, $N = 128$, total integration time for each profile $\mathcal{T} = 3 \cdot 10^5$. Details on the integration algorithm are discussed in Section 5.1.

starts decreasing; β becomes therefore negative, with a consequent change of concavity for the momentum p.d.f.. In particular, the maximum of the distribution is shifted from $p = 0$ to $p = \pm\pi$.

A practical alternative is to study the single-particle observable

$$\begin{aligned} \langle \cos(p_j/m_j) \rangle &= \int dp_j \, \rho(p_j) \cos(p_j/m_j) \\ &= \frac{I_1(\beta m_j)}{I_0(\beta m_j)} \, . \end{aligned} \tag{2.34}$$

If the dynamics satisfy reasonable ergodicity conditions, the above quantity can be measured by averaging over long-time series of data from numerical simulations. Since $B(x) = I_1(x)/I_0(x)$ is an odd function, it can be inverted to find β.

2.3 Thermometers and "thermodynamic" negative temperature

So far, we have discussed negative temperature only from the point of view of Statistical Mechanics, i.e. we have shown that in particular classes of systems the volume of the accessible phase-space region (and, as a consequence, the total entropy) is a decreasing function of the total energy of the system. In this Section we try to show that NATs are well-defined also within a thermodynamic perspective; to this end, we will discuss the possibility to extend the operative definition of "thermodynamic" temperature, related to the concept of thermal equilibrium and to the Zeroth Law, also to Hamiltonian systems with bounded kinetic terms. In other words, we will face the problem of designing a thermometer that is able to measure negative temperature. The results presented in this Section are contained in Ref. [10]. A similar study (on a lattice system) has been addressed in Ref. [26].

2.3.1 Zeroth Law and the definition of temperature

Let us assume that the macroscopic state of a system is entirely described by a set of n observables $\{\alpha_1, ..., \alpha_n\}$ (e.g. volume, pressure, magnetization...), with n much smaller than the total number of microscopic degrees of freedom. If such quantities do not change appreciably in time on a macroscopic scale, the system is said to be in a condition of thermodynamic equilibrium [85]. Moreover, if two systems $\mathcal{A}$ and $\mathcal{B}$ are put at thermal contact (i.e., they have the possibility to exchange heat) and, nonetheless, the corresponding macroscopic observables $\{\alpha_i^{\mathcal{A}}\}$ and $\{\alpha_i^{\mathcal{B}}\}$ do not change in time, $\mathcal{A}$ and $\mathcal{B}$ are in thermal equilibrium with each other.

Zeroth Law of Thermodynamics states that if two systems $\mathcal{A}$ and $\mathcal{B}$ are, separately, in thermal equilibrium with a third system $\mathcal{C}$, they are also in thermal equilibrium with each other [100]. Thermal equilibrium is thus a reflexive, transitive and symmetric property, which determines an equivalence relation between thermodynamic systems. As a consequence, Zeroth Law implies the existence of a function Θ – the "thermodynamic" temperature – which identifies the different classes of equivalence, assuming equal values for two different systems if they are at thermal equilibrium [151]. A well known result of equilibrium Statistical Mechanics [85] assures that, if a thermodynamic temperature Θ can be defined (i.e., if the considered bodies reach thermal equilibrium once they are put at contact), such quantity has to be an invertible function of $\beta = dS/dE$, whence the link between Thermodynamics and Statistical Mechanics.

The thermodynamic temperature can be measured through a thermometer, i.e. a device with the following properties:

1. it exists a physical observable of such device, function of the thermodynamic temperature only, which can be used to determine the value of Θ (at least on a suitable scale);

2. once put in contact with the system to measure, the thermometer will reach a thermal equilibrium in a finite time, without perturbing the temperature of the system in a significant way.

The very operative definition of temperature, in classical Thermodynamics, relies on the possibility to design a thermometer able to quantify such observable. In what follows we will show that for systems with bounded kinetic terms, as those discussed in Section 2.2, we can give a definition of temperature in the thermodynamic sense, through the introduction of a suitable model of "thermometer".

2.3.2 Simulating a minimal model for a thermometer

We want to verify that it is possible to design, at least in principle, a device able to measure the temperature of a system both at positive and negative temperature. The possibility of such "universal" thermometer will be tested through molecular dynamics simulations on simple Hamiltonian models. In particular, we will consider the case in which a system $\mathcal{S}$ of the type (2.26) is able to exchange energy with another system $\mathcal{T}$, so that they eventually reach thermal equilibrium; if such coupling does not perturb the initial thermodynamic state of $\mathcal{S}$, we could use $\mathcal{T}$ to "measure" the thermodynamic temperature of $\mathcal{S}$.

To this end, we will enforce molecular dynamics simulations on a Hamiltonian system composed of two interacting subsystems:

$$\begin{aligned} \mathcal{S}: &\quad H_{\mathcal{S}}(\{P_i, Q_i\}), \quad i = 1, ..., N_{\mathcal{S}} \\ \mathcal{T}: &\quad H_{\mathcal{T}}(\{p_j, q_j\}), \quad j = 1, ..., N_{\mathcal{T}}, \end{aligned} \tag{2.35}$$

with $N_{\mathcal{S}} \gg N_{\mathcal{T}}$. Due to the last requirement, it is reasonable to expect that the coupling between $\mathcal{S}$ and $\mathcal{T}$ will not lead to a significant perturbation of the initial thermodynamic state of $\mathcal{S}$, and system $\mathcal{T}$ should reach, after a sufficiently long time, a temperature very close to the one initially assumed by $\mathcal{S}$. Of course the interaction term between the two systems,

$$H_{int}(\mathbf{q}, \mathbf{Q}) = \varepsilon \sum_{i}^{N_T} V_{int}(q_i - Q_i), \quad \varepsilon \ll 1 \tag{2.36}$$

where V_{int} is some two-particles interaction potential, has to be small for the same reasons. In the following, we always choose

$$V_{int}(x) = 1 - \cos(x). \tag{2.37}$$

The total Hamiltonian of the system we are going to simulate reads:

$$H_{tot}(\mathbf{P}, \mathbf{p}, \mathbf{Q}, \mathbf{q}) = H_{\mathcal{S}}(\mathbf{P}, \mathbf{Q}) + H_{\mathcal{T}}(\mathbf{p}, \mathbf{q}) + H_{int}(\mathbf{Q}, \mathbf{q}). \tag{2.38}$$

In our numerical experiments we apply the following protocol:

1. We initialize $\mathcal{S}$ in a typical thermal state.
2. We initialize $\mathcal{T}$ in a thermal state at a different temperature.
3. We set $\varepsilon = 0$, so that no interaction is present between $\mathcal{S}$ and $\mathcal{T}$, and we let the total system evolve for some time τ_0 (much larger than the characteristic times of the subsystems' dynamics) according to the Hamiltonian evolution defined by (2.38).
4. By measuring β in the two subsystems, we verify that they are (separately) at equilibrium.
5. We set ε to a nonzero value, as to couple the two subsystems.
6. We let the total system evolve again and we measure β for $\mathcal{S}$ and $\mathcal{T}$ in time.

If the temperature of $\mathcal{S}$ is constant and it is reached by that of $\mathcal{T}$ in a finite time, we conclude that the thermometer is able to measure the temperature of $\mathcal{S}$ without perturbing it.

Our numerical simulations are based on a Verlet-like algorithm, with time step chosen to be 5×10^{-3}, in order to keep relative energy fluctuations $< 10^{-4}$. For more details, see Section 5.1. Let us just stress that our numerical simulations are fully deterministic, i.e. without coupling with external reservoirs or thermostats.

2.3.3 Characterization of $\mathcal{S}$

We are interested in the thermodynamic properties of systems of the form (2.26). A possible choice for $\mathcal{S}$ is represented by the following Hamiltonian:

$$H_{\mathcal{S}}(\mathbf{P},\mathbf{Q}) = \sum_{i=1}^{N_{\mathcal{S}}}(1-\cos P_i)+\frac{J}{2N_{\mathcal{S}}}\sum_{i,j=1}^{N_{\mathcal{S}}}(1-\cos(Q_i-Q_j))+K\sum_{i=1}^{N_{\mathcal{S}}}(1-\cos(Q_i-Q_{i-1})) \tag{2.39}$$

with $Q_0 \equiv Q_{N_{\mathcal{S}}}$, $J \ll K$, $(Q_i, P_i) \in [-\pi,\pi)^2$ (with periodic boundary conditions).

The form of the kinetic energy, and the reasons why it is particularly convenient for numerical studies, have been examined in Sec. 2.2. About the interaction potential let us remark that, if we choose $J = 0$, it reduces to the one discussed in Ref. [41] and briefly treated in Section 2.2; in this case we get a one-dimensional chain of "generalized" oscillators. At large energy the exchange of heat among the degrees of freedom of such kind of models is strongly depressed [121]. Therefore in order to avoid very slow exchange of energy, a small non local interaction contribution has been introduced. Indeed, when $J > 0$, we introduce a perturbation that has the same form of the interaction potential in the well-known HMF model [5] (a paradigm for long-range interacting systems). Such term has the mere aim of avoiding long-living metastable situations.

Remarkably enough, the equilibrium properties of systems with Hamiltonian (2.39) can be deduced analytically, in the thermodynamic limit, making use of large-deviation techniques. First we need to find the canonical equipartition function $Z_N(\beta)$, and then one has to compute the free energy per particle through the limit $-\beta f(\beta) = \lim_{N\to\infty} \log Z_N/N$. At that point, the thermodynamics of the system is fully described. This analysis is detailed in Appendix 2.B.

2.3.4 Thermometer with quadratic kinetic terms

First, we make the "naive" attempt to measure the temperature of system (2.39) by using a thermometer with the usual, quadratic kinetic energy, which is expected to mimic the behavior of a thermometer made of ordinary matter.

It is useful to recall an argument to show that the coupling of a system $\mathcal{A}$ at negative temperature with a system $\mathcal{B}$ which only admits positive values of β always produces a system with final positive temperature. Indeed, at the initial time, before $\mathcal{A}$ and $\mathcal{B}$ are put at contact, the total entropy reads

$$S_I = S^{\mathcal{A}}(E_{\mathcal{A}}) + S^{\mathcal{B}}(E_{\mathcal{B}}), \tag{2.40}$$

while, after the coupling, it becomes

$$S_F = S^{\mathcal{A}}(E'_{\mathcal{A}}) + S^{\mathcal{B}}(E'_{\mathcal{B}}), \tag{2.41}$$

where $E'_{\mathcal{A}} + E'_{\mathcal{B}} = E_{\mathcal{A}} + E_{\mathcal{B}}$ and, within our assumptions, $E'_{\mathcal{A}}$ is determined by the equilibrium condition that S_F takes the maximum possible value [85], i.e.

$$\beta_{\mathcal{A}} = \frac{\partial S^{\mathcal{A}}(E'_{\mathcal{A}})}{\partial E'_{\mathcal{A}}} = \beta_{\mathcal{B}} = \frac{\partial S^{\mathcal{B}}(E'_{\mathcal{B}})}{\partial E'_{\mathcal{B}}}. \tag{2.42}$$

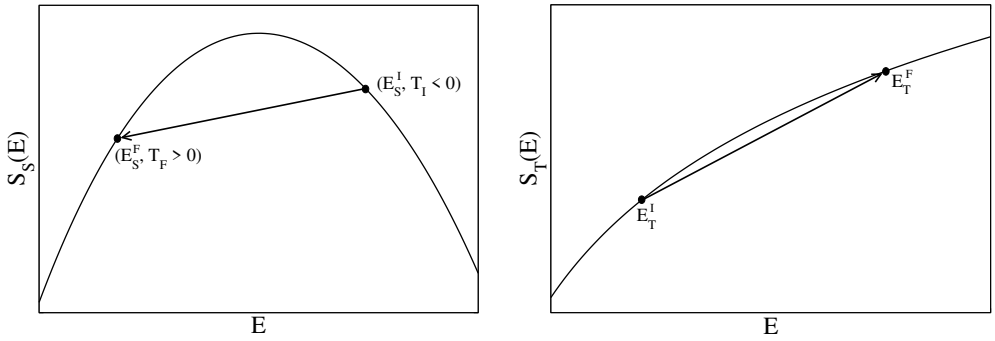

Figure 2.2. Entropy of the system $S_{\mathcal{S}}(E)$ (left panel), and of the thermometer $S_{\mathcal{T}}(E)$ (right panel), as a function of E. Before the coupling, the system's energy $E_{\mathcal{S}}^I$ corresponds to a negative temperature, $T_I < 0$; after the thermalization, due to the coupling with the thermometer with "Newtonian" kinetic energy, the total system's temperature must be necessarily positive, and a huge transfer of energy from $\mathcal{S}$ to the thermometer occurs, in such a way that $E_{\mathcal{S}}^I + E_{\mathcal{T}}^I \simeq E_{\mathcal{S}}^F + E_{\mathcal{T}}^F$. Figure from Ref. [10].

Since $\beta_{\mathcal{B}}$ is positive for every value of $E'_{\mathcal{B}}$, the final common temperature must also be positive. In Fig. 2.2 we show schematically the mechanism for the energy transfer. The result could also be expected on the basis of the discussion in Section 2.1.

In the light of the above, using as thermometer a system with "Newtonian" kinetic energy, which can only assume positive β, will result in an heavy perturbation of the system to measure (even if the size of the thermometer is much smaller than that of $\mathcal{S}$).

We have checked this argument by running molecular dynamics simulations using a thermometer with Hamiltonian given by

$$H_{\mathcal{T}}(\mathbf{p}, \mathbf{q}) = \sum_{i=1}^{N_{\mathcal{T}}} \frac{p_i^2}{2} + \sum_{i=1}^{N-1} \left[1 - \cos(q_{i+1} - q_i)\right] . \tag{2.43}$$

We compute the temperature of the thermometer by looking at the usual average $\langle p^2 \rangle$. The temperature of the system is instead measured by fitting the histograms of the momenta; in particular, we plot $\cos(p)$ vs $\log[\rho(p)]$, where $\rho(p)$ is the empirical distribution of the momenta of all particles in a certain time interval, and we make a linear fit to extrapolate the value of β (see also Ref. [41]). We repeat the operation for many consecutive time windows, in order to obtain a plot of β as a function of time t. We could also use a running observable, for instance the one discussed in Section 2.2, but with this direct inspection of the empirical distributions in time we are also able to verify that the system evolves through states of quasi-equilibrium (i.e., that temperature is well defined at any time).

Figure 2.3 shows the scenario predicted by the previous simple thermodynamic arguments. In the plots the value of β as a function of the time is displayed both for $\mathcal{S}$ and $\mathcal{T}$, starting from the instant in which the coupling ε is turned on. In the left plot we see that, if the initial equilibrium state of $\mathcal{S}$ is at negative temperature, an energy flux from the system $\mathcal{S}$ to the thermometer $\mathcal{T}$ occurs. This is coherent, of course, with the usual interpretation of negative temperature as "hotter" than positive temperature, and with the mechanism illustrated in Fig. 2.2. Such flux

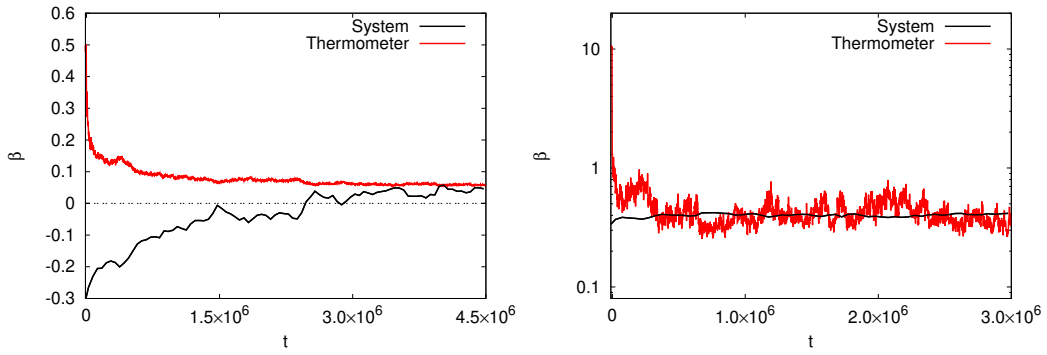

Figure 2.3. Inverse temperature β as a function of time, for the system (2.39) and the thermometer (2.43). In the left (right) panel the β corresponding to the initial energy of the system is negative (positive). $\beta(t)$ is computed for the system from a fit on the single particle momentum p.d.f.: we consider the histogram of the measured momenta from time t to time $t+\Delta t$, with $\Delta t = 50000$ in this case, and we get the value of β from the slope of $\log[\rho(p)]$, as explained in Ref. [41]. Thermometer's inverse temperature has been determined, as usual, by $\beta = \langle p^2 \rangle^{-1}$. Parameters: $N_{\mathcal{S}} = 1000$, $N_{\mathcal{T}} = 30$, $K = \gamma = 0.5$, $J = 0.05$ $\epsilon = 0.1$. Figure from Ref. [10].

ends only once thermal equilibrium is reached, i.e. when the system has released an amount of energy large enough to be in a positive-energy state. It is clear that the amount of exchanged energy is macroscopic even if the size of the thermometer is very small with respect to that of $\mathcal{S}$ (i.e. $N_{\mathcal{T}} < N_{\mathcal{S}}$). This heavy perturbation of the system to measure indicates a catastrophic failure of model (2.43) as a candidate for a "universal" thermometer.

As a side remark, let us note that system $\mathcal{S}$ reaches an equilibrium with the thermometer $\mathcal{T}$ by passing through a $\beta = 0$ state. This observation is quite obvious in the light of the above qualitative discussion, but it is useful to stress that while the states $\beta = \pm\infty$ (corresponding to $T = 0$) cannot be attained starting from systems at finite temperature, $\beta = 0$ can be actually reached: some authors, indeed, claim that such states are both unattainable, and this assumption is used to assert that the introduction of NAT leads to (apparent) paradoxes [161].

The right panel shows that no issue is encountered when the initial state of $\mathcal{S}$ is at positive temperature: in that case the temperature measured by $\mathcal{T}$ quickly reaches the original temperature of $\mathcal{S}$, which is not considerably modified by the coupling with the thermometer.

2.3.5 A proper thermometer (with bounded kinetic terms)

Let us now look at what happens when we consider a thermometer with bounded phase space of the kind (2.1), e.g. the one described by the following Hamiltonian:

$$H_{\mathcal{T}}(\mathbf{p},\mathbf{q}) = \sum_{i=1}^{N_{\mathcal{T}}}(1-\cos p_i) + \sum_{i=1}^{N_{\mathcal{T}}-1} \gamma\,[1-\cos(q_{i+1}-q_i)]\ . \tag{2.44}$$

In this case the total system, composed by $\mathcal{S}$ and $\mathcal{T}$, is still a Hamiltonian model of the kind (2.1) living in a bounded phase space, and therefore we expect that it is able to assume negative temperatures.

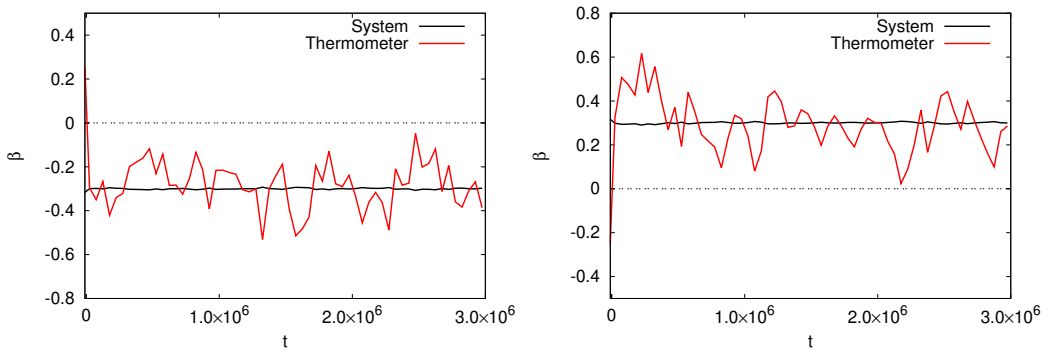

Figure 2.4. Inverse temperature β as a function of time, for the system (2.39) and the thermometer (2.44), both measured by the distribution fitting procedure explained in Fig 2.3. In the left (right) panel the β corresponding to the initial energy of the system is negative (positive). Parameters as in Fig. 2.3. Figure from Ref. [10].

If the size of the thermometer is small with respect to that of the system (i.e., if $N_{\mathcal{T}} \ll N_{\mathcal{S}}$), we can also expect that just a small exchange of energy, compared to the total energy stored in $\mathcal{S}$, is needed in order to reach thermal equilibrium. This is due to the fact that this time the subsystem $\mathcal{T}$ can reach any value of the temperature, both positive and negative, so that it does not act as a "sink" for the energy of $\mathcal{S}$ anymore. As a consequence, the thermodynamic state of $\mathcal{S}$, and its temperature, should not be perturbed too much by the coupling with $\mathcal{T}$.

Also in this case we run molecular dynamics simulations of the coupled system and we measure the inverse temperature β through the analysis of the empirical distributions of the momenta of single particles, for consecutive time intervals. Fig. 2.4 shows, as expected, that thermometer (2.44) is able to reach (and measure) the temperature of the system. In the left panel we show a case in which the initial temperature of $\mathcal{S}$ is negative, while in the right one the system starts from a positive β. In both cases the temperature measured by the thermometer quickly reaches that of $\mathcal{S}$ and fluctuates around it, with an amplitude which is expected to depend on $N_{\mathcal{T}}$ and on the time-window chosen for the measure of β.

The above results show that equilibrium negative temperature are meaningful also in the sense of Thermodynamics. A class of mechanical systems has been shown to exist such that the thermodynamic temperature Θ is well-defined, i.e. it is possible to design a suitable model of thermometer which can be used to measure it unambiguously. In the light of the above, the claim that negative-temperature states should be regarded as out-of-equilibrium (see e.g. Ref. [177]) appears inconsistent, in our opinion, with the usual definition of thermal equilibrium.

2.4 Negative temperature in absence of ensemble equivalence

Long-range interacting systems are an open research field in Statistical Mechanics, both for their practical interest and for the conceptual issues related to the non-additivity of thermodynamic potentials. It is well known, for example, that

microcanonical and canonical ensemble can be inequivalent if the internal energy of a system is not additive, and the usual results of Statistical Mechanics cannot be straightforwardly applied [32].

In this Section we study a simple Hamiltonian model with bounded kinetic terms and a mean-field potential. We will show that the equivalence of microcanonical and canonical ensemble fails; the energy regime in which the two statistical descriptions are not equivalent is characterized by negative temperature. This analysis is useful to show the non-trivial phenomenology that can be encountered, also for systems living in bounded phase spaces, when long-range interactions are involved. In particular it provides a striking example in which NATs cannot be trivially mapped into corresponding equilibrium states at positive temperature with specular properties. The results presented in this Section are discussed in Ref. [135].

2.4.1 Long-range interactions and ensemble inequivalence

It is a known fact that in physical systems with long-range interactions the equivalence of statistical ensembles can fail [50, 32]. This happens when equilibrium states described by the microcanonical p.d.f. exist, which do not correspond to any state described by the canonical one: in other words, the average of a macroscopic observable can give different results, at the same temperature T, if the system is isolated or closed. This phenomenon can be observed in a large variety of physical contexts including self-gravitating systems, perfect fluids in two dimensions and spin models with mean field interactions [145, 124, 123, 43, 44, 155, 84].

For long-range interacting systems, inequivalence of statistical ensembles is due to the lack of additivity of the total energy E, which can result in a change of concavity for the entropy $S(E)$ (i.e., negative specific heat): since the Legendre-Fenchel transform that relates the free energy $F(T)$ to $S(E)$ is not invertible in this case, there is no one-to-one correspondence between the microcanonical and the canonical description [182, 146]. In particular, it can be shown that the caloric curve T vs E in the canonical ensemble can be obtained from the microcanonical analogue through the Maxwell construction, i.e. by replacing the free energy with its convex envelope. The situation is somehow reminiscent of that arising in van der Waals equation for non ideal gases, obtained by a mean field approach, where the pressure is a non-monotonic function of the volume: Maxwell construction was indeed introduced in this context, in order to describe the coexistence of two different phases in the "unphysical" region at negative compressibility [125, 85].

In the following, we check the validity of the above scenario for Hamiltonian systems with bounded kinetic terms, belonging to the class introduced in Section 2.2. Let us remark that systems with ensemble inequivalence and negative temperature can be found, for instance, in the context of plasma physics. In Ref. [176] a guiding-center model for a plasma in a cylindric domain is studied; it is shown that the system is equivalent to a two-dimensional point vortices system, and equilibrium solutions for the corresponding mean-field Vlasov equation are studied. In a high-energy range, corresponding to a negative temperature regime, statistical ensembles are shown to be non-equivalent. Rigorous results on the Statistical Mechanics of point vortices in bounded domains have been proven [105, 28, 29], relating the inequivalence of statistical ensembles to the non-uniqueness of the solution, at high

energy and for some kind of bounded domains in two dimensions, of the mean-field equation describing the system. Recently, the problem of equivalence of statistical ensembles for systems of point vortices on a spherical surface has been also addressed [106].

2.4.2 A mean-field model with bounded kinetic terms

Let us consider a Hamiltonian system of the form (2.26) consisting of N degrees of freedom described by conjugated coordinates $\{p_i, q_i\}$, $i = 1, ..., N$. The generalized positions are, also in this case, angular variables. The total Hamiltonian reads:

$$H(\mathbf{p}, \mathbf{q}) = \sum_{i=1}^{N} (1 - \cos p_i) - N v(m) \tag{2.45a}$$

$$v(m) = \frac{J}{2} m^2 + \frac{K}{4} m^4 + \text{const.} \tag{2.45b}$$

where m is the modulus of the "magnetization" vector defined as

$$\mathbf{m}(\mathbf{q}) \equiv \frac{1}{N} \left(\sum_{i=1}^{N} \cos q_i \, , \sum_{i=1}^{N} \sin q_i \right) . \tag{2.46}$$

J and K are parameters that can assume, in general, both positive and negative values; the additive constant in Eq. (2.45b) is actually unessential for the dynamics: in the following we will choose it in such a way that the minimal energy achievable by the system is zero.

The potential term defined by Eq. (2.45b) is the one that characterize the so-called "Generalized Hamiltonian Mean Field" (GHMF) model [27] describing the mean field interactions between magnetized rotators. The GHMF is an extended version of the Hamiltonian Mean Field model [5] that includes also a quartic dependence on the magnetization; among other interesting properties, this system is paradigmatic for the study of inequivalence between canonical ad microcanonical ensembles and has been extensively studied in past years [22, 32, 11]. Let us note that the bounded phase space and the long-range interactions are two features that our model shares with two dimensional vortex systems in bounded domains [144, 176, 128].

Hamiltonian H depends on the angular positions through the magnetization modulus m, which is maximal ($m = 1$) when all the rotators are parallel and vanishes if their angular positions are homogeneously distributed in $[-\pi, \pi)$; the N factor in front of the potential is needed in order to ensure the extensivity of the system (Kac's prescription). Let us stress that for the system (2.45a) it is possible to write down an analytical computation of the equilibrium properties using large deviation approaches [146]: the procedure is quite similar to the one presented in Ref. [32], and it is explicitly carried out in Appendix 2.C.

2.4.3 Negative specific heat at negative temperature

Molecular dynamics simulations have been performed in order to study the functional dependence of the inverse temperature β on the energy E of the system.

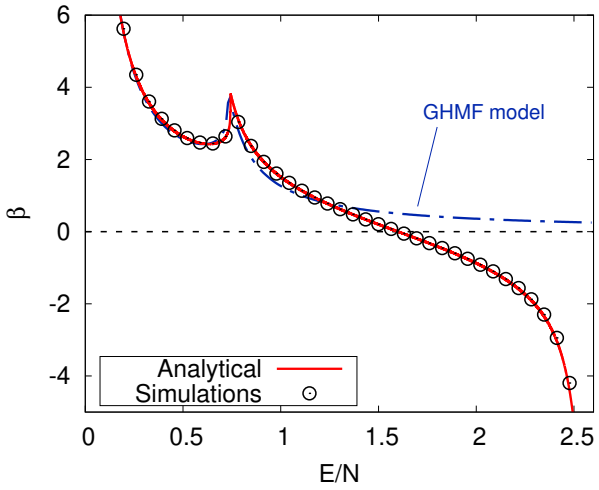

Figure 2.5. Equilibrium caloric curve $\beta(E/N)$ for model (2.45a) with $J = 0.5$, $K = 1.4$. Analytical prediction (red solid line) and results of molecular dynamics simulations (black circles) are shown. Parameters: $N = 1000$, $\Delta t = 0.25$, $\mathcal{T} = 10^8$. The caloric curve of the GHMF model with the same parameters (dash-dotted blue curve) is shown for comparison. Figure from Ref. [135].

We used a second-order symplectic Velocity Verlet-like integrator (see Section 5.1), choosing the integration step Δt so as to observe total-energy relative fluctuations $\Delta E/E \simeq O(10^{-5})$. Since we are interested in equilibrium properties, the total integration time $\mathcal{T}$ has always been chosen to be much longer than the typical characteristic times of the system. In order to fix initial conditions with the desired value of the total energy, some care has to be devoted to the fact that our kinetic terms are bounded; first, one has to choose the angular positions in such a way that $0 < E - Nv(m) < 2N$, e.g. by repeated uniform extractions over a suitable interval; once the above constraint is satisfied, momenta can be randomly extracted in such a way that the sum of the kinetic terms amounts to the residual energy. We also include a small external potential $v_{ext}(\mathbf{q}) = \cos(q_1)$, acting only on the first particle, in order to break the angular symmetry of the magnetization $\mathbf{m}$. All interesting observables are computed as temporal averages:

$$\langle A(\mathbf{X}) \rangle \simeq \frac{1}{\mathcal{T}} \int_0^{\mathcal{T}} A(\mathbf{X}(t)) dt \,. \tag{2.47}$$

In particular, we can measure the observable defined by Eq. (2.34), and infer β by inverting such relation.

In Fig. 2.5 we show the theoretical caloric curve $\beta(E/N)$ for a choice of J and K that leads to inequivalence of statistical ensembles (namely, to the existence of microcanonical equilibrium states with negative specific heat which have no canonical counterpart). In this case both J and K are positive, so that the interacting potential has a minimum for $m = 1$ ("ferromagnetic" limit).

Let us notice that the values of β measured in numerical simulations through the observable (2.34) show a very good agreement with the analytical prediction.

The figure also shows the difference between the system we are considering and

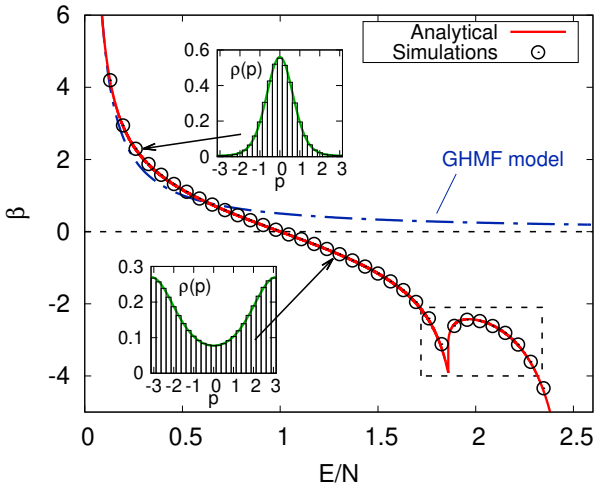

Figure 2.6. Equilibrium caloric curve for model (2.45a) with the same parameters of Fig. 2.5, but $J = -0.5$, $K = -1.4$. Insets: single-particle momentum distributions corresponding to the two cases pointed by the arrows; green solid lines represent best fits for the equilibrium p.d.f. (2.17). The fragment of the curve in the dashed rectangle is the same shown in Fig. 2.7. Figure from Ref. [135].

the corresponding GHMF model with the same parameters. At low energies the behavior of the two systems is quite similar, due to the fact that the kinetic terms are equal up to order $O(p_i^3)$ when energies are small. The scenario changes for large values of E/N: in this case, the "bounded phase-space" version of the GHMF model can reach equilibrium states with $\beta \equiv dS/dE < 0$, while the original GHMF model behaves like an ideal gas whose (positive) β asymptotically tends to zero (infinite temperature).

Fig. 2.6 shows a different example, in which both J and K are chosen to be negative; in this case $v(m)$ is minimum at $m = 0$ ("antiferromagnetic" limit). As it can be seen in the figure, in a certain energy range, negative microcanonical specific heat and negative values of β coexist – meaning that microcanonical and canonical ensembles are inequivalent for some negative temperatures. The microcanonical specific heat of the corresponding GHMF model is, instead, always positive, and the statistical ensembles are always equivalent. In the insets of Fig. 2.6 we also show the single-particle momentum distribution in a couple of cases (one at positive and one at negative β): the empirical distribution and the analytical expression for the p.d.f. given by Eq. (2.17) are in excellent agreement.

Let us now focus on the energy range in which statistical ensembles are inequivalent in this case. Fig. 2.7 shows the detail of this region. In panel (a), the microcanonical caloric curve is compared to the results of numerical simulations. The dashed line is the Maxwell's construction, which individuates the transition temperature $1/\beta^*$ in the canonical ensemble [182]: all the microcanonical equilibrium states with energies corresponding to the Maxwell's construction (red circles in the figure) are metastable or unstable [32] and have no equivalent counterpart in the canonical ensemble. The microcanonical caloric curve also shows a first order phase transition, which can be understood by looking at panel (b): the systems

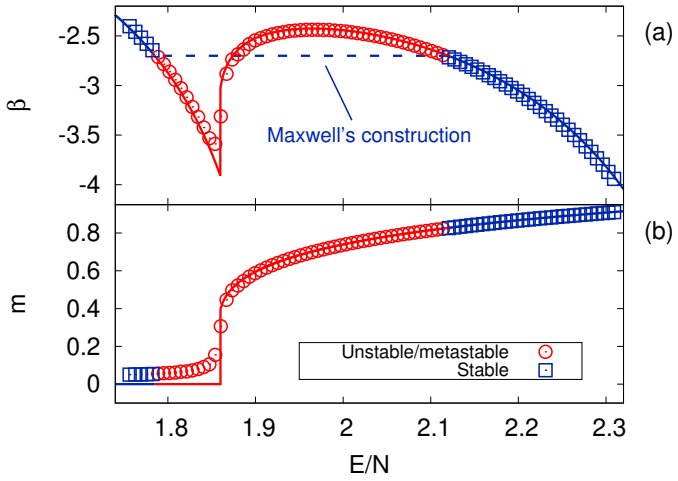

Figure 2.7. Thermodynamic behavior around the transition. Panel (a): segment of the caloric curve shown in Fig. 2.6. Blue squares represent stable equilibrium states for which ensemble equivalence holds; red circles stand for unstable or metastable microcanonical states with no canonical counterpart. The dashed blue line is the Maxwell's construction. Panel (b): the modulus m of the magnetization of the system is shown in the same conditions of panel (a). Solid lines represent, in both cases, the theoretical prediction. Figure from Ref. [135].

goes from a regime with $m = 0$ to a magnetized phase with $m > 0$.

2.4.4 Checking ensemble inequivalence

Ensemble inequivalence can be checked through numerical simulations. The idea is to prepare the system at a certain inverse temperature β and to compare the equilibrium properties that are obtained

1. by a symplectic deterministic integrator which preserves the energy of the system;

2. by a stochastic simulation which mimics the presence of a thermal reservoir at a fixed temperature β, allowing for energy fluctuations.

The integration method used in the first case is the same used before, and detailed in Section 5.1. The latter is based on a different approach, i.e. it simulates a Langevin dynamics at temperature β. The possibility to define proper Langevin equations also for negative values of β is discussed in the next Chapter. The details of the integration algorithm are presented in Section 5.2. We fix the diffusivity constant D that appears in the generalized Langevin Equation (5.10) in such a way that $1/|\beta|D$, the typical time-scale of the stochastic dynamics, is comparable to the characteristic times of the system.

Of course the first strategy is expected to reproduce the statistical properties described by the microcanonical ensemble; the second one corresponds instead to the canonical ensemble at inverse temperature β.

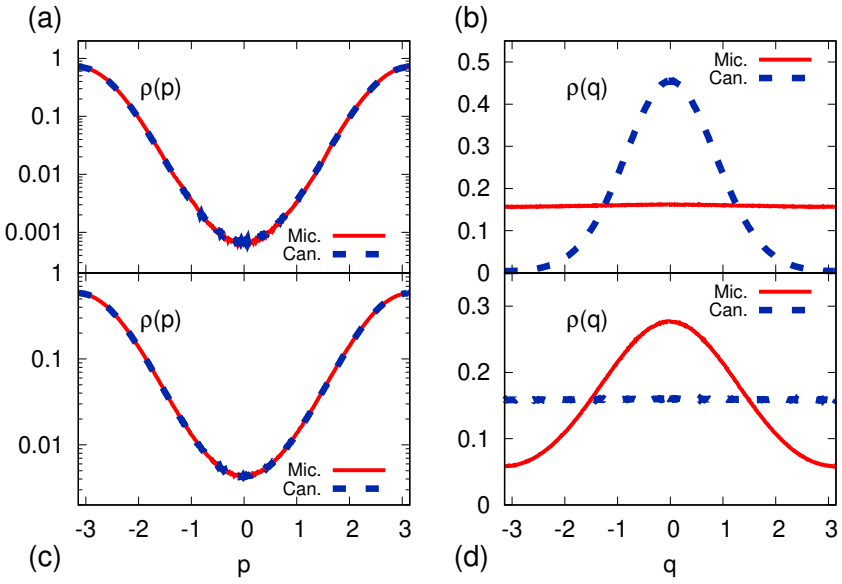

Figure 2.8. Showing ensemble inequivalence in the antiferromagnetic case $J = -0.5$, $K = -1.4$. (a) Distribution of the single-particle momentum in the microcanonical ensemble (solid red curve) and the corresponding canonical one (dashed blue curve) for $E/N = 1.84$. (b) Distribution of the single-particle position, in the same conditions of panel (a). (c-d) Same as (a-b), but for $E/N = 1.94$. Parameters: $N = 1000$, $\mathcal{T}_0 = 10^7$, $\mathcal{T}_1 = 2.5 \cdot 10^6$, $D = 0.02$. Figure from Ref. [135].

We start from an initial condition whose energy corresponds to an unstable microcanonical state, and we let the system evolve through a molecular dynamics simulation for a long time $\mathcal{T}_0$. So far the system is isolated, and we can measure the inverse temperature β of the corresponding microcanonical state by studying the above discussed observable. The final configuration is then taken as the initial condition for the two different evolution protocols described above: we run two independent simulations for an additional time $\mathcal{T}_1$, and we measure mechanical observables at equilibrium in these conditions. Of course the energy of the system is conserved in the first case, while in the stochastic simulation we fix the value of β to be the same observed during the first part of the evolution.

The results of our simulations are shown in Fig.2.8 for two choices of the initial energy that lead to unstable microcanonical states, namely $E/N = 1.84$ (panels (a) and (b)) and $E/N = 1.94$ (panels (c) and (d)). In the left part of the figure, the single-particle momentum distributions, microcanonical and canonical, are displayed: in both cases the plots are almost identical, meaning that our simulation protocol is able to mimic a canonical ensemble with the same temperature of the starting isolated state. On the right panels we show the corresponding distributions for the angular positions, from which we observe a striking difference between the two physical situations.

Panel (b) clearly shows that the zero-magnetization state which is attained in the microcanonical ensemble for $E/N = 1.84$ is lost when the constraint on the energy is

relaxed: if we only fix the temperature, i.e. if we reproduce the situation described by a canonical ensemble, the system eventually moves to a stable state at higher energy, with finite magnetization. Conversely, in panel (c) we show that starting from an unstable magnetized state, if we only fix the temperature, the system will end up in a zero-magnetization state. This is a clear evidence of ensemble inequivalence.

The fact that such inequivalence appears at negative temperature signals, as it is also evident from the caloric curve in Fig. 2.6, that the properties of the microcanonical entropy in the NAT branch are qualitatively different from those in the low-energy regime. Let us just notice that this is a striking example in which the high-energy properties of the model cannot be inferred from the low-energy regime by exploiting simple symmetry relations: in order to get a full understanding of the model at high energy, the introduction of negative temperature is mandatory. This observation is somehow significant, since among many physicists there is a diffuse feeling that NAT states are always "specular" to the positive-temperature ones, so that the introduction of the negative-temperature formalism is a cumbersome way to obtain results that could be deduced with simpler approaches. While this is true for some simple spin systems [1, 30], there is no general rule in this sense, as the present case clearly shows.

Appendix to Chapter 2

2.A Derivation of Eq. (2.33)

Here we derive the caloric curve for model (2.26) with potential (2.32). For the sake of clarity, we consider the case $m_j = 1\ \forall j$.

First we compute the canonical partition function

$$\begin{aligned} Z_N(\beta) &= \int d\mathbf{p}\, d\mathbf{q}\, e^{-\beta \mathcal{H}(\mathbf{p},\mathbf{q})} \\ &= \int d\mathbf{p}\, e^{-\beta \sum_i [1-\cos p_i]} \int d\mathbf{q}\, e^{-\beta \sum_i [1-\cos(q_i - q_{i+1})]} \\ &= e^{N[\ln 2 - \beta(1+K)]} \left\{ \frac{I_0(\beta) I_0(K\beta)}{4\pi^2} \right\}^N \end{aligned} \tag{2.48}$$

where we have introduced the modified Bessel functions of the first kind,

$$I_n(x) = \frac{1}{2\pi} \int_{-\pi}^{\pi} d\theta e^{x\cos\theta} \cos(n\theta)\,. \tag{2.49}$$

The free energy per particle reads

$$f(\beta) = -\lim_{N\to\infty} \frac{1}{\beta N} \ln Z_N(\beta) = 1 + K - \frac{1}{\beta} \ln \left[\frac{I_0(\beta) I_0(\beta K)}{8\pi^2} \right], \tag{2.50}$$

and we can infer a relation between the specific energy ε and the inverse temperature as

$$\varepsilon = \frac{d(\beta f)}{d\beta}\,, \tag{2.51}$$

from which we straightforwardly obtain Eq. (2.33).

2.B Statistical properties of model (2.39)

In this Appendix we study the statistical properties of model (2.39). The simultaneous presence of a long-range term (which can be written as a mean-field interaction) and a short-range potential can be treated by using the transfer operator strategy that has been discussed in Ref. [33] in a similar context.

As a preliminary step, let us notice that the "long-range" interaction term of the Hamiltonian can be also written as

$$\begin{aligned}\frac{J}{2N_{\mathcal{S}}}\sum_{i,j=1}^{N_{\mathcal{S}}}(1-\cos(Q_i-Q_j)) = \\ = \frac{JN_{\mathcal{S}}}{2}\left[1-\left(\frac{1}{N_{\mathcal{S}}}\sum_{i=1}^{N_{\mathcal{S}}}\cos Q_i\right)^2-\left(\frac{1}{N_{\mathcal{S}}}\sum_{i=1}^{N_{\mathcal{S}}}\sin Q_i\right)^2\right].\end{aligned} \tag{2.52}$$

Taking into account the above consideration, $Z(\beta,N)$ can be factorized into two terms:

- a kinetic part, i.e.

$$Z_K(\beta,N)=\int_{-\pi}^{\pi}dp_1...dp_N\exp\left[-\beta\sum_{i=1}^{N}(1-\cos p_i)\right]; \tag{2.53}$$

- a configurational one, i.e.

$$\begin{aligned}Z_C(\beta,N) =& e^{-\beta JN/2}\int_{-\pi}^{\pi}dQ_1...dQ_N\exp\left[\frac{\beta J}{2N}\left(\sum_{i=1}^{N}\cos Q_i\right)^2+\frac{\beta J}{2N}\left(\sum_{i=1}^{N}\sin Q_i\right)^2\right] \\ &\times\exp\left[-\beta K\sum_{i=0}^{N}(1-\cos(Q_{i+1}-Q_i))\right].\end{aligned} \tag{2.54}$$

The kinetic contribution to $f(\beta)$ can be easily computed from (2.53) in terms of the modified Bessel functions of the first kind (see Eq. (2.49)); one gets

$$-\beta f_K(\beta)\equiv\lim_{N\to\infty}\frac{1}{N}\log Z_K=-\beta+\log\left(2\pi I_0(\beta)\right).$$

The strategy to determine $Z_C\beta,N$ has been outlined in Ref. [33], where a model with a similar interacting potential has been extensively studied. The result for $\beta>0$ is

$$\begin{aligned}-\beta f_C(\beta)\equiv&\lim_{N\to\infty}\frac{1}{N}\log Z_C \\ =&-\beta K-\beta\frac{J}{2}-\min_{m\geq 0}\left(\frac{m^2}{2\beta J}-\log[\lambda(m,K\beta)]\right)\end{aligned} \tag{2.55}$$

where $\lambda(z,\alpha)$ is the maximum eigenvalue of the symmetric integral operator

$$(\mathcal{T}_{z,\alpha}\psi)(Q)=\int_{-\pi}^{\pi}dQ'\exp\left[\frac{1}{2}z(\cos Q+\cos Q')+\alpha\cos(Q-Q')\right]\psi(Q'). \tag{2.56}$$

In the following we will explicitly derive the case $\beta<0$, with the same strategy which has been used in Ref. [33] for $\beta>0$.

From Eq. (2.54), by mean of a standard Hubbard-Stratonovich transformation, we get

$$\begin{aligned} Z_C(\beta,N) &= \frac{Ne^{-\beta JN/2}}{2\pi|\beta|J}\int d\rho_x d\rho_y \exp\left[-\frac{N}{2|\beta|J}(\rho_x^2+\rho_y^2)-N\beta K\right]\times \\ &\times\int_{-\pi}^{\pi} dQ_1...dQ_N \exp\left[i\sum_{j=1}^{N}(\rho_x\cos Q_j+\rho_y\sin Q_j)+\beta K\sum_{j=1}^{N}\cos(Q_{j+1}-Q_j)\right]= \\ &= \frac{Ne^{-\beta JN/2}}{2\pi|\beta|J}\int_0^{\infty} d\rho\int_{-\pi}^{\pi} d\phi\,\rho\exp\left[-N\frac{\rho^2}{2|\beta|J}-N\beta K\right]\times \\ &\times\int_{-\pi}^{\pi} dQ_1...dQ_N \exp\left[i\rho\sum_{j=1}^{N}\cos(Q_j-\phi)+\beta K\sum_{j=1}^{N}\cos(Q_{j+1}-Q_j)\right], \end{aligned} \tag{2.57}$$

where we have introduced "polar" coordinates for the plane (ρ_x,ρ_y). Now we shift all the integration variables $\{Q_j\}$ by an angle ϕ, then we can rewrite the last term in a symmetric fashion and recover the functional form of the integral operator $\mathcal{T}$ introduced above, so that

$$\begin{aligned} Z_C(\beta,N) &= \frac{Ne^{-\beta JN/2}}{2|\beta|J}\int_0^{\infty} d\rho^2\,\exp\left[-N\frac{\rho^2}{2|\beta|J}-N\beta K\right]Tr\left[\mathcal{T}_{i\rho,\beta K}^N\right] \\ &\simeq \frac{Ne^{-\beta JN/2}}{2|\beta|J}\int_0^{\infty} d\rho^2\,\exp\left[-N\frac{\rho^2}{2|\beta|J}-N\beta K+N\log[\lambda(i\rho,K\beta)]\right] \end{aligned} \tag{2.58}$$

(reminding $Q_1\equiv Q_{N+1}$). The last equality holds in the thermodynamic limit, $N\gg 1$. Note that since $\mathcal{T}_{i\rho,\beta K}$ is not an Hermitian operator, its eigenvalues will be in general complex numbers: therefore $\lambda(z,\alpha)$ has to be defined, in this case, as the eigenvalue with the maximum modulus. Finally, one can use steepest-descent method to reduce the calculation of the integral to a minimization problem, that can be solved numerically.

2.C Study of model (2.45a)

In this Appendix we sketch the strategy we have employed to determine the equilibrium properties of model (2.45a). The problem can be addressed by mean of the methods of large-deviations theory, which turn out to be particularly useful in presence of mean-field interactions [182]. Our argument follows quite closely the usual derivation that can be done for the GHMF model (see, e.g. [32]), with an ad-hoc handling of the non-quadratic "kinetic" terms.

Let us just recall that large deviation approaches can be exploited to study the thermodynamic behavior of a Hamiltonian system of N particles (described by the state $\mathbf{X}=(\mathbf{p},\mathbf{q})$) if it is possible to write the total Hamiltonian as

$$H(\mathbf{X})=\bar{H}(\mu_1(\mathbf{X}),...,\mu_n(\mathbf{X}))\,, \tag{2.59}$$

where $\mu_j(\mathbf{X})=\sum_{i=1}^{N} g_j(q_i,p_i)/N$, $j=1,...,n$ are $n\ll N$ mean quantities, for a suitable choice of $\bar{H}$.

In such a case the following relation holds:

$$S(E) = \ln \int \prod_j d\bar{\mu}_j \delta(\bar{H}(\bar{\mu}_1, ..., \bar{\mu}_n) - E) \exp[N\bar{s}(\bar{\mu}_1, ..., \bar{\mu}_n)] \tag{2.60}$$

where $\bar{s}$ is the so-called "entropy of macrostates":

$$\bar{s}(\bar{\mu}_1, ..., \bar{\mu}_n) = \frac{1}{N} \ln \int_\Omega d\mathbf{X} \delta(\mu_j(\mathbf{X}) - \bar{\mu}_j) \,. \tag{2.61}$$

Furthermore, large deviation theory ensures that the entropy of macrostates can be computed, in the $N \gg 1$ limit, as

$$\bar{s} = \inf_{\lambda_1,...,\lambda_n} \left\{ \sum_j \lambda_j \bar{\mu}_j + \frac{\ln Z(\lambda_1, ..., \lambda_n)}{N} \right\} \tag{2.62}$$

with

$$Z(\lambda_1, ..., \lambda_n) = \int_\Omega e^{-N \sum_j \lambda_j \mu_j(\mathbf{X})} d\mathbf{X} \,. \tag{2.63}$$

In the present case, defining

$$\kappa = \frac{1}{N} \sum_{i=1}^{N} (1 - \cos(p_i)) \tag{2.64}$$

we can write Eq. (2.45a) (apart from unessential constants) as

$$\frac{H}{N} = \kappa - \frac{J}{2}(m_x^2 + m_y^2) - \frac{K}{4}(m_x^4 + 2m_x^2 m_y^2 + m_y^4) \tag{2.65}$$

where m_x and m_y are the components of the magnetization vector $\mathbf{m}$ (see Eq. (2.46)). The entropy of macrostates is equal to:

$$\begin{aligned} \bar{s} &= \inf_{\lambda_\kappa} \{\kappa\lambda_\kappa - \lambda_\kappa + \ln I_0(\lambda_\kappa) + \ln(4\pi^2)\} + \\ &\quad + \inf_{\lambda_x, \lambda_y} \{\lambda_x m_x + \lambda_y m_y + \ln I_0\left(\sqrt{\lambda_x^2 + \lambda_y^2}\right)\} \\ &= (\kappa - 1) B_{inv}(1 - \kappa) + \ln I_0(B_{inv}(1 - \kappa)) + \\ &\quad + \ln(4\pi^2) - m B_{inv}(m) + \ln I_0(B_{inv}(m)) \end{aligned} \tag{2.66}$$

where $I_n(x)$ is the n-th modified Bessel function of the first kind (see Eq. (2.49)) and $B_{inv}(x)$ is the inverse function of $I_1(x)/I_0(x)$. Let us notice that $\bar{s}$ depends actually only on κ and $m = \sqrt{m_x^2 + m_y^2}$. Now we can evaluate the microcanonical entropy $S(E)$ by using its relation with $\bar{s}(\kappa, m)$. The r.h.s. of Eq. (2.60) in the $N \gg 1$ limit can be estimated through a constrained extremal problem, namely as the supremum of $\bar{s}(\kappa, m)$ with the condition

$$\bar{H}(\kappa, m_x, m_y) = E \,. \tag{2.67}$$

It can be shown that such problem is fulfilled by the value $\tilde{m}$ of the magnetization that verifies the following condition:

$$B_{inv}(\tilde{m}) = (J\tilde{m} + K\tilde{m}^3) B_{inv}\left(1 - \frac{E}{N} - \frac{J}{2}\tilde{m}^2 - \frac{K}{4}\tilde{m}^4\right) . \tag{2.68}$$

Once $\tilde{m}$ is known (Eq. (2.68) can be solved by numerical methods) the corresponding value of κ can be found from Eq. (2.67) and we finally get

$$S(E) = N\bar{s}(\tilde{\kappa}, \tilde{m})\,. \tag{2.69}$$

In a similar way we can derive the free energy of the system:

$$F(\beta) = \inf_{\kappa,m} \left\{ H(\kappa, m) - \frac{N}{\beta}\bar{s}(\kappa, m) \right\}\,. \tag{2.70}$$

Chapter 3

Langevin Equation (also) at negative temperature

In this Chapter we face the problem of describing the coarse-grained dynamics of systems with generalized kinetic energy via effective stochastic equations. Our aim is to understand whether it is possible to define a Langevin Equation (LE) also for systems with non-quadratic kinetic energy, and in particular for the Hamiltonian models introduced in the previous Chapter. We will see that stochastic coarse-grained descriptions of the dynamics hold also when negative temperatures are involved, and we will comment on the physical meaning of this finding.

In addition, this kind of study allows to clarify some aspects of NAT states, providing, in particular, a possible answer to the question about the physical meaning of a thermal bath at negative temperature, recurrent in the literature. On the other hand, the ability of a modified LE to reproduce the action of a thermal reservoir with generalized kinetic energy turns out to be quite useful in numerical simulations on this kind of systems, as discussed in Section 5.2.

The results presented in this Chapter are discussed in Ref. [12] and Ref. [15].

3.1 Generalizing the Langevin Equation

In his celebrated paper about Brownian motion, Langevin addressed the problem of properly describing the irregular behavior of pollen particles suspended in water [114]. Following Einstein [54], he assumed that both the colloidal particle and the molecules of the fluid could be modeled as material points with masses M and $m \ll M$ respectively. The irregular motion of the heavy particle is due to the collisions with the molecules of the liquid, which are assumed to be uncorrelated. To account for the discontinuous action of the hitting molecules, Langevin relied upon the introduction of a stochastic term in the evolution equation of the colloid, namely a white Gaussian noise $\boldsymbol{\xi}(t) = (\xi_1(t), \xi_2(t), \xi_3(t))$ such that

$$\begin{aligned} \langle \xi_i(t) \rangle &= 0 \\ \langle \xi_i(t) \xi_j(t') \rangle &= \delta(t - t') \delta_{ij} \,. \end{aligned} \tag{3.1}$$

He supposed that the impulsive force acting on the colloid was proportional to this noisy function $\boldsymbol{\xi}$. On the other hand, he argued that the interaction with

the fluid resulted into an average damping force exerted on the colloidal particle, proportional to its velocity (Stokes law). The combination of the above effects leads to the celebrated Langevin Equation (LE)

$$\dot{\mathbf{P}} = -\gamma \mathbf{P} + \sqrt{2\gamma k_B T}\boldsymbol{\xi} \tag{3.2}$$

which characterizes the evolution of the momentum $\mathbf{P} = M\dot{\mathbf{Q}}$ of the heavy colloid ($\mathbf{Q}$ being its position in the three-dimensional space). Here γ is the friction term due to the interaction of the colloidal particle with the fluid, while T is the temperature and k_B is the Boltzmann constant. The noise amplitude is determined by the Einstein assumption that the interested particle is at thermal equilibrium with the fluid, so that equipartition theorem holds and

$$\langle P^2/M \rangle = 3k_B T\,. \tag{3.3}$$

Eq. (3.2) clearly shows that Brownian motion is the result of the competing actions of a damping force and a thermal noise. It seems reasonable that such mechanism should hold, under appropriate modifications, also for Hamiltonian systems with non-standard, generalized forms of the kinetic energy $\mathcal{K}(P)$, and in particular for the systems with bounded kinetic terms discussed in Section 2.2. In these cases there is no reason for the damping force to be proportional to the momentum, since the Equipartition Theorem does not hold, as discussed in Section 2.2.2. In particular, in what follow we will be interested to the possibility of deriving Langevin Equations also for systems at negative absolute temperature.

3.1.1 Generalized masses

As it will be discussed in the following, a necessary (but not sufficient) condition for the dynamics of a particle to be described by some coarse-grained Langevin-type equation is that a time-scale separation occurs between the dynamics of the observed degree of freedom and the decorrelation times of the thermal bath. A natural way to achieve such time-scale separation in systems with non-standard kinetic terms is to introduce a parameter which tunes the inertia of each degree of freedom, a "generalized mass". Then we can take the limit in which this parameter is much larger for the observed particle than for the others.

Such mass term should satisfy the following, reasonable additivity condition. Let us call $k(p, m)$ the functional form of the kinetic energy, which is assumed to fulfill all conditions detailed in Section 2.1. Let us consider n identical particles of mass m moving with the same momentum; suppose that they are stuck together, in such a way that they form a new particle with mass nm and momentum np. We require that the kinetic energy of this new particle, which is equal to $nk(p, m)$, can be expressed as $k(np, nm)$.

It is easy to verify that this condition is satisfied by any kinetic energy of the form

$$k(p, m) = mf\left(\frac{p}{m}\right)\,, \tag{3.4}$$

where $f(x)$ is a regular function which satisfies the conditions detailed in Section 2.1. Indeed, the total kinetic energy of the n particles is given by

$$nk(p,m) = nmf\left(\frac{p}{m}\right) = nmf\left(\frac{np}{nm}\right) = k(np,nm)\,, \tag{3.5}$$

i.e. it is equal to the kinetic energy of a single particle with mass and momentum n times larger.

The classical Newtonian kinetic energy is written in the form 3.4, with $f(x) = x^2/2$. Similarly, the relativistic kinetic energy in special relativity can be reconduced to such functional dependence, choosing $f(x) = \sqrt{x^2c^2 + c^4}$, where c is the velocity of light in vacuum. In the following we will always consider examples in which the functional dependence on the masses is described by Eq. (3.4).

3.1.2 A Smoluchowski-like approach

Once the dependence of the kinetic terms on the generalized masses has been established, one can try to generalize classical approaches to derive effective equations similar to Eq. (3.2). In this Section we will make a first attempt based on a generalization of the strategy proposed by Smoluchowski in his famous paper about Brownian motion [194, 40]. The idea is to consider a system composed by a heavy particle and many light molecules, which interact only through elastic collisions; we can compute the average momentum that the heavy particle exchanges in a small time interval, assuming to be in an equilibrium condition. In this way one has an explicit expression for the drift term.

Let us write the total Hamiltonian of a one-dimensional system as

$$\mathcal{H}(P,Q,\mathbf{p},\mathbf{q}) = Mk(P/M) + \sum_i mk(p_i/m) + \mathcal{U}(Q,\{q_i\})\,, \tag{3.6}$$

where the kinetic terms have been already written in the form (3.4) and all properties required in Section 2.1 are assumed to hold. Let us also require that $k'(x)$ is invertible, as it happens in the "Newtonian" case $k(x) = x^2/2$. In the above Hamiltonian (P,Q) are the coordinates of the slow degree of freedom, characterized by a mass M, while (p_i,q_i) represent the i-th light molecule, with mass $m \ll M$. The interacting potential $\mathcal{U}$ accounts for the collisions between the heavy particle and the light molecules:

$$\mathcal{U}(Q,\mathbf{q}) = \sum_i u(|Q-q_i|)\,, \tag{3.7}$$

where the function $u(x)$, defined on the positive axis, is differentiable, decays to zero within some finite range σ and verifies $lim_{x\to 0}u(x) = \infty$.

First, let us consider the case in which a small molecule collides with the large particle when the latter has zero velocity. During the collision both total energy and momentum are conserved. As a consequence, in the limit of infinite M, if the heavy particle is fixed, the momentum p of the light molecule changes its sign. In this case the exchanged momentum is given by $\Delta = 2p$: this is analogous to what happens in classical Mechanics, and it is a consequence of the assumed symmetries of the kinetic terms. If we consider the case in which M is large but finite, and the heavy particle is allowed to move with a small but non-zero velocity, we can expect

that $\Delta = 2p + \varepsilon$, where $|\varepsilon| \ll |p|$. The energy conservation before and after the collision implies

$$mk\left(\frac{p}{m}\right) - mk\left(\frac{-p-\varepsilon}{m}\right) = Mk\left(\frac{P+2p+\varepsilon}{M}\right) - Mk\left(\frac{P}{M}\right). \tag{3.8}$$

Exploiting $|\varepsilon| \ll |p| \ll |P|$ and the symmetries of $k(x)$, the above equation can be expanded to obtain

$$-\varepsilon k'\left(\frac{p}{m}\right) \simeq 2pk'\left(\frac{P}{M}\right), \tag{3.9}$$

whence

$$\Delta \simeq 2p(1 - V/v) \tag{3.10}$$

where $V = \dot{Q} = k'(P/M)$ and $v = \dot{q} = k'(p/m)$ are the velocities of the two considered particles.

Eq (3.10) can be used to derive an expression for the average drift of the momentum P of the slow particle, conditioned to its initial value. Following Smoluchowski, the average variation of P in an infinitesimal time interval can be written as

$$\left\langle \frac{dP}{dt}\Big| P \right\rangle \simeq \int_{-\infty}^{\infty} dv\, f(v)\rho|v - V|\Delta(v, V) \tag{3.11}$$

where $f(v)$ is the equilibrium distribution of the velocities for the light particles and ρ is their spatial density, supposed homogeneous. Indeed, the number of particles with velocity v which collide with the heavy one in a time interval dt is, on average, $f(v)\rho|v - V|dt$; multiplying by the corresponding contribute to the exchanged momentum and integrating over all possible values of v gives the total drift.

We can change the integration variable into $g = v - V$; then we make an expansion assuming the limit in which V is very small compared to v and we finally obtain

$$\left\langle \frac{dP}{dt}\Big| P \right\rangle \simeq -4V\rho \int_{-\infty}^{\infty} dg f(g)|\tilde{p}(g)| \tag{3.12}$$

where $\tilde{p}(x)$ is the inverse function of $k'(x/m)$. The above equation shows that it is possible to write the average drift as the product of V, the velocity of the slow particle, and a term only depending on the properties of the bath.

The above generalization of the Smoluchowski approach gives an explicit expression for the Stokes force also in cases with non-quadratic kinetic terms. However, in our derivation we used the fact that $k'(x)$ is a invertible function, an hypothesis that is not verified, for instance, by models belonging to the class discussed in Section 2.2. Moreover, the assumption of elastic collisions is not compatible, in general, with systems at negative temperature, i.e. those we are actually interested in: in a $\beta < 0$ equilibrium condition, it can be expected qualitatively that the particles tend to maximize the total energy by sticking together, so that the picture described above cannot be applied.

3.1.3 A stochastic argument

In order to obtain a suitable generalization of the LE for the systems with the bounded kinetic terms introduced in Section 2.2 we cannot always rely on the

Smoluchowski approach discussed before. An alternative strategy is based on the assumption that the action of the bath can be described as a systematic part and a delta-correlated noise independent of the value of P.

Let us consider the general case of a Hamiltonian system

$$\mathcal{H}(P, \mathbf{p}, Q, \mathbf{q}) = \mathcal{K}(P) + \sum_i \tilde{\mathcal{K}}(p_i) + \mathcal{U}(Q) + \mathcal{V}(Q, \mathbf{q}) \tag{3.13}$$

where (P, Q) are the canonical coordinates of a "slow" degree of freedom, while (p_i, q_i) represent the generalized momenta and positions of particles with a much faster dynamics. In a system with the usual quadratic kinetic energy, Q could represent the position of a particle with a mass much higher than the others; as discussed in Section 3.1.1, this notion can be generalized to other forms of $\mathcal{K}(P)$.

We can interpret $\mathcal{U}(Q)$ as the external potential which the slow particle is subjected to, while $\mathcal{V}(Q, \{q_i\})$ takes into account the interactions occurring among different degrees of freedom. For the sake of simplicity we consider here only Hamiltonian systems in one dimension, but all the results could be straightforwardly generalized to the multi-dimensional case. Let us also stress that in what follows we will limit our analysis to Hamiltonians of the form (3.13), in which the kinetic energy is the sum of single-particle contributions only depending on the momentum.

The Hamilton equations describing the motion of the slow degree of freedom read:

$$\begin{cases} \dot{Q} = \partial_P \mathcal{K}(P) \\ \dot{P} = -\partial_Q \mathcal{U}(Q) - \partial_Q \mathcal{V}(Q, \{q_i\}) \end{cases} \tag{3.14}$$

At this stage we introduce the hypothesis that the dynamics of the slow particle can be approximated by an effective, memoryless stochastic equation of the form

$$\begin{cases} \dot{Q} = \partial_P \mathcal{K}(P) \\ \dot{P} = -\partial_Q \mathcal{U}(Q) + \Gamma(P) + \sqrt{2D}\xi(t)\,. \end{cases} \tag{3.15}$$

Here the term $\Gamma(P)$ can be seen as a generalization of the Stokes force, while D is a constant which determines the amplitude of the noise. In this way we are ignoring the details of the interactions between the slow and the fast degrees of freedom. We are implicitly assuming that the dynamics of the slow process is Markovian on the considered time scale: let us notice that this assumption is not a direct consequence of the time-scale separation between the typical characteristic times of the dynamics of Q and of those of q_i, which however is a necessary condition. Furthermore, we are assuming that the amplitude of the noise term, $\sqrt{2D}$, does not depend on the momentum (i.e., we are only considering non-multiplicative processes).

The possibility to perform such averaging procedure on rigorous mathematical grounds is a non-trivial, largely studied problem in the field of dynamical systems [71, 107]: the above approximation should be therefore viewed as an ansatz, whose validity needs to be checked *a posteriori*. The results that are discussed in the following are expected to hold only in physical situations in which the above hypotheses are verified.

We aim at finding some kind of generalized Einstein relation between the constant D and $\Gamma(P)$. Let us introduce the steady probability density $f(Q, P)$ (to

be determined) of the considered degree of freedom, and the corresponding steady probability currents:

$$\begin{cases} J_Q(Q,P) = f(Q,P)\partial_P \mathcal{K}(P) \\ J_P(Q,P) = -f(Q,P)\partial_Q \mathcal{U}(Q,P) + \Gamma(P) f(Q,P) - D\partial_P f(Q,P)\,. \end{cases} \tag{3.16}$$

In terms of the above quantities, the Fokker-Planck equation corresponding to Eq. (3.15) reads:

$$\partial_Q J_Q(Q,P) + \partial_P J_P(Q,P) = 0\,. \tag{3.17}$$

We assume now that the system is in thermal equilibrium (which is the same hypothesis done by Einstein and Langevin when applying the equipartition theorem (3.3)). We require therefore that detailed balance is satisfied, i.e. that the irreversible part of J_P vanishes, so that

$$\Gamma(P) f(Q,P) - D\partial_P f(Q,P) = 0\,. \tag{3.18}$$

Exploiting the factorization of the equilibrium distribution $f(Q,P) = f_Q(Q) f_P(P)$, and the form of the momentum-dependent term,

$$f_P(P) \propto e^{-\beta \mathcal{K}(P)}\,, \tag{3.19}$$

one easily finds from Eq. (3.18):

$$\Gamma(P) = -D\beta\partial_P \mathcal{K}(P) = -\gamma \dot{Q}\,. \tag{3.20}$$

The last equation states that, if the hypotheses discussed above are satisfied, the Stokes law is proportional to (minus) the velocity $\dot{Q} = \partial_P \mathcal{K}(P)$, no matter what the form of the kinetic energy is. Furthermore, the ratio γ between such generalized viscous force and the velocity of the particle is fixed by

$$\gamma = D\beta\,. \tag{3.21}$$

This last equation can be seen as a generalization of the Einstein relation to cases with non-quadratic kinetic energy.

A couple of observations are in order. First, let us notice that in the usual, Newtonian case $\mathcal{K}(P) = P^2/2M$, the Einstein relation is recovered, as it should. Second, in the above discussion we never assumed that the parameter β had to be positive. We can expect that for systems with bounded kinetic terms as those discussed in Section 2.2, which admit negative temperature, relation (3.21) holds also at $\beta < 0$.

3.2 LE at negative temperature: case with "mechanical" baths

In the previous Section we addressed the problem of deriving a proper Langevin equation for the slow degree of freedom in Hamiltonian systems described by Eq. (3.13), where the kinetic term can assume a non-quadratic form. We deduced a generalized

version for the Einstein relation (3.21), which is expected to hold also at negative temperature, since in our derivations we never assumed $\beta > 0$ explicitly. Now we want to verify such result by numerically simulating Hamiltonian systems which can model the interaction between a slow degree of freedom and a thermal bath.

The possibility to model thermal baths through mechanical systems, in suitable limits, is well known. In the 60's several papers showed that the motion of a single, heavy particle inside a chain of many harmonic oscillators with mass m could be rigorously described by a Brownian motion, in the limit $M/m \gg 1$ (where M is the mass of the heavy particle) [162, 186, 180, 131, 59]. These results were generalized by Zwanzig, who could extend such rigorous approach to nonlinear systems coupled to baths of harmonic oscillators [200].

If the kinetic terms are not quadratic, the results just mentioned cannot be rigorously proven; however, it is reasonable to expect that in systems composed by one heavy particle and many light molecules, in the sense discussed in Section 3.1.1, a qualitatively similar situation appears. We can simulate the dynamics of such kind of system and study the behavior of the slow degree of freedom, in order to verify, *a posteriori*, whether the generalization of the LE discussed in the previous Section applies. In particular, we will consider a case in which also negative temperature can be achieved. The methodology that will be used in this Section is discussed in some detail in Section 5.3, where it is applied to an exactly solvable case as those mentioned above and some technical and conceptual issues are discussed.

3.2.1 A preliminary example

As a preliminary example, let us consider the mechanical system described by the following Hamiltonian:

$$\mathcal{H}(P,\mathbf{p},Q,\mathbf{q}) = \frac{P^4}{4M^3} + \sum_{i=\pm 1,\dots,\pm N} \frac{p_i^4}{4m_i^3} + \frac{k}{2}\sum_{i=-N}^{N+1}(q_i - q_{i-1})^2, \qquad q_{-N-1} \equiv q_{N+1} \equiv 0\,, \tag{3.22}$$

i.e. a chain of $2N+1$ generalized oscillators with quartic kinetic terms. All oscillators have generalized mass m, apart from the central one (characterized by momentum P and position $Q \equiv q_0$), whose inertia is given by some $M \gg m$; the kinetic terms depend on the masses in the way identified by Eq. (3.4).

Our aim is to show that the generalized Einstein relation (3.21) holds in this case with non-standard kinetic terms. To this end, we perform molecular dynamics simulations of the whole system (3.22) and we measure P, the momentum of the heavy particle. Assuming that the dynamics of P can be approximated by a Markov process, it must be described by a LE of the form

$$\dot{P} = F(P) + \sqrt{2D(P)}\xi \tag{3.23}$$

where ξ is a white Gaussian noise with unitary variance. If this is the case, we should be able to infer the functional form of $F(P)$ and $D(P)$ from the study of the conditioned moments

$$A(P_0,\Delta t) = \left\langle \frac{P(t+\Delta t) - P(t)}{\Delta t} \middle| P(t) = P_0 \right\rangle \tag{3.24}$$

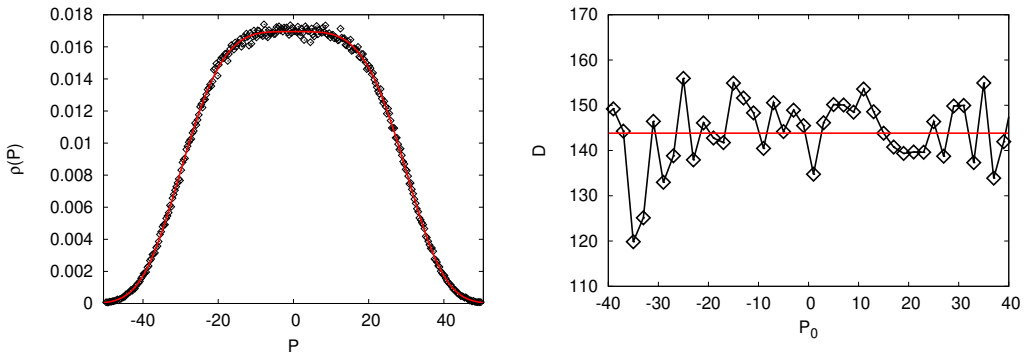

Figure 3.1. Effective behavior of the slow particle in model (3.22). Left panel shows the p.d.f. of P, measured in simulations. The solid red line is the best fit with the expected functional dependence, Eq (3.26), which gives a value of the parameter β close to 0.446. The right panel shows the result of the numerical analysis detailed in Section 5.3 to infer the diffusivity $D(P_0) = \lim_{\Delta t \to 0} B(P_0, \Delta t)$, where B is defined in Eq. (3.25). The solid red line is a constant fit. Black lines are guides for the eyes. Parameters: $M = 50$, $k = 2500$, $2N = 2000$.

and

$$B(P_0, \Delta t) = \left\langle \frac{[P(t+\Delta t) - P(t)]^2}{2\Delta t} \Big| P(t) = P_0 \right\rangle \tag{3.25}$$

respectively, in the limit of $\Delta t \to 0$ [65, 63]. The procedure we use to reconstruct numerically the coefficients of the Langevin equation is detailed in Section 5.3, as well as the range of applicability of this method and possible practical issues related to its usage.

We have to verify that the hypotheses discussed in Section 3.1.3 are fulfilled. First, we need to check that the action of the bath (represented here by the chain of particles with mass m) maintains the heavy particle at equilibrium at some inverse temperature β; then, assuming that the process is Markovian, we measure the amplitude of the noise induced on such particle through formula (3.25), taking the limit $\Delta t \to 0$, and we verify that it does not depend on P (i.e., the noise is additive). Such checks are shown in Fig. 3.1. The left panel of the figure shows the histogram of P during the simulation; this distribution can be fitted through the equilibrium Boltzmann p.d.f.

$$\rho(P) = \frac{e^{-\beta P^4/4M^3}}{\int_{-\infty}^{\infty} dP\, e^{-\beta P^4/4M^3}} = \frac{\sqrt{2}\beta^{1/4} e^{-\beta P^4/4M^3}}{\Gamma(1/4) M^{3/4}} \tag{3.26}$$

in order to achieve the value of β. Here $\Gamma(x)$ is the Euler Gamma function. The right panel shows the diffusivity as a function of the momentum. No clear trend appears with our analysis, and it seems reasonable that a model in which D it is independent of P should catch the essential features of the dynamics. If this is the case, the hypotheses for the derivation presented in Section 3.1.3 are satisfied, and Eq. (3.20) should be verified.

This is indeed what we find with the analysis shown in Fig. 3.2. Here we compare the results of our procedure to reconstruct the drift term from data with the

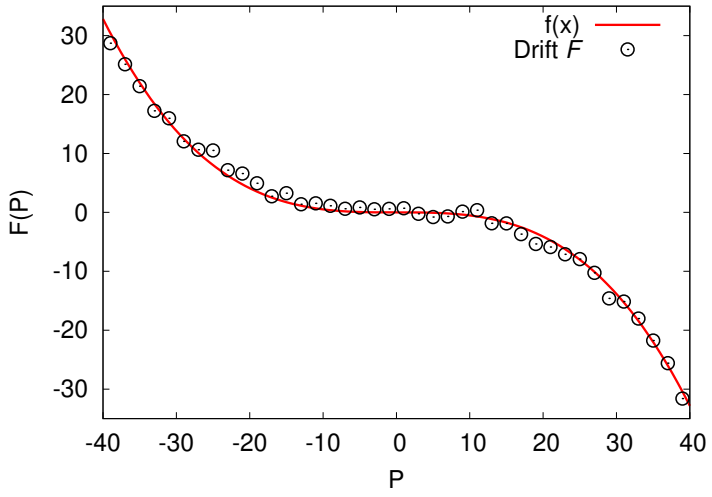

Figure 3.2. Drift term $F(P)$ for the coarse-grained dynamics of the heavy particle in model (3.22), in the same conditions of Fig. 3.1. Circles represent the results of the numerical analysis detailed in Section 5.3, i.e. the limit $\lim_{\Delta t \to 0} A(P, \Delta t)$. The solid red line is determined by Eq. (3.20), where the parameters are inferred from the analysis shown in Fig. 3.1 (no fitting).

expected curve

$$F(P) = -\beta D (P/M)^3 \,, \tag{3.27}$$

where β and D are those inferred in Fig. 3.1. The agreement is very good, meaning that, provided that a thermal bath satisfies some reasonable requirements, a precise relation between the viscous term and the diffusivity can be established, also for systems with non-quadratic kinetic energy.

3.2.2 A "mechanical" bath with bounded kinetic terms

In order to test the possibility of a LE at negative temperature, in this Section we study a model of generalized oscillators of the form (3.13), characterized by the kinetic energy introduced in Section 2.2. This deterministic model can be investigated through molecular dynamics simulations. In the spirit of the data-driven analysis already applied in Section 3.2.1, we use long-time series of data for the momentum P of the slow particle to infer numerically the terms of the LE which approximates its dynamics to the best extent. We can then verify that Eq. (3.21) holds, both for positive and negative values of β.

Also in this case we want to study the effective motion of a "heavy" oscillator subjected to the action of a thermal bath of "light" particles. In the following, we will model the bath as a chain of N generalized oscillators with equal masses m:

$$\mathcal{H}_{chain}(\mathbf{p}, \mathbf{q}) = \sum_{i=1}^{N} m \left[1 - \cos\left(\frac{p_i}{m} \right) \right] + \epsilon \sum_{i=1}^{N+1} \left[1 - \cos(q_i - q_{i-1}) \right] \tag{3.28}$$

where (p_i, q_i) is the $i-$th pair of canonical coordinates, and $q_{N+1} \equiv q_0 \equiv 0$. The kinetic energy is modeled on the one introduced in Section 2.2, and we have set

$c = 1$. A constant parameter ϵ tunes the intensity of the mutual interaction between neighbor particles. Let us notice that the kinetic terms depend on the masses in the way prescribed by Eq. (3.4). Of course this system can assume both positive and negative temperature, depending on its internal energy, as discussed in Section 2.1.

We couple the above chain to a slow degree of freedom (P, Q) with mass $M \gg m$ and the same form of the kinetic term. The total Hamiltonian reads

$$\mathcal{H}(P, Q, \mathbf{p}, \mathbf{q}) = \mathcal{H}_{chain} + M[1 - \cos(P/M)] + k \sum_{i=1}^{\lfloor N/n \rfloor} [1 - \cos(Q - q_{i \cdot n})] , \quad (3.29)$$

where n is an integer parameter in the range $1 \ll n \ll N$ and $\lfloor x \rfloor$ represents the integer part of x. In other words, the heavy particle is only coupled to those oscillators whose label is an integer multiple of n.

One could wonder if it is necessary to deal with this kind of coupling, instead of simply replacing the central particle of chain (3.28) with an heavier intruder, as in the case discussed in Section 3.2.1; the reason for this choice is twofold. First, since interaction terms are now bounded, heat exchange between the various parts of the chain is much slower: a more "connected" geometry surely enhances the thermalization process, and the system is expected to reach equilibrium at the temperature of the reservoir on relatively fast time scales. Secondly, it is reasonable that the composition of several interactions with different particles of the system will result in an uncorrelated noise for the heavy particle; the thermal noise is then expected to be memoryless, as required for the argument discussed in Section 3.1 to be valid.

3.2.3 An effective Langevin equation for both positive and negative temperature

The Hamiltonian chain (3.28) represents a "deterministic" bath. The total system (3.29) can be simulated through the usual generalized Verlet algorithm discussed in Section 5.1. We measure the trajectory of the observable P, then we apply the strategy already used in Section 3.2.1 and detailed in Section 5.3: we assume as working hypothesis that in the limit $M/m \gg 1$ and $N \gg 1$, the variable P can be described by a Langevin equation with the shape

$$\dot{P} = F(P) + \sqrt{2D}\xi \quad (3.30)$$

where ξ is a white noise such that $\langle \xi(t)\xi(t') \rangle = \delta(t - t')$; then we compute the conditioned moments (3.24) and (3.25), and take the limit $\Delta t \to 0$.

The results of such extrapolation procedure are shown in Fig. 3.3, where we consider two different values of the total energy of the system, corresponding to two different β with opposite sign. In both cases, D is quite constant with respect to the momentum, therefore equation (3.20) is expected to apply; indeed, $F(P)$ seems to match quite well our phenomenological prediction

$$F(P) = -\beta D \sin(P/M) . \quad (3.31)$$

Let us notice that relation (3.21) holds both at positive and at negative temperature. In particular, as it is clear from the figure, passing from positive to negative β the proportionality factor between $F(P)$ and $\partial_P \mathcal{K}(P)$ changes its sign.

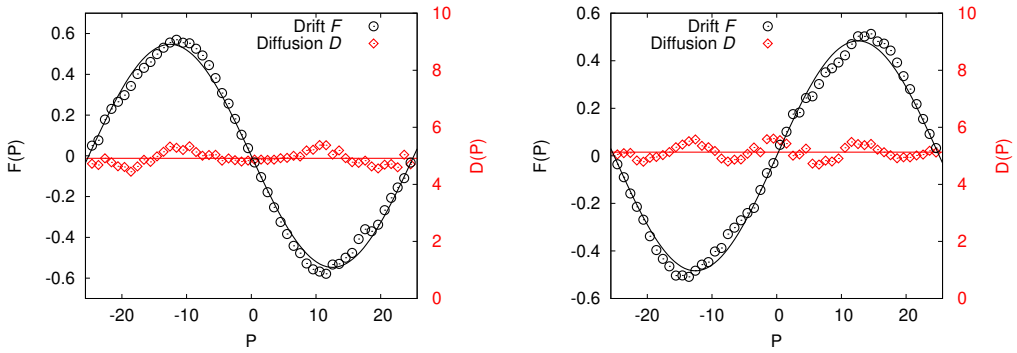

Figure 3.3. Drift and diffusivity evaluated with the discussed data-driven approach (points) and corresponding fits (solid lines). Left: $\beta \simeq +0.11$. Right: $\beta \simeq -0.10$. Drift terms are fitted with sinusoidal functions, diffusivities with constant values. Parameters of the simulations: $M = 8$, $m = 1$, $k = 0.5$, $N = 600$, $n = 15$. Figure from Ref. [12].

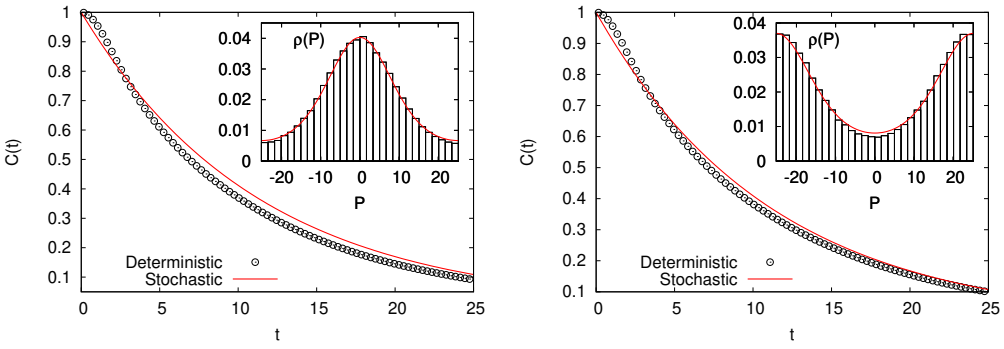

Figure 3.4. Autocorrelation functions of the velocity in the original dynamics (circles) and in the coarse-grained model (solid lines) at $\beta = 0.11$ (left) and $\beta = -0.10$ (right). In the insets, probability density functions of P in the two cases, both for the original dynamics (boxes) and for the reconstructed model (solid lines). Figure from Ref. [12].

Of course there is a natural pragmatic way to verify the goodness of the effective stochastic equation provided by the above approach: we can compare the behavior of some observable in the original dynamics and in the coarse-grained one. To this end, we simulate the stochastic process (3.30) with the reconstructed parameters by using a standard stochastic integration algorithm (see Ref. [127] for details).

In Fig. 3.4 we show the velocity autocorrelation functions of the original dynamics and those that are obtained through a stochastic simulation of the LE. The similarity between the two curves is a good indicator that the reconstructed coarse-grained dynamics actually catches the relevant features of the slow particle's evolution, including the typical time-scales. Similarly, the stationary p.d.f. of P obtained by a stochastic simulation of the LE is compared to its histogram in the original, compete deterministic dynamics, and the agreement is very good also in this case.

3.2.4 Some remarks

If the generalized Einstein relation (3.21) holds for $\beta < 0$, it means that $F(P)$, in such regime, must be positive when $P > 0$ and negative when $P < 0$, contrary to what happens at positive temperature. In other words, the Stokes force gives energy to the particle, instead of subtracting it. At first sight this behavior may appear very unphysical. However, one has to remember that systems with $\beta < 0$ are characterized by an entropy which decreases when the energy increases; random fluctuations due to thermal noise are expected to increase the entropy of the considered system, so that their average effect is to subtract heat from it. In order to maintain thermal equilibrium, the viscous term must compensate this loss, by providing energy to the system.

A similar situation arises in the context of bi-dimensional hydrodynamics. Several studies have shown that also in that case the effective dynamics of a single vortex can be described by a stochastic equation which respects a generalized Einstein relation [46, 45, 197, 197]; since the statistical properties of two-dimensional vortices can be described by models which admits negative temperature states (as briefly discussed in Section 1.1.1), it is not surprising that such relation holds true also for $\beta < 0$. The physical interpretation is on the lines of that sketched above [197]

The fact that it is possible to write down a Langevin-like equation with $\beta < 0$, which properly reproduces the behavior of a slow degree of freedom subjected to the action of a bath, sounds quite relevant in the context of the long-lasting debate about negative temperatures, briefly accounted for in Section 1.2. On the one hand, we stress that the above results can be only understood in terms of negative β: if the alternative thermostatistical description based on S_G is adopted, the straightforward extension of the Einstein relation (3.21) to cases with bounded kinetic terms cannot be done. On the other hand, the above results show that it is possible to design thermal baths at negative temperature, so that the notion of thermal equilibrium at some negative temperature seems completely justified.

Finally, let us note that the LE described in this section can be used to mimic the action of a thermal bath in stochastic simulations, i.e. it provides a practical way to simulate the canonical ensemble. In Section 5.2 an example of algorithm based on this finding is developed.

3.3 LE at negative temperature: case with spin baths

The reasoning in Section 3.1 provides a general relation between D and γ, but it is not sufficient to determine γ (or D) from the knowledge of the Hamiltonian. When the nature of the bath is specified, one may try perturbative methods in the limit of large scale separation to derive the parameters of the effective equation. In the following we consider an analytically tractable case, where the thermal bath is constituted by a large number of Ising spins kept at a fixed temperature (which can be both positive or negative) by a stochastic dynamics. The "slow" degree of freedom is an oscillator characterized by the generalized kinetic energy discussed before. All spins feel a magnetic field which depends on the position of the oscillator: if the typical frequency of the oscillator is much slower than the rate of the stochastic dynamics, a Chapman-Engsok expansion of the Fokker-Planck equation of the particle

can be performed. This analysis shows that Eq. (3.21) is verified also in this case, but now the diffusivity explicitly depends on the position of the oscillator.

The results presented in this Section are discussed in Ref. [15]. A fruitful collaboration with Prof. Antonio Prados, who elaborated the analytical approach sketched in the following, is acknowledged.

3.3.1 A spin bath with a stochastic dynamics

We consider the following Hamiltonian for a slow particle with canonical coordinates (P, Q) coupled to a thermal bath composed of N Ising spins $\boldsymbol{\sigma} \equiv (\sigma_1, \sigma_2, ..., \sigma_N)$:

$$\mathcal{H}(P, Q, \boldsymbol{\sigma}) = \mathcal{K}(P) + \mathcal{U}(Q) - \mu\lambda(Q) \sum_{j=1}^{N} \sigma_j \,. \tag{3.32}$$

The particular form of the kinetic energy $\mathcal{K}(P)$ is not important to the analytical derivation we will discuss in this Section, so we will not specify it for the moment; $\mathcal{U}(Q)$ is the external potential felt by the particle, while the last term rules the interaction with the spins. In the case discussed here, the particle interacts with the bath through the total magnetization of the spins $\sum_{j=1}^{N} \sigma_j$; each spin σ_j can assume only the values $+1$ or -1. They feel an external field $\mu\lambda(Q)$, where parameter μ is a constant which scales like $O(N^{-1/2})$, while $\lambda(Q)$ is a function of the oscillator's position only. Let us stress that this kind of models have some relevance in the biophysical context, in which the spins are employed to model some internal degrees of freedom of macromolecules [21, 20, 166].

The dynamics of the oscillator is determined by the usual Hamilton equations. The spin bath experiences instead a stochastic evolution which keeps it at a fixed equilibrium temperature, the widely used Glauber dynamics [72]. The basic idea is that each spin changes its sign with a rate depending on the inverse temperature β and on the external field, in such a way that the conditioned equilibrium distribution

$$\mathcal{P}(\sigma_j = \pm 1 | Q) = \frac{e^{\pm\beta\mu\lambda(Q)}}{2\cosh[\beta\mu\lambda(Q)]} = \frac{1}{2}\{1 \pm \tanh[\beta\lambda(Q)]\} \tag{3.33}$$

is achieved. Due to the particular form of the Hamiltonian, each spin evolves independently of the others, once the position Q of the oscillator is given.

We denote by R_j the operator that flips the j-th spin, leaving the remainder unchanged. Starting from the generic spin configuration $\boldsymbol{\sigma}$, the rate of transition to the configuration $\boldsymbol{\sigma}'_j = R_j\boldsymbol{\sigma}$, in which the j-th spin has been flipped, is given by

$$\omega(\boldsymbol{\sigma} \to \boldsymbol{\sigma}'_j | Q) = \frac{\alpha}{2}\{1 + \sigma_j \tanh[\beta\lambda(Q)]\} \,, \tag{3.34}$$

where α is a parameter which fixes the overall velocity of the process with respect to the typical time scales of the oscillator's dynamics. In the following we will adopt the compact notation

$$W_j(\boldsymbol{\sigma}|Q) \equiv \omega(\boldsymbol{\sigma} \to \boldsymbol{\sigma}'_j | Q) \,. \tag{3.35}$$

Let us notice that the detailed balance (at fixed Q) is automatically satisfied, since

$$\mathcal{P}(\boldsymbol{\sigma}|Q) W_j(\boldsymbol{\sigma}|Q) = \mathcal{P}(\boldsymbol{\sigma}'_j|Q) W_j(\boldsymbol{\sigma}'_j|Q) \tag{3.36}$$

by construction.

We can write a Liouville-master equation for the time evolution of the joint p.d.f. $\mathcal{P}(Q,P,\boldsymbol{\sigma},t)$:

$$\sum_{j=1}^{N}(R_j-1)W_j(\boldsymbol{\sigma}|Q)\mathcal{P}(Q,P,\boldsymbol{\sigma},t) = \\ = \left[\partial_t + \mathcal{K}'(P)\partial_x + \left(-\mathcal{U}'(Q)+\mu\lambda'(Q)\sum_i \sigma_i\right)\partial_p\right]\mathcal{P}(Q,P,\boldsymbol{\sigma},t)\,. \tag{3.37}$$

In the limit $\alpha \to 0$ (infinitely slow Glauber dynamics), the l.h.s. vanishes and the above relation reduces to the usual, "collisionless" Liouville evolution equation for the p.d.f. of the canonical coordinates of an Hamiltonian particle.

If, instead, α is finite, there is a net probability current due to the evolution of the spins,

$$\sum_j \mathcal{P}(Q,P,\boldsymbol{\sigma}'_j,t)W_j(\boldsymbol{\sigma}'_j|Q) - \mathcal{P}(Q,P,\boldsymbol{\sigma},t)\sum_j W_j(\boldsymbol{\sigma}|Q)\,, \tag{3.38}$$

which is exactly the l.h.s. of Eq. (3.37).

3.3.2 Analytical derivation of the LE

We will study Eq. (3.37) with the aim of deriving an effective LE for the slow degree of freedom, averaging over the effect of the spin bath. First, we derive an equation for the marginal probability $f(Q,P,t)$ for the particle variables,

$$f(Q,P,t) = \sum_{\boldsymbol{\sigma}} \mathcal{P}(Q,P,\boldsymbol{\sigma},t)\,, \tag{3.39}$$

valid when the spins are much faster than the particle. Then we obtain a Fokker-Planck equation for f, whence we can deduce the LE we are searching for [65].

The strategy that we will follow is based on the Chapman-Enskog method [42], originally introduced to derive the hydrodynamic equations of a gas from the Boltzmann equation. The idea is to expand the dynamical equation for the p.d.f. in powers of some small parameter ε. In our case, since we are interested in the $\alpha \gg 1$ limit (i.e., spins much faster than the oscillator), a reasonable choice is given by

$$\varepsilon = \alpha^{-1}\,. \tag{3.40}$$

In this way we will be able to find the first terms of the expansion for the drift and the diffusivity of the LE.

The canonical distribution

$$\mathcal{P}_{eq}(Q,P,\boldsymbol{\sigma}) = \frac{1}{\mathcal{Z}}e^{-\beta\mathcal{H}(Q,P,\boldsymbol{\sigma})}\,, \tag{3.41}$$

where $\mathcal{Z}$ is the partition function, is a time-independent solution of the dynamical equation (3.37) (see Refs.[21, 200] for a proof of an H-theorem for this kind of system, specifically for quadratic $\mathcal{K}(P)$, $\mathcal{U}(Q)$ and linear $\lambda(Q)$, although these particular shapes are not required in the proof). Since the spins are fast, they will be

close to equilibrium at all times. This time-scale separation allows us to introduce the following expansion for the solution of Eq. (3.37),

$$\mathcal{P}(Q,P,\boldsymbol{\sigma},t) = \mathcal{P}^{eq}(\boldsymbol{\sigma}|Q)f(Q,P,t) + \sum_{l=1}^{\infty} \varepsilon^l \mathcal{P}^{(l)}(Q,P,\boldsymbol{\sigma},t)\,, \tag{3.42}$$

where the conditioned equilibrium distribution for the spins is given by

$$\mathcal{P}^{eq}(\boldsymbol{\sigma}|Q) = \frac{e^{\beta\mu\lambda(Q)\sum_j \sigma_j}}{2^N\{\cosh(\beta\mu\lambda(Q))]\}^N} \tag{3.43}$$

and we assume that

$$\sum_{\boldsymbol{\sigma}} \mathcal{P}^{(l)}(Q,P,\boldsymbol{\sigma},t) = 0\,, \quad \forall l \geq 1\,. \tag{3.44}$$

Let us notice that if assumption (3.44) is fulfilled, $f(Q,P,t)$ is the exact marginal distribution of the particle. Then we can expand the dynamical equation for $f(Q,P,t)$, following the Chapman-Enskog approach, as

$$\partial_t f = \sum_{l=0}^{\infty} \varepsilon^l F^{(l)}(Q,P,t)\,. \tag{3.45}$$

Now we insert the above expressions for $\mathcal{P}(Q,P,\boldsymbol{\sigma},t)$ and $\partial_t f$ into Eq. (3.37), we consider each order of the ε expansion separately and, after some calculations, we find the following equations:

$$\varepsilon^0 : \quad \hat{W}\mathcal{P}^{eq}(\boldsymbol{\sigma}|Q)f(Q,P,t) = 0 \tag{3.46a}$$

$$\varepsilon^1 : \quad \hat{W}\mathcal{P}^{(1)}(Q,P,\boldsymbol{\sigma},t) = \mathcal{P}^{eq}(\boldsymbol{\sigma}|Q)F^{(0)} + \\ + \left[K'(P)\partial_Q + \left(-V'(Q) + \mu\lambda'(Q)\sum_{i=1}^{N}\sigma_i\right)\partial_P\right]\mathcal{P}^{eq}(\boldsymbol{\sigma}|Q)f(Q,P,t) \tag{3.46b}$$

$$\varepsilon^2 : \quad \hat{W}\mathcal{P}^{(2)}(Q,P,\boldsymbol{\sigma},t) = \mathcal{P}^{eq}(\boldsymbol{\sigma}|Q)F^{(1)} + \partial_t\mathcal{P}^{(1)}(Q,P,\boldsymbol{\sigma},t) + \\ + \left[K'(P)\partial_Q + \left(-V'(Q) + \mu\lambda'(Q)\sum_{i=1}^{N}\sigma_i\right)\partial_P\right]\mathcal{P}^{(1)}(Q,P,\boldsymbol{\sigma},t)\,. \tag{3.46c}$$

In the above equations we introduced the operator

$$\hat{W} = \frac{1}{\alpha}\sum_{j=1}^{N}(R_j - 1)W_j(\boldsymbol{\sigma}|Q)\,, \tag{3.47}$$

characterized in Appendix 3.A. Note that, with this definition, the matrix elements of $\hat{W}$ do not scale with α (or ε). One can exploit the mathematical properties of $\hat{W}$ to solve Eq. (3.46): a sketch of the solution is presented in Appendix 3.B. Eq. (3.46a) is always verified, due to detailed balance. Eq. (3.46b), first order in ε, gives

$$\begin{aligned} F^{(0)} &= -\mathcal{K}'(P)\partial_Q f + \{\mathcal{U}'(Q) - \mu\lambda'(Q)N\tanh[\beta\mu\lambda'(Q)]\}\,\partial_P f \\ &\simeq -\mathcal{K}'(P)\partial_Q f + \left\{\mathcal{U}'(Q) - \tilde{\mu}^2\beta\lambda(Q)\lambda'(Q)\right\}\partial_P f \end{aligned} \tag{3.48}$$

in the thermodynamic limit, where we have introduced the rescaled coupling constant

$$\tilde{\mu} = N^{1/2}\mu\,, \tag{3.49}$$

which is of order 1 due to the original assumption on the scaling of μ. The $O(\varepsilon^2)$ equation leads to

$$F^{(1)} = \left(\tilde{\mu}\lambda'(x)\right)^2 \partial_p \left(\beta K'(p) f + \partial_p f\right)\,. \tag{3.50}$$

Taking into account the above expressions for $F^{(0)}$ and $F^{(1)}$, we can truncate Eq. (3.45) to the first order in ε. We obtain the following Fokker-Planck equation for f:

$$\partial_t f = -\boldsymbol{\nabla}\cdot(\mathbf{A}f) + \frac{1}{2}\boldsymbol{\nabla}\cdot(\boldsymbol{\nabla}\cdot \mathrm{B}f) \tag{3.51}$$

where $\boldsymbol{\nabla} = (\partial_Q, \partial_P)$ and

$$\mathbf{A} = \begin{pmatrix} \mathcal{K}'(P) \\ -\mathcal{U}_R'(Q) - \beta\mathcal{K}'(P)D(Q) \end{pmatrix} \qquad \mathrm{B} = \begin{pmatrix} 0 & 0 \\ 0 & 2D(Q) \end{pmatrix}\,. \tag{3.52}$$

In the above equations, $\mathcal{U}_R$ is the "renormalized" potential

$$\mathcal{U}_R = \mathcal{U} - \frac{\beta}{2}\tilde{\mu}^2\lambda^2(x)\,, \tag{3.53}$$

which reduces to the original potential when $\tilde{\mu} \to 0$, i.e. when the interaction with the spin bath is negligible. The additional term, which comes from the coupling with the reservoir, results in a systematic force acting on the oscillator. The quantity $D(Q)$, i.e. the diffusivity of the dynamics of P, has the form

$$D(Q) = \varepsilon\tilde{\mu}^2[\lambda'(Q)]^2\,. \tag{3.54}$$

Let us notice that $D(Q)$ is always positive, as it should.

The LE for $\boldsymbol{\Gamma} = (Q, P)$ can be straightforwardly obtained from the corresponding Fokker-Planck equation (3.51):

$$\partial_t\boldsymbol{\Gamma} = \mathcal{A} + \mathrm{B}\boldsymbol{\xi} \tag{3.55}$$

where $\boldsymbol{\xi} = (\xi_1, \xi_2)$ is a two-dimensional delta-correlated Gaussian noise verifying $\langle\xi_i\rangle = 0$ and $\langle\xi_i(t)\xi_j(t')\rangle = \delta_{ij}\delta(t-t')$.

3.3.3 Numerical simulations

In order to check the consistency of the previous theoretical approach, we perform numerical simulations of the complete dynamics (3.37) in the $\alpha \gg 1$ limit (fast spins): our aim is to compare the actual values of significant observables to those predicted by the coarse-grained description provided by the Fokker-Planck equation (3.51) (or, equivalently, by the LE (3.55)). Specifically, we consider a case in which the kinetic energy of the slow oscillator is given by

$$\mathcal{K}(P) = 1 - \cos P\,, \tag{3.56}$$

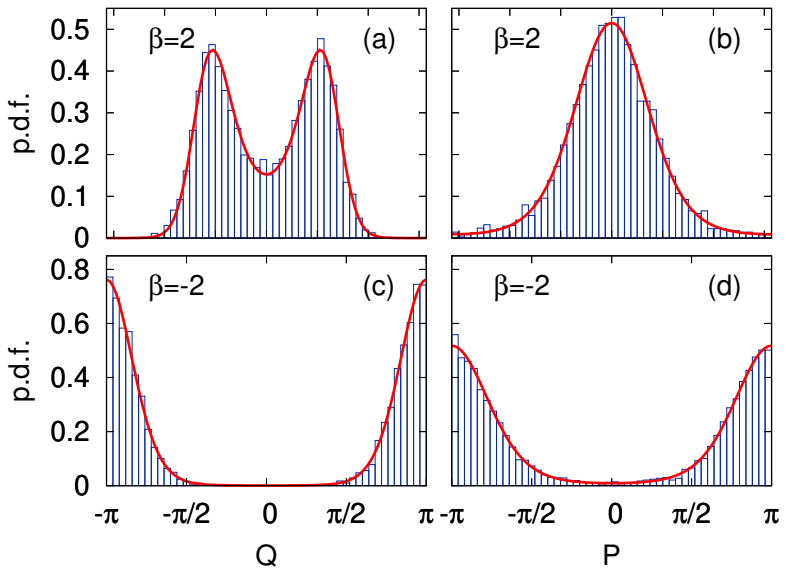

Figure 3.5. Equilibrium p.d.f. of the particle variables (Q, P). The top (bottom) panels correspond to $\beta = 2$ ($\beta = -2$). Histograms are computed from numerical simulations of the microscopic dynamics (3.37); red solid lines are the best fits to the Boltzmann distribution (3.58). Parameters: $N = 10^4$, $\alpha = 10$, $\mu = 10^{-2}$, $dt = (\alpha N)^{-1}$. Figure from Ref. [15].

i.e. it is the same discussed in Section 2.2, while the external potential and the coupling with the bath read, respectively,

$$\mathcal{U}(Q) = (1 - \cos Q)^2 \qquad \lambda(Q) = \sin Q \,. \tag{3.57}$$

In our simulations, the spins are started from an unmagnetized configuration in which $\sigma_j = \pm 1$ with equal probability. Then, for each time-step dt thereof, our algorithm performs two actions:

1. it evolves the state (Q, P) of the particle through a (deterministic) Velocity Verlet integration step (described in Section 5.1);

2. it chooses one spin with uniform probability, and "tries" to flip it according to the Glauber dynamics (3.34).

The waiting time between two extractions of the same spin is, on average, Ndt; as a consequence, the probability to flip the spin once it has been selected is given by $Ndt\, W_j(\boldsymbol{\sigma}|Q)$; in order to keep it of the order of unity, we choose $dt \sim O[(\alpha N)^{-1}]$.

As a first check for the validity of our description, we verify the renormalization of the potential that arises in our theoretical framework. Specifically, we check the shape of the equilibrium p.d.f. for the particle variables (Q, P), which is given by

$$f_{eq}(Q, P) = \frac{1}{Z} \exp\{-\beta[\mathcal{K}(P) + \mathcal{U}_R(Q)]\} \,. \tag{3.58}$$

Making use of Eq. (3.53), we find that the renormalized potential $\mathcal{U}_R(Q)$ is

$$\mathcal{U}_R(Q) = (1 - \cos Q)^2 - \frac{\beta}{2}\tilde{\mu}^2 \sin^2 Q \,. \tag{3.59}$$

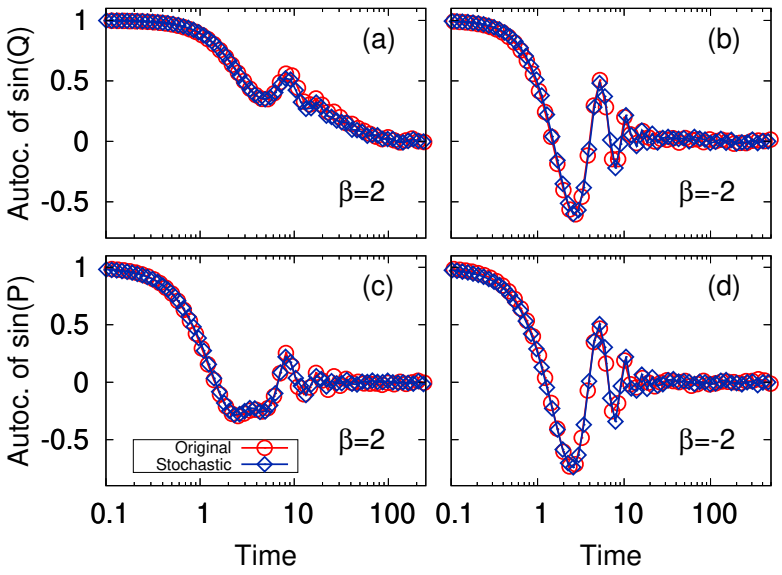

Figure 3.6. Equilibrium autocorrelation functions. Specifically, we consider two observables, $\sin Q$ above and $\sin P$ below, for $\beta = 2$ (left panels) and $\beta = -2$ (right panels). Red circles represent the simulations of the original dynamics (3.37), whereas blue diamonds are the numerical integration of the Fokker-Plank equation (3.51), with a time-step $h = 10^{-4}$. Other parameters as in Fig. 3.5. Figure from Ref. [15].

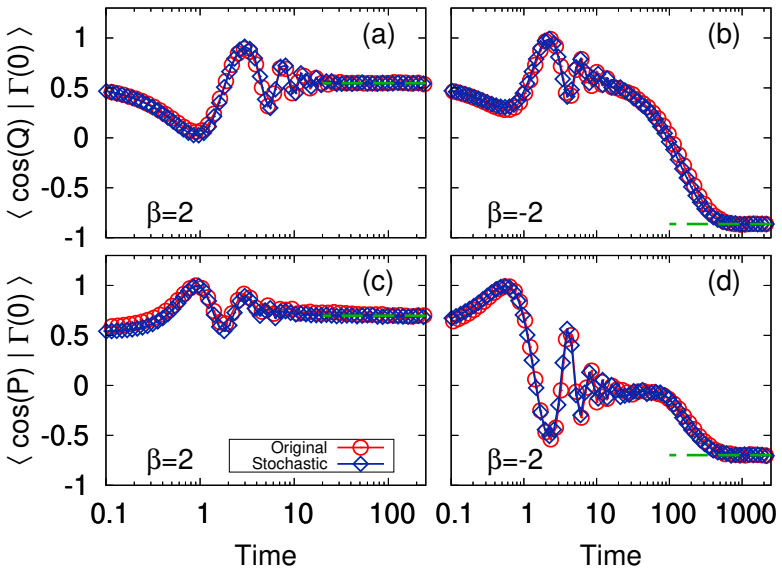

Figure 3.7. Relaxation to equilibrium. We plot the time evolution of the averages of $\cos Q$ (top) and $\cos P$ (bottom), for $\beta = 2$ (left panels) and $\beta = -2$ (right panels). In all cases, the particle starts from the initial condition $\mathbf{\Gamma}(0) = (Q(0), P(0)) = (1, 1)$. As in Fig. 3.6, the original dynamics (red circles) is compared with the Fokker-Planck equation (blue diamonds), with a time-step $h = 10^{-4}$. Other parameters as in Fig. 3.5. Figure from Ref. [15].

For positive temperatures, $\mathcal{U}_R(Q)$ corresponds to a bistable potential with symmetric minima at some $Q \in [-\pi, \pi)$ verifying $\cos Q = 2/(2 + \beta\tilde{\mu}^2)$, and maxima at $Q = 0, \pm\pi$, whereas for negative temperatures $\mathcal{U}_R(Q)$ has only one minimum at $Q = 0$ and attains its maximum value at $Q = \pm\pi$. Thus, the most probable value of Q – given by the maximum of $\exp[-\beta\mathcal{U}_R(Q)]$ – changes discontinuously from $Q = \pm\tilde{\mu}\sqrt{\beta}$ for $\beta = 0^+$ to $Q = \pm\pi$ for $\beta = 0^-$.

In Fig. 3.5, we show the histograms of Q and P at equilibrium, for two values of the temperature with opposite signs: the agreement between the numerical and the theoretical results are excellent. By fitting each plot with the corresponding Boltzmann factor, we infer values of the parameter β that are compatible with the original ones used in the simulations, within the confidence interval for the fit.

Second, we check the accuracy of the derived LE for describing the dynamics of the particle variables. We want to compare the behavior of dynamical quantities in the original dynamics to that of the same observables in a coarse-grained model ruled by Eq. (3.55). With this aim, we numerically integrate such LE using a standard algorithm for stochastic differential equations [127]. The variant of the algorithm that has been chosen for such simulations is accurate up to order $O(h^{3/2})$, where h is the time-step for the integration.

Several time-dependent quantities which can be computed from the Fokker-Planck equation (3.55) are compared with those obtained by simulating the original Liouville-master equation (3.37). In Fig. 3.6, we look into time correlation functions at equilibrium, namely, into the autocorrelations of $\sin Q$ and $\sin P$, for two different values of β with opposite sign. In Fig. 3.7, we study the relaxation to equilibrium of some dynamical observables. In particular, we have evaluated $\langle \cos Q \rangle$ and $\langle \cos P \rangle$, conditioned to fixed initial values of the particle variables $\mathbf{\Gamma}(0) \equiv (Q(0), P(0))$. Also in this case, we consider a case with positive β and one at negative temperature. The asymptotic values of the observables, computed analytically, are also shown for reference. As the figures show, in all cases the agreement is very good.

3.3.4 Some remarks

The results presented in Section 3.3.2 provide an exact analytical form for the generalized Klein-Kramers equations of a stochastic process which can take place also at NAT, when the parameter β for the considered bath is negative. The simulations discussed in Section 3.3.3 are in good agreement with the analytical predictions.

Remarkably, also in this case it is possible to find a generalized Einstein relation of the form (3.21), as it is clear from the P-dependent part of the drift term for P in Eq. (3.55). An interesting difference from the examples discussed before is given by the fact that in this case D is a function of Q. This is of course a consequence of the particular nature of the bath, and of the way in which it interacts with the considered slow particle.

The above consideration raises a subtle issue. In this case an analytical derivation shows that D is not constant during the dynamics, even if it does not depend on P. In other words, it would not be possible to write down a one-variable LE for P only, since its dynamics is not Markovian. How can we be sure that in the previously discussed examples (see Section 3.2) D was not a function of Q? The question is legitimate, since our data-driven method for the inference of the diffusivity (see

Figs. 3.1 and 3.3) is based on the assumption that D can only depend on P. If this hypothesis was not verified in the first place, the observed profiles of $D(P)$ would be an average over the position of some function $D^{(2)}(Q, P)$. Of course, this scenario could be excluded with a 2-variable version of the approach used in Section 3.2 (similar generalizations are discussed in Sections 5.4 and 5.5). In the specific cases discussed before, however, the system presents translational invariance in the thermodynamic limit (rotational invariance when the generalized positions are angles), and an explicit dependence on Q would break this symmetry. As a consequence, D must be constant. As far as we know, however, there is no systematic procedure to be sure, *a priori*, that the set of coordinates chosen for the coarse-grained representation is described by a Markovian dynamics, and one is usually forced to compare, *a posteriori*, the outcomes of the effective description and the original dynamics to check the level of accuracy of the considered approximation. This point is discussed in Section 5.4 in a particular case.

Another interesting point is represented by the renormalization of the potential (3.53), which is again an effect of the coupling with the spin bath. The additional potential depends on the temperature, and in particular it can assume qualitatively different shapes depending on the sign of β (see example shown in Fig. 3.5). This is another situation in which the presence of negative temperature leads to scenarios which cannot be straightforwardly reconduced to corresponding positive-temperature cases.

Appendix to Chapter 3

3.A Properties of operator $\hat{W}$

In this Appendix we discuss some properties of the operator $\hat{W}$ defined by Eq. (3.47). Such characterization will be useful for the solution of Eq. 3.46, which will be carried out in Appendix 3.B.

Let us consider the space of spin configurations $\boldsymbol{\sigma}$, where we define the following scalar product:

$$\langle f, g \rangle = \sum_{\boldsymbol{\sigma}} \frac{1}{\mathcal{P}^{eq}(\boldsymbol{\sigma}|Q)} f(\boldsymbol{\sigma}) g(\boldsymbol{\sigma}) \,. \tag{3.60}$$

First, we show that $\hat{W}$ is self-adjoint with respect to this scalar product. To this end, consider

$$\begin{aligned} \langle f, \hat{W} g \rangle &= \sum_{\boldsymbol{\sigma}} \frac{1}{\mathcal{P}^{eq}(\boldsymbol{\sigma}|Q)} f(\boldsymbol{\sigma}) \hat{W} g(\boldsymbol{\sigma}) \\ &= \sum_{\boldsymbol{\sigma}} \frac{1}{\alpha \mathcal{P}^{eq}(\boldsymbol{\sigma}|Q)} f(\boldsymbol{\sigma}) \left[\sum_{j=1}^{N} \omega(\boldsymbol{\sigma}'_j \to \boldsymbol{\sigma}) g(\boldsymbol{\sigma}'_j) - \sum_{j=1}^{N} \omega(\boldsymbol{\sigma} \to \boldsymbol{\sigma}'_j) g(\boldsymbol{\sigma}) \right] . \end{aligned} \tag{3.61}$$

Due to detailed balance,

$$\omega(\boldsymbol{\sigma}'_j \to \boldsymbol{\sigma}) \mathcal{P}^{eq}(\boldsymbol{\sigma}'_j|Q) = \omega(\boldsymbol{\sigma} \to \boldsymbol{\sigma}'_j) \mathcal{P}^{eq}(\boldsymbol{\sigma}|Q) \,, \tag{3.62}$$

so that the first term in the r.h.s. of Eq. (3.61) can be also written as

$$\sum_{j=1}^{N} \sum_{\boldsymbol{\sigma}} \frac{1}{\alpha \mathcal{P}^{eq}(\boldsymbol{\sigma}'_j|Q)} f(\boldsymbol{\sigma}) \omega(\boldsymbol{\sigma} \to \boldsymbol{\sigma}'_j) g(\boldsymbol{\sigma}'_j) \,. \tag{3.63}$$

Now we observe that the sum over the configurations $\boldsymbol{\sigma}$ can be equivalently replaced by a sum over $\boldsymbol{\sigma}'_j$, once j has been fixed, since there is a one-to-one correspondence between the realizations of $\boldsymbol{\sigma}$ and those of $\boldsymbol{\sigma}'_j$. Then we can exchange the role of the two dummy indexes $\boldsymbol{\sigma}$ and $\boldsymbol{\sigma}'_j$; the resulting expression can be substituted into Eq. (3.61) to give

$$\begin{aligned} \langle f, \hat{W} g \rangle &= \sum_{\boldsymbol{\sigma}} \frac{1}{\alpha \mathcal{P}^{eq}(\boldsymbol{\sigma}|Q)} g(\boldsymbol{\sigma}) \sum_{j=1}^{N} \left[\omega(\boldsymbol{\sigma}'_j \to \boldsymbol{\sigma}) f(\boldsymbol{\sigma}) - \omega(\boldsymbol{\sigma} \to \boldsymbol{\sigma}'_j) f(\boldsymbol{\sigma}) \right] \\ &= \sum_{\boldsymbol{\sigma}} \frac{1}{\mathcal{P}^{eq}(\boldsymbol{\sigma}|Q)} g(\boldsymbol{\sigma}) \hat{W} f(\boldsymbol{\sigma}) = \langle \hat{W} f, g \rangle \,, \end{aligned} \tag{3.64}$$

which shows that $\hat{W}$ is self-adjoint.

Let us now consider a generic function $f(\boldsymbol{\sigma})$ defined on the space of spin configurations. We have

$$\begin{aligned}\sum_{\boldsymbol{\sigma}} \hat{W} f(\boldsymbol{\sigma}) &= \sum_{\boldsymbol{\sigma}} \frac{1}{\mathcal{P}^{eq}(\boldsymbol{\sigma}|Q)} \mathcal{P}^{eq}(\boldsymbol{\sigma}|Q) \hat{W} f(\boldsymbol{\sigma}) \\ &= \langle \mathcal{P}^{eq}(\boldsymbol{\sigma}|Q), \hat{W} f(\boldsymbol{\sigma}) \rangle = \langle \hat{W} \mathcal{P}^{eq}(\boldsymbol{\sigma}|Q), f(\boldsymbol{\sigma}) \rangle = 0\,,\end{aligned} \tag{3.65}$$

where we have used the self-adjointness of $\hat{W}$ just discussed and the detailed balance property $\hat{W}\mathcal{P}^{eq}(\boldsymbol{\sigma}|Q) = 0$. In other words, $\hat{W} f(\boldsymbol{\sigma})$ is orthogonal to the equilibrium distribution $\mathcal{P}^{eq}(\boldsymbol{\sigma}|Q)$ with respect to the scalar product (3.60) for every choice of $f(\boldsymbol{\sigma})$.

Let us also stress that $\mathcal{P}^{eq}(\boldsymbol{\sigma}|Q)$ is the only solution of $\hat{W} f = 0$, but for multiplicative constants, since it is the only equilibrium distribution for the dynamics associated to $\hat{W}$ (an H-theorem can be shown to hold in this case; see Ref. [21] for details).

3.B Sketch of the solution of Eqs. 3.46

In this Appendix we briefly sketch the strategy that can be employed to solve Eqs. 3.46. First, let us observe that Eq. 3.46a is always verified, due to detailed balance.

The l.h.s. of Eq. 3.46b can be written as $\hat{W}\mathcal{P}^{(1)}(Q, P, \boldsymbol{\sigma}, t)$. In the light of the discussion outlined in Appendix 3.A, such function is orthogonal to $\mathcal{P}^{eq}(\boldsymbol{\sigma}|Q)$ and, as a consequence, also the r.h.s. verifies the same property, i.e.:

$$F^{(0)}(Q,P,t) + \left[\mathcal{K}'(P)\partial_Q - \mathcal{U}'(Q)\partial_P + \mu\lambda'(Q)\sum_{\boldsymbol{\sigma}}\sum_{j=1}^{N}\sigma_j\partial_P\right]\mathcal{P}^{eq}(\boldsymbol{\sigma}|Q) f(Q,P,t) = 0\,. \tag{3.66}$$

The above equation leads to Eq. (3.48). Such expression for $F^{(0)}$ can be inserted again into Eq. 3.46b to obtain, after some straightforward calculations,

$$\hat{W}\mathcal{P}^{(1)}(Q,P,\boldsymbol{\sigma},t) = \mu\lambda'(Q)\left(\beta\mathcal{K}'(P) f + \partial_P f\right)\sum_j(\sigma_j - \langle\sigma\rangle_{eq})\mathcal{P}^{eq}(\boldsymbol{\sigma}|Q)\,. \tag{3.67}$$

The above equation characterizes the first-order term of the expansion of $\mathcal{P}(Q, P, \boldsymbol{\sigma}, t)$. We can search for solutions of the form

$$\mathcal{P}^{(1)}(x,p,\boldsymbol{\sigma},t) = \mu\lambda'(x)\left(\beta K'(p) f + \partial_p f\right)\Phi(\boldsymbol{\sigma}|x)\,, \tag{3.68}$$

where $\Phi(\boldsymbol{\sigma}|x)$ satisfies

$$\hat{W}\Phi(\boldsymbol{\sigma}|x) = \mathcal{P}^{eq}(\boldsymbol{\sigma}|Q)\sum_{j=1}^{N}(\sigma_j - \langle\sigma\rangle_{eq})\,. \tag{3.69}$$

It is easy to verify that the r.h.s. of the above equation is an eigenfunction of $\hat{W}$, with eigenvalue -1. Eq. (3.44) assures that Φ is orthogonal to $\mathcal{P}^{eq}(\boldsymbol{\sigma}|Q)$ (and

therefore to the kernel of $\hat{W}$, as discussed in Appendix 3.A): we can conclude that

$$\Phi(\boldsymbol{\sigma}|x) = -\sum_{j=1}^{N}(\sigma_j - \langle\sigma\rangle_{eq})\,, \tag{3.70}$$

which, once substituted into Eq. (3.68), gives the searched expression for $\mathcal{P}^{(1)}$.

Now we can apply the same strategy to the third of equations (3.46). Its l.h.s. is orthogonal to $\mathcal{P}^{eq}(\boldsymbol{\sigma}|Q)$ and, as before, the sum over all spin configurations of the r.h.s. has to vanish, too. This observation leads, through some straightforward calculations, to

$$F^{(1)} = \frac{1}{\alpha}N\left(\mu\lambda'(Q)\right)^2\left[1-\tanh^2\left(\beta\mu\lambda(Q)\right)\right]\partial_P\left(\beta\mathcal{K}'(P)f+\partial_P f\right)\,, \tag{3.71}$$

which in the thermodynamic limit reduces to Eq. (3.50).

Chapter 4

Negative temperature out of equilibrium

In this Chapter we present some results for the behavior of Hamiltonian systems living in bounded phase spaces in typical out-of-equilibrium conditions. We aim at showing that negative temperatures correctly describe the high-energy regime of these models also in the context of non-equilibrium Statistical Mechanics.

First, we study some cases in which the system is driven out of equilibrium by a time-dependent perturbation, showing how response theory applies to states described by negative β. Then, the problem of Fourier transport along one-dimensional chains in presence of negative-temperature baths is investigated.

Some of the results presented in Section 4.1 are discussed in Ref. [135]. Results of Section 4.2 are part of a work (in preparation) in collaboration with S. Iubini.

4.1 Linear response theory

The classical theory of linear response accounts for the effect of small perturbations on Hamiltonian systems initially in equilibrium [75, 129]. Let us consider a mechanical model described by some Hamiltonian $\mathcal{H}_0(\mathbf{p}, \mathbf{q})$, and let us assume that at time t_0 it stays in an equilibrium state, whose p.d.f. is given by $f_0(\mathbf{p}, \mathbf{q})$. At time t_0 the Hamiltonian is perturbed by an additional term $-\mathcal{F}(t)\mathcal{A}(\mathbf{p}, \mathbf{q})$, where $\mathcal{A}$ is some function of the canonical coordinates, while $\mathcal{F}(t)$ can be seen as a time-dependent external field. We are interested in the time-dependent behavior of the generic mechanical observable $\mathcal{B}(\mathbf{p}, \mathbf{q})$.

The Fluctuation-Dissipation Relation (FDR) [31, 129] assures that the average deviation from the equilibrium value, $\langle \Delta\mathcal{B}(t) \rangle = \langle \mathcal{B}(t) - \mathcal{B}(t_0) \rangle$, has the form

$$\langle \Delta\mathcal{B}(t) \rangle = \int_{t_0}^{t} dt' R(t - t')\mathcal{F}(t') \,, \tag{4.1}$$

where $R(t)$, the "response function", reads

$$R(t) = \beta \langle \dot{\mathcal{A}}(t_0)\mathcal{B}(t) \rangle_{eq} \,. \tag{4.2}$$

In the above expressions, $\langle \cdot \rangle$ represents the average over the perturbed, time-dependent p.d.f. of the state, while $\langle \cdot \rangle_{eq}$ is the average over $f_0(\mathbf{p}, \mathbf{q})$. Let us stress

that Eq. (4.2) is deduced under the assumption that the equilibrium state of the system is properly described by a canonical distribution $f_0(\mathbf{p},\mathbf{q}) \propto \exp[-\beta\mathcal{H}_0(\mathbf{p},\mathbf{q})]$ at inverse temperature β. The importance of the above result lies in the link between a non-equilibrium quantity (the time-dependent response to an external perturbation) to an average over equilibrium fluctuations. Let us notice that Eq. (4.1) reduces to the Kubo relations in the $t \to \infty$ limit.

The FDR can be generalized to cases in which the system does not obey a Hamiltonian dynamics, provided that its evolution is mixing and that the invariant measure is smooth and nonvanishing [56, 129]. Let us assume that the system is described by a vector $\mathbf{X}$. At time t_0, an instantaneous infinitesimal perturbation $\mathbf{X} \to \mathbf{X}' = \mathbf{X} + \delta\mathbf{X}(t_0)$ occurs. The average displacement of the observable $\mathcal{B}(\mathbf{X})$ from its unperturbed trajectory at time t is given by

$$\overline{\delta\mathcal{B}(t)} = -\sum_j \left\langle \mathcal{B}(\mathbf{X}(t)) \frac{\partial \ln \rho(\mathbf{X})}{\partial X_j}\Big|_{t=t_0} \right\rangle \delta X_j(t_0)\,, \tag{4.3}$$

where $\bar{\cdot}$ indicates an average over several realizations of the perturbation at time t_0, on states initially distributed according to the invariant measure $\rho(\mathbf{X})$; average $\langle\cdot\rangle$ is instead computed on $\rho(\mathbf{X})$ itself. The above formulation reduces to Eq. (4.1) in the case of Hamiltonian dynamics.

In what follows, we examine some cases in which a small perturbation is applied to a system at negative temperature.

4.1.1 External field

Let us consider the following Hamiltonian

$$\mathcal{H}(\mathbf{p},\mathbf{q};t) = \sum_{i=0}^{N}[1-\cos p_i] + k\sum_{i=1}^{N+1}[1-\cos(q_i - q_{i-1})] - \lambda(t)\sum_{i=1}^{N}\sin q_i\,, \tag{4.4}$$

where $\{p_i\}$ and $\{q_i\}$ are the usual canonical coordinates, defined on $[-\pi,\pi)$, and $q_0 \equiv q_{N+1} \equiv 0$. If the generalized positions are orientations of spins rotating on a xy plane, we can interpret the mechanical observable $M(\mathbf{q}) = \sum_i \sin q_i$ as the extensive y-axis magnetization. The time-dependent parameter $\lambda(t)$ assumes then the meaning of an external field.

If the external field is small, we can predict the behavior of the magnetization using the classical response theory. For instance, we can imagine that the system evolves according to the unperturbed Hamiltonian until some time t_0 (i.e. $\lambda(t) = 0$ for $t < t_0$); then, at time t_0, a small external field is switched on, and its intensity is kept constant for very long times. In other words, we are considering the case

$$\lambda(t) = h\Theta(t - t_0)\,, \tag{4.5}$$

where $\Theta(x)$ is the Heaviside step-function and $0 < h \ll 1$. According to Eq. (4.1), the average deviation of $M(t) = M(\mathbf{q}(t))$ from its unperturbed equilibrium value is given by the FDR

$$\langle \Delta M(t)\rangle = \beta h \int_{t_0}^{t} dt' \langle \dot{M}(t_0) M(t')\rangle_{eq}\,. \tag{4.6}$$

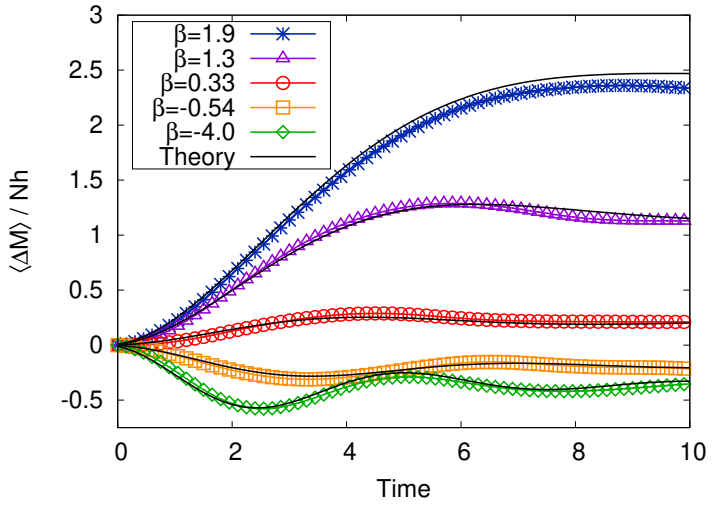

Figure 4.1. Magnetization of the system (4.4) after the external field has been switched on at time $t_0 = 0$. Symbols represent the variation $M(t) - M(t_0)$ with respect to the intensity of the small constant field $h = 0.02$, averaged over $\mathcal{N} = 10^4$ realizations and divided by the number of total particles N. Black solid lines are computed according to linear response theory (Eq. (4.6)) performing simulations in the unperturbed equilibrium state. $N = 128$, $k = 0.5$, $\tau = 300$.

Let us notice that the inverse temperature β appearing in the previous equation can assume negative values.

We perform numerical simulations in order to check the validity of the above scenario. First we initialize the system in a (microcanonical) equilibrium state at some energy E. The system is evolved with the unperturbed Hamiltonian ($\lambda = 0$) for a total time $\mathcal{N}\tau$, where τ is much longer than the typical time-scales of the dynamics: we get $\mathcal{N}$ trajectories of length τ for the unperturbed equilibrium dynamics at energy E. Now we simulate $\mathcal{N}$ "alternative" dynamics, starting from the microscopic configurations at $t_n = n\tau$, $n = 0, ..., \mathcal{N}-1$; this time we take $\lambda = h$, and we consider the deviation from the corresponding unperturbed trajectory. Finally, we average over the $\mathcal{N}$ realizations.

The results of our simulations are shown in Fig. 4.1. We also report the prediction of linear response theory, computed through equilibrium simulations at the same energies. Two qualitatively different scenarios appear when considering positive and negative temperatures. In the first case, the system is already "magnetized" at equilibrium, since the spins are aligned in the same direction, on average, due to the interaction terms; however $\langle M \rangle_{eq}$, which measures the alignment of the rotators to the y-axis, is zero for symmetry reasons. When the field is turned on, each spin tends to reach the minimum of the external potential, $q_i = \pi/2$. In the case of negative temperature, the spins are initially in a state such that neighbor rotators tends to have a relative angular distance of π, maximizing the total energy. The response is then smaller in modulus, and the sign of the magnetization is opposite to that of the field in this case.

Let us notice that the agreement between the numerical results and linear response theory is quite good, also in the case of negative β.

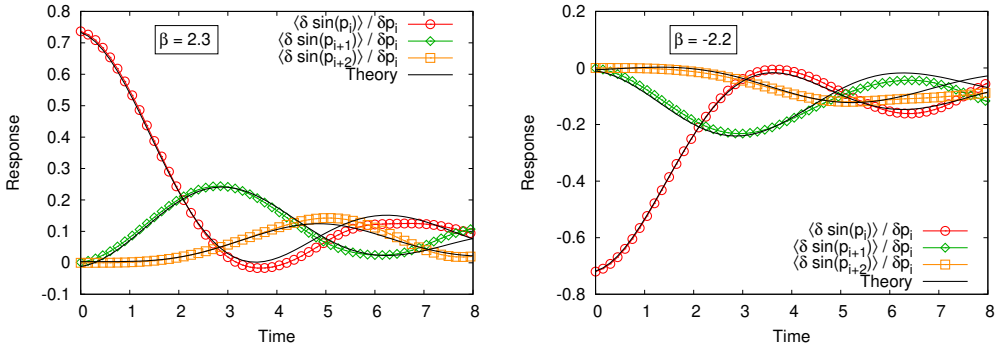

Figure 4.2. Average response of the velocity $\sin p_j$ of the j-th particle to a small perturbation, at time $t_0 = 0$, of the i-th rotator's momentum by a small quantity $\delta p = 0.01$. Two cases are considered, one at positive (left) and one at negative β (right); the average deviations from the unperturbed velocity are plotted (with different symbols) for $j = i$, $j = i + 1$ and $j = i + 2$. Black solid lines are theoretical predictions from Eq. (4.7), computed through equilibrium simulations. $N = 128$, $\mathcal{N} = 10^4$, $k = 0.5$, $\tau = 300$, $i = 50$.

4.1.2 Local perturbation

Another typical case that can be studied with linear response theory is that of a small perturbation of a single degree of freedom. For instance, it can be interesting to study how a small, instantaneous "kick" on a particle (a sudden variation of its momentum) affects its velocity at later times, and how such effect propagates through the system.

Let us consider again Hamiltonian (4.4), in absence of external field (i.e. $\lambda(t) = 0$). At time t_0, the i-th particle's momentum is instantaneously changed by a small quantity δp, and we study the average response on the velocity of the j-th particle, $\sin p_j$, as a function of time. Eq. (4.3) reduces in this case to the generalized FDR

$$\overline{\delta \sin p_j} = \beta \langle \sin(p_j(t)) \sin(p_i(t_0)) \rangle \delta p_i \,. \tag{4.7}$$

Let us notice that, also in this case, the above expression is derived assuming a canonical distribution at inverse temperature β.

Again, we perform numerical simulations at equilibrium, at fixed energy, comparing the unperturbed trajectories to those obtained by suddenly adding $\delta p = 0.01$ to the momentum of the i-th particle. Fig. 4.2 shows the average velocity response of three particles (the perturbed one, the first and the second neighbors) after the perturbation, compared with the theoretical expectation given by Eq. (4.7). The perturbed rotator experiences, obviously, an immediate deviation from the original velocity, while the maximum average deviations of its neighbors happen after some delay.

The linear response theory gives accurate predictions also in this case, and also when the system is prepared at negative temperature. In the latter case, the response to a positive perturbation of the momentum is clearly negative for the velocity; this can be easily explained by remembering that at negative temperature the momentum distribution is peaked in $p_i = \pm\pi$. The success of Eq. (4.7) shows

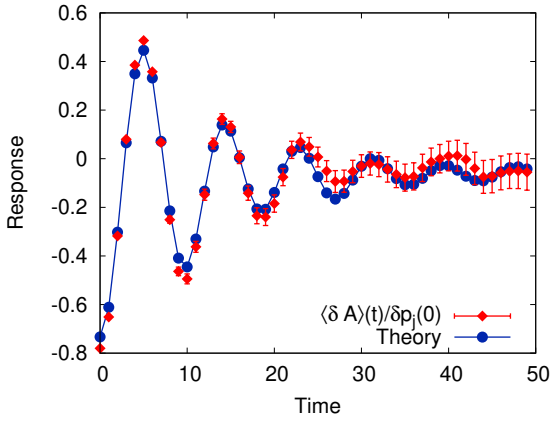

Figure 4.3. Check of the FDR for system (4.8) by a direct measure of the velocity response to a momentum perturbation δp (red diamonds) and comparison with the theory, Eq. (4.7) (blue circles). The case with specific energy $E/N = 1.9$, corresponding to $\beta = -2.6$, is considered. Parameters: $J = -0.5$, $K = -1.4$ $N = 250$, $M = 10^5$, $\tau = 50$, $\delta p_i(0) = 0.01$. Figure from Ref. [135].

the necessity of adopting negative values of β in order to get a consistent response theory in the high-energy regime.

4.1.3 A case in absence of ensemble equivalence

A non-trivial case in which the applicability of response theory could appear questionable is represented by the Hamiltonian described in Section 2.4, namely

$$\mathcal{H}(\mathbf{p},\mathbf{q}) = \sum_i (1-\cos p_i) - \frac{J}{2}Nm^2 - \frac{J}{4}Nm^4 \tag{4.8}$$

where m is the modulus of the intensive "magnetization"

$$\mathbf{m} = \left(\frac{1}{N}\sum_i \cos q_i, \frac{1}{N}\sum_i \sin q_i\right) . \tag{4.9}$$

As discussed in Chapter 2, this system shows ensemble inequivalence at negative temperature, in a suitable energy range. Here we are interested in the study of FDR in such regime.

We consider again a small perturbation of the i-th momentum, and we study the response of velocity. In this case the only meaningful velocity to consider is that of the i-th particle itself, since the mean-field interaction which rules the dynamics does not allow to consider proper "neighbors". The FDR is still given by Eq. (4.7), where the equilibrium average is now computed considering Hamiltonian (4.8).

The numerical strategy is the same as before, and again we consider the average deviation from the unperturbed trajectory. The results are shown in Fig. 4.3, for a choice of the total energy corresponding to an unstable state (i.e., a proper microcanonical state which does not correspond to any canonical equilibrium state).

Also in this case, not surprisingly, the correct β to consider in order to recover linear response theory is negative. Let us notice that this is true even if the canonical

distribution does not correctly describe the equilibrium state considered here, due to ensemble inequivalence.

4.2 Energy transport and Fourier's law at negative temperature

One of the main topics of irreversible thermodynamics and out-of-equilibrium Statistical Mechanics is represented by thermal conduction. It is empirically well known that energy can flow through matter under the action of a temperature gradient; this principle is established by Fourier's law

$$\mathbf{J} = -\kappa \nabla T \tag{4.10}$$

where $\mathbf{J}$ is the heat flux and κ is a tensor, the thermal conductivity. Although the above law has been experimentally verified in innumerable cases, its full understanding, especially for low-dimensional systems, is still lacking; in particular, it has not been possible, so far, to derive it directly from first principles [117, 51, 115].

During the last decades, a large number of models have been proposed to study thermal conduction. The typical framework is constituted by a one-dimensional chain, whose extremities are able to exchange heat with thermal baths at different temperatures. Many numerical techniques have also been investigated to reproduce the action of such reservoirs; a recent account can be found in Ref. [115].

One of the most interesting phenomena emerging in this context is anomalous transport, which is encountered when κ does not reach finite values as the size of the chain tends to infinity. It has been recognized that this behavior is typical of systems ruled by momentum-conserving dynamics; the divergence of κ in the limit of infinite size can be related to energy superdiffusivity, nonintegrable power-law decay of the heat flux autocorrelation and superexponential relaxation of spontaneous fluctuations; such phenomena are expected to obey proper hyperscaling laws, which could allow a classification into universality classes [116, 118, 16]. Systems whose dynamics does not conserve momentum, on the other hand, tend to show normal transport [117].

A noticeable exception to the above scheme is represented by Hamiltonian chains of rotors: even if the total (angular) momentum of such models is a conserved quantity, this property does not seem to hinder the possibility of normal transport, at least for not-too-low temperatures (i.e., when the model is far enough from its integrable limit at low energies). It has been argued that this behavior could depend on the periodicity of positions, whose continuous passage from π to $-\pi$ and vice versa is equivalent to an instantaneous "kick" in the opposite direction [69, 67, 89].

In the following, we will first discuss a stochastic simplified model, which should mimic the dynamics of a chain of nuclear spins coupled to two thermal baths at its extremities. Then we will consider a Hamiltonian system strictly related to the rotors model, i.e. a variant with bounded kinetic terms. Our motivation for the study of these setups is the possibility to investigate thermal conduction at negative temperature.

4.2.1 Exclusion process on a spin chain: a simplified model for Fourier transport

First, let us study a simple model mimicking the dynamics of N magnetic spins $\{\sigma_i = \pm 1\}$, with $i = 1, ..., N$, on a one-dimensional lattice. The chain is subjected to the action of two thermal baths, which fix the temperatures at the extremities. An external field h is present, so that the energy of the chain is simply given by

$$E = nh - (N - n)h = (2n - N)h \tag{4.11}$$

where n is the number of positive spins.

Locally, the dynamics of the system is expected to conserve energy. As a consequence, the i-th spin can "flip" from $+1$ to -1 (or vice-versa) only if the $(i+1)$-th or the $(i-1)$-th spin experience a simultaneous change with opposite sign. The resulting evolution is equivalent to an exclusion process (EP) in which the i-th site is considered "occupied" by a particle if the spin is positive, while it is "empty" if the spin is negative. Particles can move to an adjacent site only if it is empty. In numerical simulations, the stochastic nature of the process is mimicked by choosing, at each time step, one *ordered* pair of adjacent sites, with uniform probability among the $2N - 2$ possible couples. If the first site of the couple is occupied and the second is empty, the particle moves from the first to the second site; in all other cases, nothing happens. A generalization of this dynamics has been used, e.g., in Ref. [91] to provide a toy model for the study of discrete breathers in the DNLS equation.

If the distribution of the values for the i-th spin was determined by an equilibrium dynamics at inverse temperature β, its average magnetization would result

$$m_i = \mathcal{P}(+1) - \mathcal{P}(-1) = \frac{e^{-\beta h} - e^{\beta h}}{e^{-\beta h} + e^{\beta h}} = -\tanh(\beta h)\,, \tag{4.12}$$

where $\mathcal{P}(\pm 1)$ is the probability of extracting a spin value ± 1. The above relation provides a natural definition for a local (inverse) temperature,

$$\beta_i = -\frac{\operatorname{atanh}(m_i)}{h}\,. \tag{4.13}$$

In order to study the problem of heat transport along the chain, we need to impose fixed temperatures at the extremal sites of the unidimensional lattice. To this end, the leftmost spin is extracted with an equilibrium distribution corresponding to some inverse temperature β_L, while the rightmost one is kept at inverse temperature β_R with the same mechanism. The extremal temperatures can assume, of course, negative values. Let us notice that, besides the (potentially relevant) practical difficulties, this situation could be reproduced, in principle, in real experiments on nuclear spins.

In our simulations, one time unit consists of $2N - 2$ trials of the exclusion process, so that, irrespectively of their signs, both extremal spins have, on average, one chance to flip during a unitary time interval (if the adjacent spin has opposite value). The number of time units between two successive extractions of the extremal spins is determined by an exponential distribution $\gamma e^{-\gamma t}$, where the parameter γ

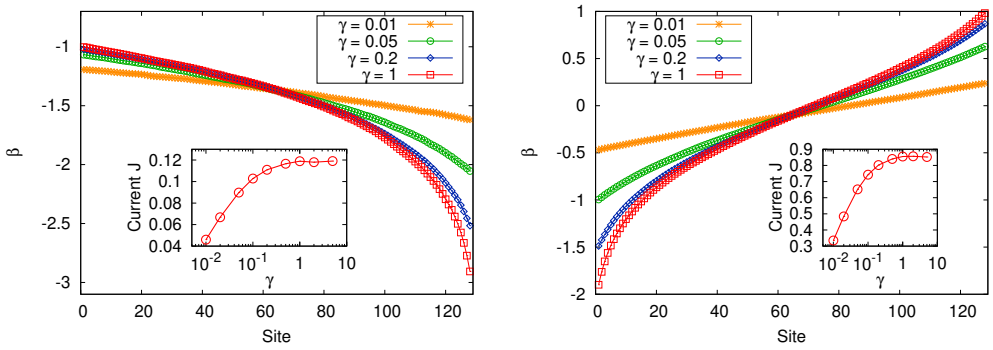

Figure 4.4. Temperature profiles in a spin chain ruled by an EP, for different values of γ. Left panel: $\beta_L = -1$, $\beta_R = -3$. Right panel: $\beta_L = -2$, $\beta_R = 1$. Insets show how the current of particles depends on γ. Total integration time $\mathcal{T} = 10^7$ (after the stationary state has been reached), $N = 128$, $h = 1$.

fixes the rate of such Poisson process. The simulations are initialized with random initial conditions, in which each spin can be $+1$ or -1 with equal probability. We let the system evolve until a stationary state is reached. Then we start measuring, for each site of the chain, the magnetization m_i, averaging over a (long) time $\mathcal{T}$. We infer a local temperature using Eq. (4.13).

Fig. 4.4 shows some temperature profiles for two different situations involving negative temperature: in the left panels β_L and β_R are both negative, while in the right one they have opposite signs. Let us notice that the external baths are actually able to fix the temperatures of the extremal sites only if γ is large enough. The choice of the rate is a delicate point when working with stochastic baths [117]. Some insight can be obtained from the study of the current of particles of the EP (which corresponds to an energy flux in the spin-system picture). For each pair of adjacent sites $(i, i+1)$, we define

$$J_i = w_{i\to i+1} - w_{i+1\to i} \tag{4.14}$$

where $w_{i\to j}$ is the rate of the transition of a particle from site i to site j in the EP. The corresponding energy flux in the spin dynamics is simply $h(2J_i - 1)$. Being the current associated to a locally conserved quantity, $\langle J_i \rangle = J$ is independent of site in the stationary state. The insets of Fig. 4.4 show that such current crucially depends on γ, and a plateau is reached for values $O(1)$. This is reasonable, since the EP that determines the internal movements along the chain involves each of the extremal spins just once in a time unit: larger update frequencies are, in this sense, useless. Values of γ much smaller than one, on the other hand, do not assure a current large enough for the stationary process between the two temperature to be sustained.

Figure 4.5 shows several temperature profiles, with various choices of β_L and β_R. Let us notice that in each case the (inverse) temperature continuously change from the value assumed at the left extremity to the rightmost one. When these values have opposite signs, the profile passes through a state of local equilibrium at vanishing β (i.e., infinite temperature). This is an additional evidence of the fact that β is the "right" variable to consider when dealing with systems which can

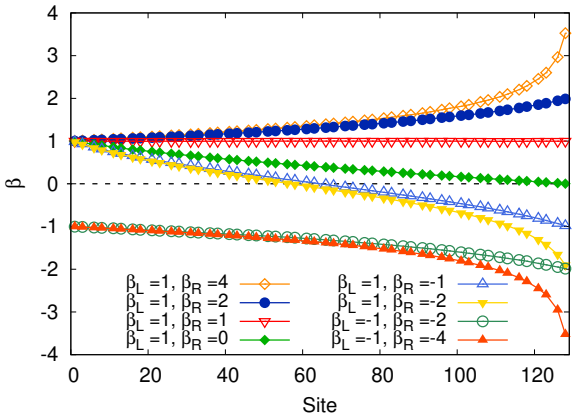

Figure 4.5. Temperature profiles for various choices of the extremal baths. The dashed line signals the passage, through $\beta = 0$, from positive to negative temperatures. $\mathcal{T} = 10^7$, $N = 128$, $h = 1$, $\gamma = 1$.

assume both positive and negative temperature.

4.2.2 A Hamiltonian chain between two baths

Let us now discuss the much more complex case in which the chain is represented by an Hamiltonian system, whose evolution is ruled by a deterministic dynamics (with the only exceptions of the extremal baths, whose dynamics is stochastic). We will deal with the already discussed model

$$\mathcal{H}(\mathbf{p},\mathbf{q}) = \sum_{i=0}^{N+1}(1-\cos p_i) + \varepsilon \sum_{i=1}^{N+1}[1-\cos(q_i - q_{i-1})]\,, \tag{4.15}$$

where the canonical coordinates $\{p_i, q_i\}$ are, as usual, angular variables. The label i represents the site in which the corresponding degree of freedom is located. This model is a version with bounded kinetic terms of the chain of Hamiltonian rotators which has been studied in several works on Fourier transport [69, 67].

This time the 0-th and $(N+1)$-th particles are not fixed; instead, they are subjected to a stochastic dynamics which fixes their temperature. From a computational point of view, this requirement is fulfilled by mean of the quasi-symplectic algorithm discussed in Section 5.2, which is able to integrate the generalized Klein-Kramers equation

$$\begin{pmatrix}\dot{q}\\ \dot{p}\end{pmatrix} = \begin{pmatrix}\partial_{p_i}\mathcal{H}\\ -\partial_{q_i}H - D_i\beta_i\partial_{p_i}\mathcal{H} + \sqrt{2D_i}\xi(t)\,,\end{pmatrix} \tag{4.16}$$

and reduces to the Verlet algorithm when $D_i = 0$ (i.e., when there is no stochastic bath and the Hamilton equations are recovered). As discussed in Chapter 3, the above dynamics is the proper generalization of the LE for systems with non-quadratic kinetic energies. In the following, we will consider the case $D_i = 0$ $\forall i : 1 \leq i \leq N$, choosing instead a nonvanishing value for $D_0 = D_{N+1} = D$. We fix the time-step for the integration in such a way that, setting $D = 0$ (completely

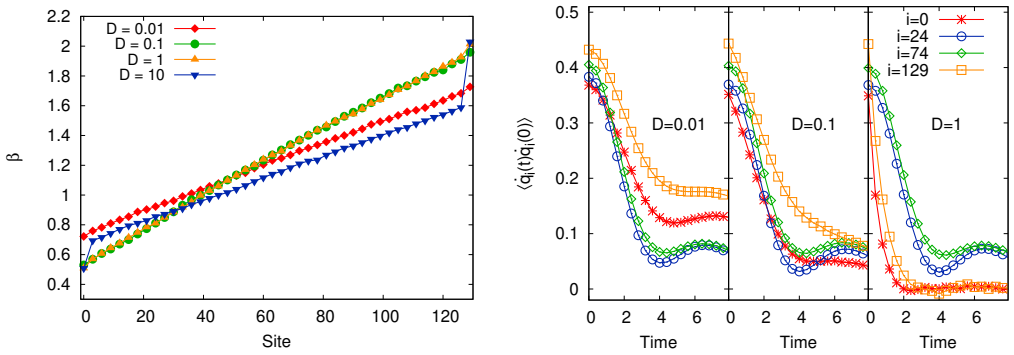

Figure 4.6. Effects of the choice of D on the dynamics. Left: temperature profiles obtained, for fixed $\beta_L = 0.5$ and $\beta_R = 2$, with different values of D. Right: autocorrelation functions for the velocities of the extremal particles compared to those of two rotators of the bulk; three cases are considered, for different choices of D. Parameters: $\varepsilon = 0.5$, $N = 128$.

deterministic dynamics) energy is conserved up to relative fluctuations of order 10^{-5}.

As in the EP discussed before, there is a natural way to define a local temperature for this system; as mentioned in Section 2.2, we can measure a suitable function $\mathcal{A}(p_i)$ of the i-th momentum (e.g., $\cos p_i$) and infer the value of β from its average over long times, inverting the relation which expresses $\langle \mathcal{A} \rangle$ as a function of β. Of course, this is only true if the chain is locally at equilibrium; as a preliminary check, we have to verify that the i-th momentum distribution is correctly described by $\rho(p_i) \propto \exp(\beta \cos p_i)$.

As discussed also for the simple case of the EP mimicking the spin dynamics, the choice of the typical rates of the baths is a crucial point for the simulations. In Fig. 4.6 (left) we show some different temperature profiles that can be obtained through the described setup by simply varying the parameter D (which fixes a typical time scale for the evolution of the reservoirs). When D is too small (case $D = 0.01$ in the figure), the action of the baths fails to maintain the extremal particles at the corresponding temperature. On the other hand, when the parameter is too high ($D = 10$ in the considered case), the extremal particles are found at the right temperature, but they are unable to establish a local equilibrium at that β with the neighbors. This is a known issues of stochastic baths, which is also encountered in cases with quadratic kinetic terms [117]. Good choices for the rates of the baths should lead to autocorrelation times of the same order of the those of the "bulk. Fig. 4.6 (right) shows the velocity autocorrelation functions of the extremal particles, compared to those of some rotators inside the chain, for three values of D, whence it is clear that this parameter should be chosen between 0.1 and 1.

4.2.3 Heat flux

As in the case of the EP, some more quantitative information about the range for D can be obtained from the study of the heat flux. Let us observe that in the

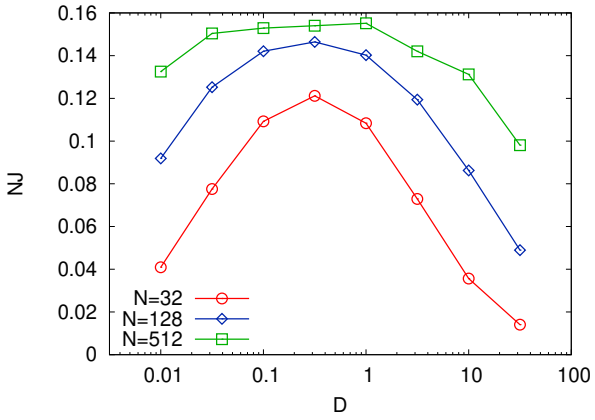

Figure 4.7. Heat flux of model (4.15), computed according to Eq. (4.21) and multiplied by the number of elements of the chain, as a function of D, the parameter which rules the rate of the thermal baths. Lines are guides for the eyes. Different values of N, the length of the chain, are considered. The inverse temperatures of the baths are $\beta_L = 1$, $\beta_R = 2$. Total integration time: $\mathcal{T} = 5 \cdot 10^7$. Other parameters of the dynamics as in Fig. 4.6.

considered system the momentum transport is expected to be null on average (as it can be verified numerically), so energy current and heat flux coincide.

The proper definition of energy current through an Hamiltonian chain with the usual, quadratic kinetic energy is discussed in Ref. [117]; the idea is to exploit the continuity equation, resulting from the local conservation of energy, to individuate a suitable mechanical observable with the meaning of an energy flux. Let us generalize this result to cases with non-quadratic kinetic terms.

Let us consider the Hamiltonian model

$$\mathcal{H}(\mathbf{p},\mathbf{q}) = \sum_{i=1}^{N} \mathcal{K}_i(p_i) + \sum_{i=1}^{N-1} \mathcal{U}_i(q_{i+1} - q_i)\,. \tag{4.17}$$

We will restrict to cases, as the one discussed in this Section, in which the i-th particle is located in the i-th site, and q_i does not indicate a translational displacement along the direction of the chain, but instead an internal degree of freedom or a position on a plane perpendicular to the chain itself (e.g., the angle of the i-th rotator). All pairs of adjacent sites are at the same distance a.

We can define the local energy associated to the i-th site as

$$h_i = \mathcal{K}_i(p_i) + \frac{1}{2}\left[\mathcal{U}_i(q_{i+1} - q_i) + \mathcal{U}_{i-1}(q_i - q_{i-1})\right] \tag{4.18}$$

where the $1/2$ factor in front of the potential terms implies that the energy contribution due to the interaction between adjacent sites is equally divided among the two. Taking the derivative of the above expression w.r.t. time, and bearing in mind the Hamilton equations, we get

$$\begin{aligned}\dot{h}_i = \frac{1}{2}\mathcal{U}_i'(q_{i+1} - q_i)[\mathcal{K}_{i+1}'(p_{i+1}) + \mathcal{K}_i'(p_i)] + \\ - \frac{1}{2}\mathcal{U}_{i-1}'(q_i - q_{i-1})[\mathcal{K}_i'(p_i) + \mathcal{K}_{i-1}'(p_{i-1})]\,.\end{aligned} \tag{4.19}$$

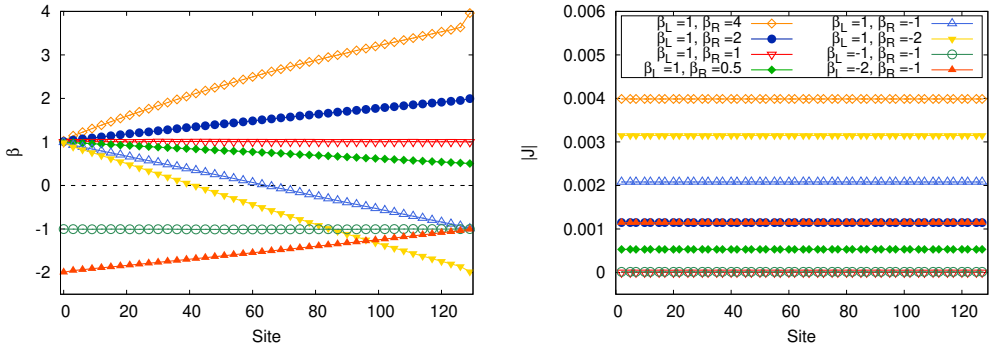

Figure 4.8. Stationary states of chain (4.15) subjected to the action of stochastic baths. Left: temperature profiles of the chain for several choices of β_L and β_R. Right: corresponding modulus of $\langle J_i \rangle$. Here $D = 0.4$, $N = 128$, other parameters as in Fig. 4.6.

We can compare the above expression with the discretized continuity equation

$$\dot{h}_i + \frac{J_i - J_{i-1}}{a} = 0\,, \tag{4.20}$$

where a, the lattice spacing, can be chosen to be unitary without loss of generality. J_i is the energy flux between the i-th and the $(i+1)$-th site. We get

$$J_i = -\frac{1}{2}\mathcal{U}_i'(q_{i+1} - q_i)[\mathcal{K}_i'(p_i) + \mathcal{K}_{i+1}'(p_{i+1})]\,. \tag{4.21}$$

In the specific case of Hamiltonian (4.15), where the functional forms of the kinetic and interaction terms do not explicitly depend on the site, the above equation leads to

$$J_i = -\frac{\varepsilon}{2}\sin(q_{i+1} - q_i)[\sin p_i + \sin p_{i+1}]\,. \tag{4.22}$$

In Fig. 4.7 we show the values of $J = \langle J_i \rangle$ (we drop the dependence on the index i since in the stationary state there is no dependence on the site, as expected) versus the choice of D. We notice that a maximum is found around $D \simeq 10^{1/2}$ for typical values of the external baths, this result being quite independent of the length of the chain. A qualitatively similar behavior is encountered also in different models, as the Fermi-Pasta-Ulam-Tsingou chain subjected to Langevin stochastic baths [117].

Figure 4.8 shows several temperature profiles obtained with a choice of D close to the one that maximizes the energy flux, and the corresponding values of $\langle J_i \rangle$. Not surprisingly, in the stationary state their value does not depend on the site, but only on the temperatures of the baths. Also for this Hamiltonian chain, as for the EP discussed before, when the signs of β_L and β_R are opposite, the temperature profile passes continuously from positive to negative values, crossing the $\beta = 0$ line.

It can be interesting to study the scaling of the flux with the size of the chain (i.e., the number of its particles), e.g. to understand, for instance, if we are in presence of normal or anomalous heat transport. In Fig. 4.9 we plot the conductivity, operatively defined as

$$\kappa = \frac{JN}{\beta_L^{-1} - \beta_R^{-1}}\,, \tag{4.23}$$

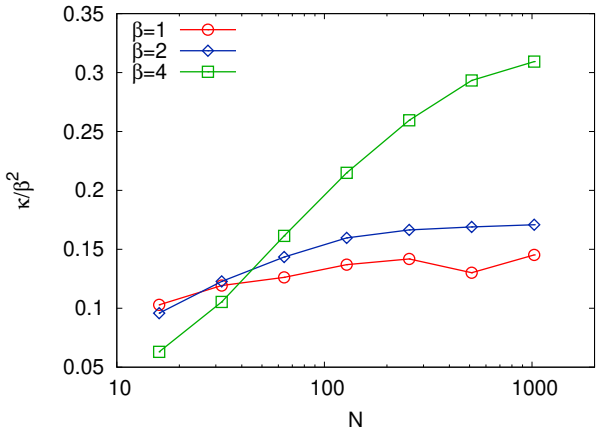

Figure 4.9. Scaling with the size of the chain. Thermal conductivity (4.23) (divided by β^2) as function of N. Profiles are computed for three choices of the temperature of the external baths, i.e. $\beta_{R,L} = (1 \pm 0.05)\beta$ for three values of β. Lines are guides for the eyes. Total integration time $> 2 \cdot 10^8$ in all cases. $D = 0.4$, other parameters as in Fig. 4.6.

versus N. Three cases are considered, for three different average β: the temperatures of the baths are given by $\beta_{R,L} = (1 \pm 0.05)\beta$. While for $\beta \simeq 1$ and $\beta \simeq 2$ the conductivity seems to reach a finite value for infinite N, the behavior is completely different in the case $\beta = 4$. This could be reminiscent of the transition between anomalous and normal transport in rotators chains, observed for $T \simeq 0.3 \div 0.4$ [67]; however, the data available at now do not allow for a definitive answer on this point.

4.2.4 Some remarks

Even if the considered model (4.15) may appear not particularly interesting *per se*, it shows that thermal conduction at negative temperature, and between thermal baths whose temperatures have opposite signs, are possible in principle.

The continuous transition between positive and negative values of β in the temperature profiles, through $\beta = 0$, seems to suggest that a generalization of Fourier's law to cases with both signs of the temperature is meaningful. In particular, Eq. (4.10) may be rewritten in terms of β in this context, to avoid the discontinuity that is encountered at $T = \pm\infty$. The β gradient has, on the other hand, an immediate interpretation, since it determines the local entropy increase associated to an infinitesimal displacement of energy. The formulations with T and β are of course equivalent in all interesting cases with only positive temperature.

An important case-study for energy transport is represented by the DNLS equation briefly discussed in Section 1.1.4. Several works have studied its behavior in out-of-equilibrium conditions, when the extremities are at contact with thermal baths, or characterized by purely dissipative conditions. The rich phenomenology that is observed, which includes the emergence of breathers (typical of negative-temperature states) also when only baths with $\beta \geq 0$ are involved, steel needs to be completely understood; however, the coupled transport of heat and momentum is recognized to play a major role [90, 88, 93]. The set-up discussed here, and possible

modifications aiming at allowing the transport of a second conserved quantity, could provide useful analogies for the understanding of such non-trivial phenomenology.

Chapter 5

Computational and technical aspects

Many of the results discussed in the previous Chapters are based on numerical simulations and data-processing methods. This Chapter is devoted to a careful analysis of the techniques employed throughout this Thesis, both from a mathematical and from an applicative point of view.

First, we review the basic properties of the symplectic integration algorithm we applied for molecular dynamics simulations of Hamiltonian systems. We also generalize such algorithm in order to include thermal baths, possibly at negative temperature. Then we focus our attention on the strategy used in Chapter 3 to infer from numerical data the LE which approximates a given process to the best extent, discussing some practical aspects of its application. The motion of a heavy particle in a harmonic chain, whose description in terms of LE is well-known, is analyzed with this procedure as a first check. Finally we switch to two less trivial cases: the activated dynamics of a simple polymer model moving in a two-well potential, from which the role of Markovianity for the applicability of the method is evident, and the actual experimental case of rotational diffusion in granular medium, whose study allows to fully appreciate the power, and the limits, of the discussed technique.

5.1 A symplectic algorithm for Hamiltonian systems with generalized kinetic energy

Here we review some basic results from the theory of symplectic integrators. A detailed exposition of the topic can be found, e.g., in Refs. [61] and [77].

Given an open set $D \in \mathbb{R}^{2N}$, a differentiable function $\mathbf{f} : U \to \mathbb{R}^{2N}$ is said to be symplectic if its Jacobian matrix M, defined as $M_{ij} = \partial_j f_i$, verifies

$$M^T J M = J \,, \tag{5.1}$$

where

$$J = \begin{pmatrix} 0 & I_N \\ -I_N & 0 \end{pmatrix} . \tag{5.2}$$

In the above equation, I_N is the $N \times N$ identity matrix.

Let us call $\mathbf{X} = (\mathbf{q}, \mathbf{p})$ the vector of positions and momenta of a Hamiltonian $\mathcal{H}$, so that the evolution equations can be rewritten as

$$\frac{d\mathbf{X}}{dt} = J\boldsymbol{\nabla}\mathcal{H}\,. \tag{5.3}$$

For a generic Hamiltonian defined on a $2n$-dimensional phase-space let us introduce the flow

$$\boldsymbol{\varphi}_t(\mathbf{X}_0) = \mathbf{X}(\mathbf{X}_0, t)\,, \tag{5.4}$$

being $\mathbf{X}(\mathbf{X}_0, t)$ the position of the phase-space that the system occupies after a time t, if it starts in $\mathbf{X}_0$ at time 0. Exploiting formulation (5.3) of the Hamilton equations, it is easy to prove a well-known theorem (Poincaré [148]) which assures that $\boldsymbol{\varphi}_t$ is symplectic for any time t.

5.1.1 Symplectic algorithms

In Statistical Physics, molecular dynamics simulations are often employed to sample the phase-space of a certain system at fixed energy E; assuming ergodicity, an average of some mechanical observable over long time-trajectories of the system is equivalent to a microcanonical average at energy E. Let us remark that, strictly speaking, ergodicity in generic Hamiltonian systems does not hold; however one can fairly assume its validity for a certain class of interesting functions, those obtained as averages over a large number of particles [104]. As a consequence, an important point in the choice of the integration algorithm concerns its ability to conserve energy up to very long times in Hamiltonian systems.

It has been shown [17] that conservation of total energy is strictly related, in numerical integration algorithms, to symplecticity. Let us call h the time-step, and let us assume that each iteration is constituted by a transformation $\mathbf{f}_h$ such that:

1. its Jacobian matrix M verifies condition (5.1);
2. $\mathbf{f}_h$ reduces to the identity in the limit $h \to 0$;
3. the error with respect to the true dynamics is of order $O(h^{n+1})$, i.e.

$$|\mathbf{f}_h(\mathbf{X}_0) - \boldsymbol{\varphi}_h(\mathbf{X}_0)| \simeq O(h^{n+1})\,,$$

with $n \geq 1$(in this case the algorithm is said to be "of order n").

If the above conditions hold, it can be proved that energy conservation holds, within an error $O(h^n)$, up to times exponentially long in h^{-1}.

Moreover, the dynamics described by such update, leaving apart the effects related to numerical roundoff error, is exponentially close to the flow $\tilde{\boldsymbol{\varphi}}_t(\mathbf{X}_0)$ of some Hamiltonian $\tilde{\mathcal{H}}$, which differs from the original Hamiltonian $\mathcal{H}$ only up to terms of order $O(h^n)$. In particular, it can be shown that

$$|\mathbf{f}_h^{(k)}(\mathbf{X}_0) - \tilde{\boldsymbol{\varphi}}_{kh}(\mathbf{X}_0)| < C_1 e^{-C_2/h}\left(e^{C_3 kh} - 1\right)\,, \tag{5.5}$$

where $\mathbf{f}_h^{(k)}$ is the transformation obtained by the composition of k iterations $\mathbf{f}_h$, i.e. the result of the simulation at time $t = kh$, while C_1, C_2 and C_3 are constants of

order 1. The above result implies that such distance possibly diverges only after $k \simeq h^{-2}$ iterations, corresponding to times of order h^{-1}. Let us stress that after such (quite long) time the trajectory of the simulation could possibly diverge from that of the original system; also in this case, however, the dynamics will stay on the constant-energy surface, up to an error $O(h^n)$, due to the previous result on energy conservation.

5.1.2 The generalized Verlet algorithm

One of the most popular symplectic integrators is the so-called "Verlet algorithm" [191]. In its version for separable Hamiltonians with generic kinetic terms,

$$\mathcal{H}(\mathbf{p},\mathbf{q}) = \mathcal{K}(\mathbf{p}) + \mathcal{U}(\mathbf{q})\,, \tag{5.6}$$

it reads

$$\begin{cases} \mathbf{p}^\star = \mathbf{p}_0 - \frac{h}{2}\boldsymbol{\nabla}_\mathbf{q}\mathcal{U}(\mathbf{q}_0) \\ \mathbf{q}_h = \mathbf{q}_0 + h\boldsymbol{\nabla}_\mathbf{p}\mathcal{K}(\mathbf{p}^\star) \\ \mathbf{p}_h = \mathbf{p}^\star - \frac{h}{2}\boldsymbol{\nabla}_\mathbf{q}\mathcal{U}(\mathbf{q}_h) \end{cases} \quad \text{or} \quad \begin{cases} \mathbf{q}^\star = \mathbf{q}_0 + \frac{h}{2}\boldsymbol{\nabla}_\mathbf{p}\mathcal{K}(\mathbf{p}_0) \\ \mathbf{p}_h = \mathbf{p}_0 - h\boldsymbol{\nabla}_\mathbf{q}\mathcal{U}(\mathbf{q}^\star) \\ \mathbf{q}_h = \mathbf{q}^\star + \frac{h}{2}\boldsymbol{\nabla}_\mathbf{p}\mathcal{K}(\mathbf{p}_h) \end{cases} \tag{5.7}$$

("Velocity Verlet Update" and "Position Verlet Update", respectively). The subscripts 0 and h identify the values of the canonical variables before and after the integration step, while $\mathbf{p}^\star$ and $\mathbf{q}^\star$ are temporary variables.

To show that the above integrators are symplectic, let us first notice that they can be obtained as compositions of the two Euler algorithms

$$\begin{cases} \mathbf{p}_k = \mathbf{p}_0 - k\boldsymbol{\nabla}_\mathbf{q}\mathcal{U}(\mathbf{q}_0) \\ \mathbf{q}_k = \mathbf{q}_0 + k\boldsymbol{\nabla}_\mathbf{p}\mathcal{K}(\mathbf{p}_k) \end{cases} \quad \text{and} \quad \begin{cases} \mathbf{q}_k = \mathbf{q}_0 + k\boldsymbol{\nabla}_\mathbf{p}\mathcal{K}(\mathbf{p}_0) \\ \mathbf{p}_k = \mathbf{p}_0 - k\boldsymbol{\nabla}_\mathbf{q}\mathcal{U}(\mathbf{q}_k)\,, \end{cases} \tag{5.8}$$

choosing $k = h/2$. A well-known result from Hamiltonian theory states that a transformation $\mathbf{f} : (\mathbf{p},\mathbf{q}) \to (\mathbf{P},\mathbf{Q})$ is symplectic if and only if

$$\mathbf{Q}\cdot d\mathbf{P} + \mathbf{p}\cdot d\mathbf{q} = d(\mathbf{P}\cdot d\mathbf{q} + F_2) \text{ for some function } F_2(\mathbf{P},\mathbf{q})$$

or, equivalently,

$$\mathbf{P}\cdot d\mathbf{Q} + \mathbf{q}\cdot d\mathbf{p} = d(\mathbf{p}\cdot d\mathbf{Q} - F_3) \text{ for some function } F_3(\mathbf{p},\mathbf{Q})\,.$$

It is easy to show that both Euler integrators verify such condition, the first with $F_2(\mathbf{P},\mathbf{q}) = h\mathcal{H}(\mathbf{P},\mathbf{q})$, the second with $F_3(\mathbf{p},\mathbf{Q}) = h\mathcal{H}(\mathbf{p},\mathbf{Q})$. They are thus symplectic and, as a consequence, also their compositions (5.7) share this property.

Verlet algorithm is second order. To prove this property, it is sufficient to observe that (5.7), up to order $O(h^2)$, reads

$$\begin{aligned} \mathbf{q}_h &\simeq \mathbf{q}_0 + h\boldsymbol{\nabla}_\mathbf{p}\mathcal{K}(\mathbf{p}_0) - \frac{h^2}{2}\boldsymbol{\nabla}_\mathbf{p}\left[\boldsymbol{\nabla}_\mathbf{p}\mathcal{K}(\mathbf{p}_0)\cdot\boldsymbol{\nabla}_\mathbf{q}\mathcal{U}(\mathbf{q}_0)\right] \\ \mathbf{p}_h &\simeq \mathbf{p}_0 - h\boldsymbol{\nabla}_\mathbf{q}\mathcal{U}(\mathbf{q}_0) + \frac{h^2}{2}\boldsymbol{\nabla}_\mathbf{q}\left[\boldsymbol{\nabla}_\mathbf{p}\mathcal{K}(\mathbf{p}_0)\cdot\boldsymbol{\nabla}_\mathbf{q}\mathcal{U}(\mathbf{q}_0)\right]\,, \end{aligned} \tag{5.9}$$

which is exactly the $O(h^2)$ Taylor expansion of the Hamilton dynamics.

5.2 Quasi-symplectic algorithms for LE with generalized kinetic energy

In this Section we introduce a stochastic Verlet-like integrator that can be used to simulate Hamiltonian systems with generic kinetic terms, subjected to a thermal bath at fixed β. This algorithm is also considered in Ref. [135].

We search for a simulation scheme able to reproduce the "generalized" LE discussed in Section 3.1.3

$$\dot{\mathbf{X}} = \begin{pmatrix} \dot{q} \\ \dot{p} \end{pmatrix} = \begin{pmatrix} \partial_p \mathcal{K} \\ -\partial_q \mathcal{U} - D\beta \partial_p \mathcal{K} + \sqrt{2D}\xi(t) \end{pmatrix} \tag{5.10}$$

where $\xi(t)$ is a white noise with unitary variance and D is a positive constant. Here we consider a one-dimensional dynamics; the discussion can be straightforwardly generalized to the multi-dimensional case.

Since in the limit $D = 0$ the dynamics reduces to that of an isolated Hamiltonian system, it is quite natural to ask that the algorithm becomes symplectic in this limit. This problem has been addressed in Ref. [133] for the case of quadratic kinetic energy: in the following we apply the same reasoning to a wider class of Hamiltonian systems.

It can be shown [83] that the integration of Eq. (5.10) over a time-step h leads to errors of order $h^{3/2}$ if the deterministic and the stochastic parts are evolved independently. In order to improve the stability of the algorithm one can alternate the integrations of position and momentum during the single time-step of total length h, as it happens in the usual Position Verlet discussed in the previous Section. We first evolve the position for a time-interval $h/2$, then the momentum advances for a time h, and finally we evolve again the position for the remaining half time-step $h/2$.

Specifically, the integration of the position for half time-step $h/2$ can be trivially written as

$$q_{h/2} \simeq q_0 + \partial_p \mathcal{K}(p_0)\frac{h}{2} + O(h^2) \tag{5.11}$$

where (q_0, p_0) is the state for the considered degree of freedom at time t_0.

We are left with the problem of evolving the momentum for a time-step h; we have to solve the following stochastic differential equation:

$$\dot{p} = F_0 - D\beta \partial_p K(p) + \sqrt{2D}\xi(t) \tag{5.12}$$

where $F_0 = -\partial_q \mathcal{U}(q_{h/2})$. If $\mathcal{K}(p) = p^2/2m$, an exact solution of such equation can be found; in the general case we can rely on the approximation

$$\partial_p K(p) \simeq \partial_p K\Big|_{p_0} + \partial_p^2 K\Big|_{p_0}(p - p_0) + O[(p - p_0)^2]\,. \tag{5.13}$$

Substituting the above expression into Eq. (5.12) we get an equation of the form

$$dp = (A + Bp)dt + \sqrt{2D}dw\,, \tag{5.14}$$

where we are neglecting terms of order dt^2 and

$$\begin{aligned} A &= -\partial_q H\Big|_{q^\star} - D\beta\left(\partial_p K\Big|_{p_0} - \partial_p^2 K\Big|_{p_0} p_0\right) \\ B &= -D\beta\partial_p^2 K\Big|_{p_0} \end{aligned} \tag{5.15}$$

are constant during the integration step. The above equation can be solved [65].

Combining the above evolutions for position and momentum, the final result is a Position Verlet-like integration scheme:

$$\begin{cases} q^\star = q_0 + \partial_p K\Big|_{p_0}\frac{h}{2} \\ p_h = e^{Bh}p_0 + \frac{A}{B}(e^{Bh}-1) + \sqrt{2D}\mathcal{N}\left(\frac{1}{2B}(e^{2Bh}-1)\right) \\ q_h = q^\star + \partial_p K\Big|_{p_h}\frac{h}{2}\,, \end{cases} \tag{5.16}$$

where $\mathcal{N}(x)$ is a random Gaussian variable with zero mean and variance x. An equivalent Velocity Verlet-like algorithm can be found by inverting the integration order.

5.3 Inferring LEs from data

In this Section we discuss the numerical method that has been employed in Chapter 3 to infer drift and diffusivity terms for Langevin Equations of some quantity from data. The basic idea is to exploit well-known relations between such functions and suitable conditioned moments of the stochastic dynamics. This approach has been used in several contexts, ranging from physics to biology and finance [63, 147, 14].

5.3.1 Method

Let us consider a Markovian stochastic process $x(t)$, whose dynamics is described by the Langevin Equation

$$\dot{x} = F(x) + \sqrt{2D(x)}\xi\,, \tag{5.17}$$

where $\xi(t)$ is a delta-correlated noise with zero mean and unitary variance. Here we consider the one-dimensional case, but, as it is shown in the next sections, the discussion can be easily generalized to the multi-dimensional case. It is well known that the drift term $F(x)$ and the diffusivity $D(x)$ can be computed, in principle, from the temporal evolution of x by using the relations [65]

$$F(x_0) = \lim_{\Delta t\to 0}\frac{1}{\Delta t}\langle \Delta x | x(t_0) = x_0\rangle \tag{5.18a}$$

$$D(x_0) = \lim_{\Delta t\to 0}\frac{1}{2\Delta t}\left\langle [\Delta x - F(x)\Delta t]^2 \Big| x(t_0) = x_0\right\rangle\,, \tag{5.18b}$$

where Δt is a time interval and

$$\Delta x = x(t_0+\Delta t) - x(t_0)\,. \tag{5.19}$$

In other words, we can estimate the numerical value of the Langevin coefficients as functions of x_0 by looking at the average behavior of the trajectory after it passes through x_0. In what follows we face the problem of the practical application of the above idea to discrete temporal series of data $x(kdt)$, where dt is the time-step and k is an integer, as those typically produced by a numerical simulation or acquired during a real experiment.

A first issue comes from the fact that we need to evaluate averages which are conditioned to the realization of the event $x(t) = x_0$, i.e. a condition which, strictly speaking, is verified with zero probability if the trajectory is discretized in time. This problem can be clearly bypassed by discretizing also the space. Specifically, let $I = (a, b)$ be a typical range for the considered stochastic process $x(t)$, i.e., such that the time which $x(t)$ spends outside the interval I is negligible with respect to that of the whole trajectory. We can divide I into n smaller intervals $I_1, I_2, ..., I_n$ of equal length; every N time steps the algorithm checks in which interval the variable $x(t)$ is situated, namely for what j (if any) the relation $x(t) \in I_j$ holds; then it measures the value of $x(t + \Delta t) - x(t)$ (for several Δt). In order to avoid correlations, the delay Ndt between two measures has to be chosen $\geq \tau$, where τ is a typical decorrelation time of the considered dynamics. At the end of the process, conditioned averages on the r.h.s. of equations (5.18) can be computed as functions of both j and Δt; the dependence on j is then replaced by that on the central value of the corresponding bin. Let us stress that such approximation is meaningful if the drift and diffusivity terms are not expected to vary too much on a scale $(b - a)/n$.

Once the quantities on the r.h.s. of Eqs. (5.18) have been estimated as functions of x_0 and Δ, we are left with the problem of inferring the limit $\Delta t \to 0$. One could be tempted to take a very small value of Δt, say $\Delta t \ll \tau$, and evaluate the conditioned averages for that value. For instance, one could consider the time interval between two subsequent data acquisitions. In most cases, however, this choice needs some additional care; indeed, physically meaningful processes can be usually approximated as a stochastic process of the form (5.17) only on suitably large time scales, while for shorter times the motion is deterministic. It is well known that the autocorrelation functions $C_D(t)$ and $C_L(t)$ in a deterministic and in a Langevin process, respectively, can be expanded as

$$C_D(t) = 1 - \frac{t^2}{\tau_D^2} + O(t^3) \tag{5.20a}$$

$$C_L(t) = 1 - \frac{t}{\tau_L} + O(t^2)\,, \tag{5.20b}$$

for small times t. Comparing the two expressions, one finds that the differences between C_D and C_L are not negligible, at least until some typical time $\tau_M \sim O\left(\frac{\tau_D^2}{\tau_L}\right)$. This observation is a clear hint that a deterministic motion cannot be approximated as a stochastic process on time-scales smaller than such τ_M. This threshold is sometimes called "Markov-Einstein time" [63].

At a practical level, a good strategy consists in evaluating the quantities (5.18) (for a fixed starting value x_0) as functions of the time interval Δt, then looking at their behavior in a range $\tau_M < \Delta t < \tau$, fitting it with some low-order polynomial and extrapolating the limit $\Delta t \to 0$ from the inferred function. In the following Section we illustrate this procedure with an example.

5.3.2 A first test on a Hamiltonian system

First, we will test our procedure on a Hamiltonian system which is well-known to reproduce the Brownian motion in the thermodynamic limit, i.e. a harmonic chain with an heavy "intruder":

$$\mathcal{H} = \frac{P^2}{2M} + \sum_{i=\pm 1,\ldots,\pm N} \frac{p_i^2}{2m} + \frac{k}{2} \sum_{i=-N}^{N+1} (q_i - q_{i-1})^2, \qquad Q \equiv q_0 \,. \tag{5.21}$$

Here (p_i, q_i), $i = -N, ..., -1, 1, ..., N$ are the canonical coordinates of the "light" particles, with equal masses m, while (P, Q) are those of the heavy intruder of mass $M \gg m$; k is the elastic constant. We consider fixed boundary conditions $q_{-N-1} \equiv q_{N+1} \equiv 0$. The above model, and other similar harmonic chains, have been analytically studied since the 1960's and represent one of the few examples in which stochastic differential equations can be exactly derived starting from first principles [162, 186, 59, 200].

Hamiltonian (5.21) is integrable, so that the energy assigned to each normal mode at the beginning of the dynamical evolution is conserved; as a consequence, if the system is initialized in such a way that energy is shared among only few degrees of freedom, thermodynamic equilibrium will never be reached and the Langevin description (3.2) will necessarily fail. If, conversely, the system starts at equilibrium, it can be rigorously shown that the dynamics of P is approximated by a Markovian stochastic process, whose autocorrelation function reads

$$C(t) \simeq \exp\left(-\frac{2\sqrt{km}}{M} t\right) + O(m/M) \,. \tag{5.22}$$

In order to check the validity of the extrapolation method discussed in the previous Section we can perform computer simulations of system (5.21) and compare the effective behavior of the slow particle with the stochastic description given by Eq. (5.17). We numerically simulate Hamiltonian (5.21) with a standard velocity Verlet update, choosing the time-step in such a way that the relative fluctuations on the total energy are of order $O(10^{-5})$. We start from equilibrium initial conditions. The numerical integration of the whole system results in a discretized time-series of $P(t)$, from which we can extrapolate $F(P)$ and $D(P)$ following the procedure discussed above.

Fig. 5.1 shows the conditioned averages (5.18) as functions of Δt, for several starting values P_0. As discussed before, at very small time scales the process is not expected to be described by a LE, so that it is reasonable to fit the data on intermediate time-scales. Fig. 5.2 shows the functional forms of drift and diffusivity extrapolated from the $\delta t \to 0$ limit of the fitting functions found in Fig. 5.1. As expected, the drift linearly depends on the momentum and the diffusivity is constant. By the way, relation (3.21) is also verified.

To check the goodness of our extrapolation method one could, of course, compare the results to the analytical predictions valid for $M/m \to \infty$ in the thermodynamic limit. In this case, anyway, the resulting deviation of the measured values from the theoretical ones would be affected not only by the actual errors in the extrapolation procedure, but also by the fact that considering $P(t)$ as a stochastic process is by

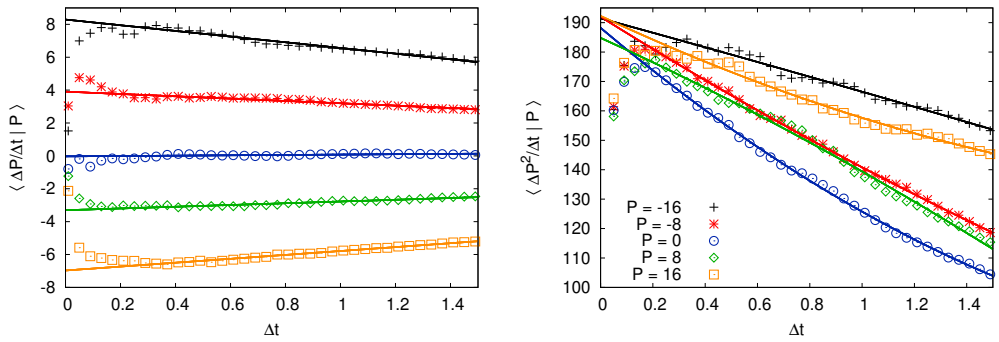

Figure 5.1. Evaluation of the conditioned moments on the r.h.s. of Eq. (5.18). We numerically compute such quantities as functions of Δt (points), then we fit the curves with low-order polynomials (solid lines) and we consider the limits for $\Delta t \to 0$. Left: r.h.s. of Eq. (5.18)a, linear fit. Right: r.h.s. of Eq. (5.18)b, parabolic fit. Different colors and shapes of the points correspond to different values of the initial value of P. All fits are computed between $\Delta t = 0.25$ and $\Delta t = 1.5$. Parameters of the simulation $M = 200$, $m = 1$, $k = 2500$, $2N = 2000$, $\beta \simeq 1.0$. Figure from Ref. [12].

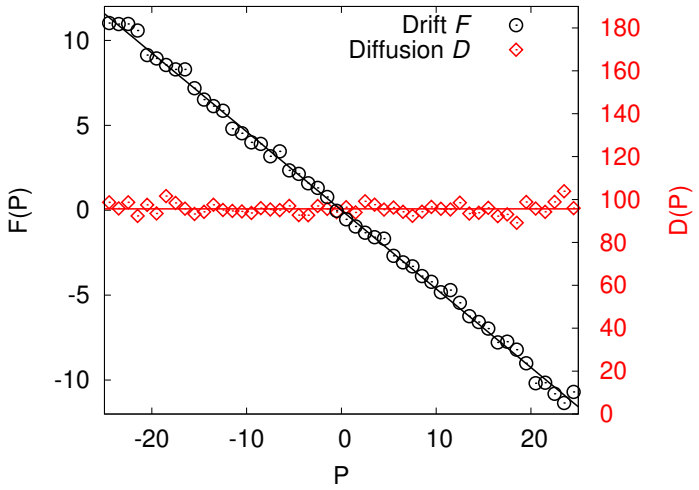

Figure 5.2. Drift term $F(P)$ and diffusivity $D(P)$ of the process $P(t)$ as determined by the data-driven procedure discussed in the text. Red circles (black diamonds) represent the values obtained for the drift (diffusivity) from the limits (5.18); solid lines are linear fits. Figure from Ref. [12].

itself an approximation. At least in the case of the harmonic chain, however, we can do better than this: since the conditioned p.d.f of P is known, there is an easy way to compute the Langevin parameters from data without performing the limit $\Delta t \to 0$, and we can compare these values to the results of the previous method in order to estimate the precision of the extrapolation.

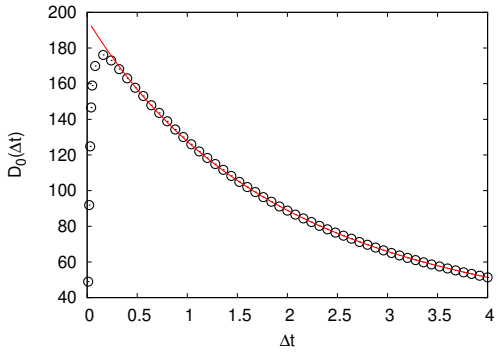

Figure 5.3. Evolution of $D_0(\Delta t)$ with the time interval. The red line is the result of a fit with the functional form (5.25). Figure from Ref. [12].

To this end, let us note that since the conditioned p.d.f. of P is given by [162]:

$$f(P(t+\Delta t)|P(t)) = \frac{1}{\sqrt{2\pi k_B T M(1-C(\Delta t)^2)}} \exp\left\{-\frac{[P(t+\Delta t)-P(t)C(\Delta t)]^2}{2k_B T M(1-C(\Delta t)^2)}\right\}, \tag{5.23}$$

we can explicitly compute the averages in equation (5.18), assuming that the Markovian limit holds and that the autocorrelation function actually verifies $C(\Delta t) = \exp(-\Delta t/\tau)$ for some τ. For the diffusion term we get

$$\frac{1}{\Delta t}\langle \Delta P(\Delta t)^2 | P(t) = P\rangle = D_0(\Delta t) + D_1(\Delta t)P^2 \tag{5.24}$$

where

$$D_0(\Delta t) = \frac{k_B T M}{\Delta t}\left(1 - e^{-2\Delta t/\tau}\right), \qquad D_1(\Delta t) = \frac{\left(1-e^{-\Delta t/\tau}\right)^2}{\Delta t} P^2 . \tag{5.25}$$

We can fit our data with the previous formulae: in particular, from the fit of $D_0(\Delta t)$ (Figure 5.3), we can infer both T and τ and calculate the corresponding values of drift and diffusion for Brownian motion [65],

$$F(P) = -P/\tau , \qquad D(P) = 2Mk_B T/\tau .$$

The resulting values and the previously extrapolated coefficients differ by less than 3%, which is a quite satisfactory precision for our qualitative analysis.

In order to check that the reconstructed LE actually reproduces the behavior of the slow particle, we can do an additional check: we can compute the steady probability density and the autocorrelation function in this new coarse-grained dynamics and compare them to the original, deterministic evolution. In this simple case, since the dynamics is linear, we can determine such observables analytically once we know $F(P)$ and D; in more complex cases one can rely on numerical simulations of the stochastic process. Fig. 5.4(a) shows both quantities in the original and in the reconstructed dynamics: the agreement is quite good. Finally, we have

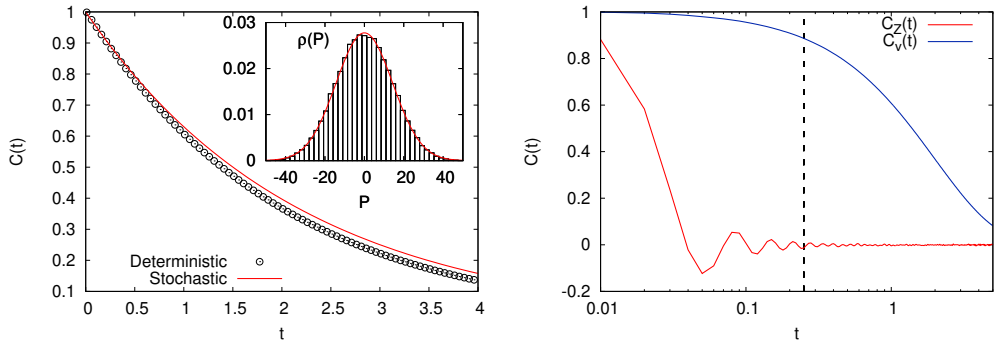

Figure 5.4. Left: autocorrelation function of the velocity in the original dynamics (circles) and in the reconstructed stochastic process (solid line). In the inset, the steady probability density functions for the deterministic evolution (boxes) and for the stochastic one (solid red line) are compared. Right: autocorrelation function of the velocity (blue) compared to the one of the "thermal noise" defined by Eq. (5.26) (red). Figure from Ref. [12].

to check that time-scale separation hypothesis is valid, i.e. that the "thermal noise"

$$\zeta(t) = \dot{P}(t) - F(P(t)) \tag{5.26}$$

decorrelates much faster than P. The autocorrelation functions of the two quantities are shown in Fig. 5.4(b): the time-scale separation is evident.

5.3.3 Some remarks on the method

The method discussed here is quite general and can be applied in a variety of contexts. However one should always keep in mind that the success of this technique relies on the possibility to approximate a given series of data $x(t)$ as a Markovian stochastic process described by the LE (5.17), at least on suitably large time-scales. This point is not trivial at all.

First, let us stress that the presence of a mechanism which induces time-scale separation between a fast "noise" and a slow systematic drift is not sufficient, in general, to imply the Markovianity of the process. The dynamics could keep some memory of the previous values of the considered variable, resulting in a failure of the described procedure. A typical scenario of this kind happens when we deal with a two-dimensional Markov process and we focus only on the time series of a single component of the vector.

It is easy to understand that the first, crucial step when one tries to build an effective stochastic equation from data is the selection of the "right" set of variables, i.e. a vector of quantities whose coupled evolution can be fairly approximated by a memoryless stochastic process. This observation can be found in the seminal work by Onsager and Machlup on fluctuations and irreversible processes [143].

Several systematic methods have been developed to give a partial answer to this problem. The most widely used is *principal component analysis* (PCA) [98], which searches for independent linear combinations of available observables with maximal variance. *Dynamic mode decomposition* (DMD) [185], *variational approach of*

conformation dynamics (VAC) [141], *time-lagged independent component analysis* (TICA) [136] are some of the many, related, techniques used to project the evolution of the coordinates describing the full system into a smaller set of relevant variables [109]. This is usually done by considering linear combinations of the original ones and exploiting the methods of linear algebra. In recent years, neural networks and deep learning techniques have been applied to enhance such algorithms; specifically, they can select combination of nonlinear functions (from libraries of possible candidates) to encode original data into a space with reduced dimension [195, 24].

However, no matter if the set of variables is chosen by a systematic approach or based on physical intuition, the best way to be sure that the dynamics could be actually approximated by a Markov process in lower dimension is to check, a posteriori, that the inferred LE fairly reproduces interesting dynamical observables. The next Section is devoted to the illustration of a concrete example in which these remarks are crucial.

5.4 A case with two variables: a simple model for polymer translocation

So far we have discussed an algorithmic procedure to infer a LE from series of data and, to check its validity, we have applied it to an exactly solvable case. Now we will examine its applicability to a far less trivial case, where the considered process describes an activated dynamics. In this context, the role played by the Markovianity assumption results completely clear; in particular, for some choices of the external parameters it will be necessary to enlarge the set of considered variables, in order to achieve a satisfactory description. The results presented here are discussed in Ref. [9].

5.4.1 Model and simple remarks

Let us consider the problem of a polymer crossing the barrier of a double-well energy profile, which is related to the transport of biomolecules across nano-scale pores [19, 101, 134, 86, 3, 171]. In many practical situations channels are so narrow that the transport dynamics of biopolymers and ions occurs on a single axis, thus, as a matter of fact, it can be considered one-dimensional [48, 122, 4, 96]. In this crude approximation, the polymer is composed by a chain of N beads (point particles), interacting via nearest-neighbors forces and subjected to a thermal noise at temperature T.

The nanopore is portrayed as a region of the translocation axis where the polymer feels the effect of an energy barrier, which acts independently on each particle and separates the left-side and right-side of the pore [140, 3, 149]. As customary, in this kind of phenomenology we can assume the evolution of each monomer to be accessible on time-scales long enough to neglect the effect of inertia. Accordingly,

the polymer beads are governed by the overdamped Langevin dynamics:

$$\begin{aligned} \gamma\dot{x}_1 &= -V'(x_1) + U'(x_2 - x_1) + \xi_1 \\ \gamma\dot{x}_i &= -V'(x_i) + U'(x_{i+1} - x_i) - U'(x_i - x_{i-1}) + \xi_i \\ \gamma\dot{x}_N &= -V'(x_N) - U'(x_N - x_{N-1}) + \xi_N \end{aligned} \tag{5.27}$$

with $i = 2, \ldots, N-1$, where x_j is the position of the j-th bead. V represents here the external potential, due to the nanopore action on the chain. U is the nearest-neighbor interparticle potential that is chosen to be an even and convex function of $x_i - x_{i-1} - \sigma$, where σ is the equilibrium distance between consecutive particles. Each ξ_i is a Gaussian noise, with average $\langle \xi_i(t) \rangle = 0$ and correlation $\langle \xi_i(0)\xi_j(t) \rangle = 2\gamma T \delta_{ij}\delta(t)$, where γ is a dimensional constant, that we will put equal to 1 in the following.

In order to study the collective dynamics of the polymer we need to identify proper reaction coordinates (RCs) that describe the state of the system, and then we have to infer effective equations for their evolution.

A natural choice seems to be the center of mass Q of the polymer, which roughly indicates the spatial position of the chain:

$$Q = \frac{1}{N} \sum_{i=1}^{N} x_i \,. \tag{5.28}$$

Its dynamical equation is obtained by just summing up Eqs. (5.27) for all the particles and dividing by N,

$$\dot{Q} = -\frac{1}{N} \sum_{i=1}^{N} V'(x_i) + \sqrt{\frac{2T}{N}}\, \eta_Q \tag{5.29}$$

where the reciprocal elimination of internal forces has been taken into account, as well as the mutual independence of the noises $\{\xi_i\}$ that combine into a delta-correlated Gaussian noise with zero mean and such that $\langle \eta_Q(0)\eta_Q(t) \rangle = \delta(t)$.

By posing $x_i = Q + u_i$, Eq. (5.29) can be recast as

$$\dot{Q} = -\frac{1}{N} \sum_{i} V'(Q + u_i) + \sqrt{\frac{2T}{N}}\, \eta_Q \,. \tag{5.30}$$

The above equation is formally exact, but it is not very useful in this form, since it depends on all the u_i terms.

The simplest approximation that can be done to achieve a closed form for Eq. (5.30) is to assume that the force term due to the external potential can be written as a (possibly complicated) function of Q only. In this case, a one-variable, memoryless model of the kind

$$\frac{dQ}{dt} = F(Q) + \sqrt{2D}\, \eta_Q \,, \tag{M1}$$

should catch the relevant features of the macroscopic evolution of the system, where $D = T/N$. Assuming that the above approximation holds, the specific form of $F(Q)$ can be inferred from data with the method discussed in Section 5.3.

Let us notice that Eq. (M1) describes a Markovian stochastic process for the variable Q, and it is expected to give a reasonable approximation of the real dynamics only when the knowledge of Q suffices to determine the macroscopic state of the system. For instance, Eq. (M1) gives a good approximation of the real dynamics in the limit of high-rigidity chain.

In general, however, the above one-variable model will not be valid, meaning that it will not be possible to find any form of $F(Q)$ able to reproduce the dynamical properties of the original system in an accurate way. This is due to the fact that the dynamics of Q, in general, is not Markovian: in order to achieve a satisfactory coarse-grained description, one possibility is to modify Eq. (M1) by introducing memory-dependent terms, which in some cases can be found analytically by mean of projection methods [199, 200, 74]. To avoid such dependence on memory kernels, which are often difficult to manipulate, the only possibility is to search for (at least) a second RC of the system, such that the vector composed by Q and this new variable obeys a Markovian dynamics.

The additional RC can be individuated through the methods briefly mentioned in the previous Section, or it can be suggested by physical intuition. In our case, if the bond fluctuations are large enough, it is reasonable that the elongation $L = x_N - x_1$ have a role in the macroscopic dynamics. We can then guess an effective model of the form:

$$\begin{cases} \dfrac{dQ}{dt} = F_Q(Q, L) + \sqrt{2D_Q}\,\eta_Q \\ \\ \dfrac{dL}{dt} = F_L(Q, L) + \sqrt{2D_L}\,\eta_L\,. \end{cases} \tag{M2}$$

Again, assuming that the dynamics of (Q, L) is fairly described by a Markov process, the best choices for F_Q, F_L, D_Q, D_L can be found with the data-driven approach discussed before. However, one has then to verify that the chosen RCs are actually "valid" macroscopic variables, i.e. that the coarse-grained dynamics (M2) reproduces the macroscopic features of the original system.

In the remaining part of this Section, we will try to implement this program in a specific case. In particular we will show that, as expected, the stiffness of the polymer plays an important role in the choice of the right set of RCs.

We consider now the case in which the external potential $V(x)$ in Eq. (5.27) is a double-well. This simple model allows us to study some properties of thermally activated barrier crossing as, for instance, the dependence of the jump rate r on the physical parameters. The general problem of activated dynamics has been extensively studied since the seminal work by Kramers, and the reaction-rate theory provides many analytic methods to compute jump times in different contexts (see Ref. [80] and reference therein). Important results have been derived also for polymeric chains [99, 172, 171].

The external potential reads, in this case,

$$V(x) = \frac{B^2}{4}(x^2 - A^2)^2 \tag{5.31}$$

where A and B are suitable constants. The typical dynamics of the center of mass, $Q(t)$, is therefore characterized by jumps over the barrier separating the two minima

of the potential (two-state model). For the interaction potential we choose the form $U(r) = K(r-\sigma)^2/2$.

In the following, we will always consider the limit $N\sigma \simeq A$, i.e. the case in which the equilibrium length of the polymer is comparable to the half distance between the well minima: it is reasonable to expect that in these conditions the value of the bond rigidity affects the qualitative behavior of the chain in a relevant way.

Our aim is to show that for high values of K the model described by Eq. (M1) suffices to reproduce the quantitative macroscopic behavior of the system; whereas, as soon as K becomes comparable to B^2A^2/σ, the evolution of Q is no more Markovian and any attempt to describe it through model (M1) is doomed to failure. However, if the phase-space is expanded by including a suitable additional RC, it is still possible that the evolution of the new RCs vector turns out to be Markovian, so that a dynamical description based on Eq. (M2) can be accurate enough.

The validity of such scenario can be tested by using the data-driven approach discussed in the previous Section. We first perform numerical simulations of the whole system by using a Stochastic Runge-Kutta algorithm [83] and measuring the relevant RCs of the system at every time step. As a first attempt, from long time-series of such data we build an effective stochastic equation for Q only, in the form of Eq. (M1); then we apply the extrapolation procedure to the dynamics of the two-dimensional vector (Q, L), obtaining an M2-like model. The "goodness" of M1 and M2 is tested by measuring the Kramers' transition times of the reconstructed models and comparing the corresponding jump rates to the original ones.

5.4.2 1-variable model

Before applying the mentioned extrapolation method to infer numerically the functional form of the terms appearing in Eq. (M1), let us derive analytically an effective equation for Q for the high-stiffness limit, $K \gg B^2A^2/\sigma$. In this case we can assume that the position of two consecutive beads is fixed and equal to σ. Due to the simple form of the external potential $V(x)$, the drift term in Eq. (5.30) can be exactly computed in this case:

$$\begin{aligned} -\frac{1}{N}\sum_{i=1}^{N} V'(Q+u_i) &= -\frac{B^2}{N}\sum_{i=1}^{N}\left[(Q+u_i)^3 - A^2(Q+u_i)\right] \\ &= -\frac{B^2}{N}\sum_{i=1}^{N}\left[3Qu_i^2 + Q^3 - A^2Q\right] . \end{aligned} \tag{5.32}$$

where we have used the fact that, due to the rigidity of the polymer, $\sum_i u_i^3 = \sum_i u_i = 0$.

Now we substitute the explicit expression for the relative positions of the polymer beads, $u_i = (2i - N - 1)\sigma/2$, and after straightforward algebra we get

$$\begin{aligned} -\frac{1}{N}\sum_{i=1}^{N} V'(x_i) &= -B^2Q\left(Q^2 - A^2 + \frac{\sigma^2}{4}(N+1)(N-1)\right) \\ &= -B^2Q\left(Q^2 - A^2_{\text{eff}}\right) \end{aligned} \tag{5.33}$$

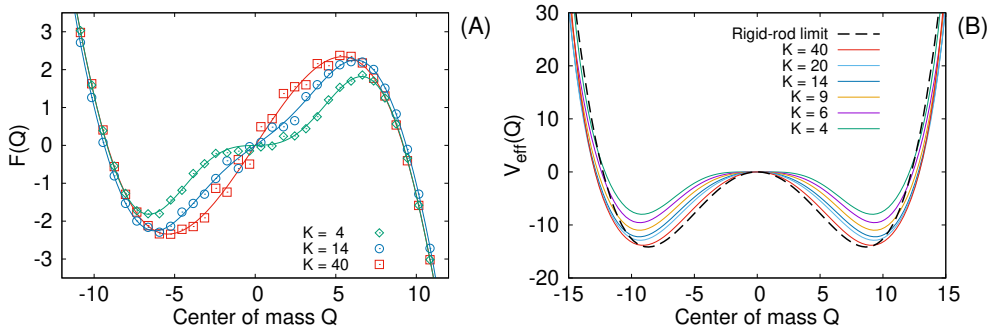

Figure 5.5. (A): drift term $F(Q)$ of model (M1) as reconstructed from data (points) and fitted with a 9-th degree odd polynomial (solid lines), for three different values of K. (B): Effective potential obtained by integration of $F(Q)$. Parameters for the simulations of the complete system: $A = 10$, $B = 0.1$, $T = 30$, $\sigma = 1$, using a time-step $dt = 10^{-5}$. Simulations on model (M1) have been run with a time-step $dt = 10^{-4}$.

with

$$A_{\text{eff}} = A\sqrt{1 - \frac{L^2(N+1)}{4A^2(N-1)}}\,, \tag{5.34}$$

where we have used the definition of the polymer length for the rigid case, $L = (N-1)\sigma$. Let us notice that the above drift corresponds to an effective potential

$$V_{\text{eff}}(Q) = \frac{B^2}{4}(Q^2 - A_{\text{eff}}^2)^2\,, \tag{5.35}$$

i.e. a "rescaled" version of the original external potential (5.31).
We can now use the theory of escape times [65] to estimate the jump rate r for the effective potential (5.35). The average waiting time between two consecutive jumps can be computed through the formula [65]

$$\begin{aligned}\tau =& \frac{1}{D}\int_{-A}^{A} dy\, e^{V(y)/D}\int_{-\infty}^{y} dz\, e^{-V(z)/D} \\ =& \frac{1}{D}\int_{-A}^{A} dy\, e^{\frac{B^2}{4D}\left[y^4 - 2A_{\text{eff}}^2 y^2\right]}\int_{-\infty}^{y} dz\, e^{-\frac{B^2}{4D}\left[z^4 - 2A_{\text{eff}}^2 z^2\right]}\end{aligned} \tag{5.36}$$

where $D = T/N$ is the diffusivity associated to Q. The jump rate r is then found as

$$r = \frac{1}{\tau}\,. \tag{5.37}$$

The above equations, which are only valid in the rigid-rod limit, will be a useful touchstone to evaluate the level of accuracy of the model inferred numerically.

We apply now the extrapolation method to infer the right functional forms for the terms of the Langevin equation (M1), assuming that the dynamics of Q is Markovian and a 1-variable description in the form of model (M1) holds. We find that D (not shown here) is always basically constant and equal to T/N, as it would be expected if the process was Markovian, while the drift shows a more complex shape (Fig. 5.5A); we fit the data by a 9-th degree, odd polynomial, then

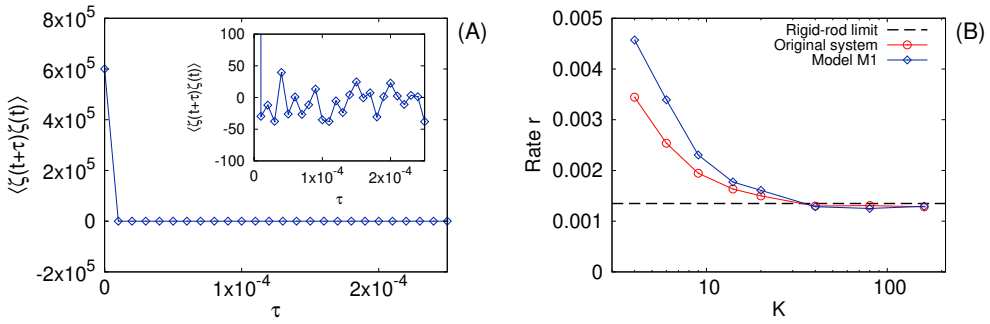

Figure 5.6. Checking the validity of model (M1). (A) Autocorrelation $\langle \zeta(t)\zeta(t+\tau)\rangle$ of the "noise" term (5.38) vs. τ. The inset is a zoom. It is apparent the fast decay with τ that can be considered effectively a delta-correlation, since the time-step of the integration algorithm generating the dynamics is $dt = 10^{-5}$. Here, $K = 14$. (B): Jump rates as functions of K in the original system (red circles) and in simulations of the reconstructed M1 (blue diamonds). The rigid-rod approximation (dashed line) is reported as reference. Parameters as in Fig. 5.5.

we integrate the resulting function in order to get an effective potential, which is reported in Fig. 5.5B for several values of K. In the large-K limit, as expected, we recover a quartic effective potential: terms of higher order become relevant when the bond stiffness is low, and their effect is to flatten the potential barrier between the two wells.

As mentioned above, the validity of Eq. (M1) relies on the assumption that the evolution of Q is Markovian, which has to be checked. First, one can define and measure the following quantity:

$$\zeta(t) = \dot{Q}(t) - F(Q(t))\,, \tag{5.38}$$

which represents the "noise" of Eq. (M1), if the dynamics of Q is Markovian. We can compare the autocorrelation time of $\zeta(t)$ and verify that it is much shorter than any characteristic time-scale of the dynamics of Q. In our case, $\zeta(t)$ always decorrelates on the scale of the time-step of the integration algorithm, dt (see Fig. 5.6A).

This first check suggests the existence of a clear time-scale separation between the dynamics of the center of mass and its "noise". However, this does not imply that the original dynamics of Q has to be Markovian: in order to check that, we also have to verify the consistency with the original dynamics. If the one-variable description is able to catch the relevant features of the whole system, we can conclude, *a posteriori*, that the evolution of Q was Markovian also in the complete dynamics; if not, a different description has to be taken into account.

Fig. 5.6B shows, for several values of the rigidity, the jump rates measured in the original dynamics and those observed in the reconstructed model, using a standard stochastic integration algorithm (the one discussed in Ref. [127], up to order $dt^{3/2}$). In the high-K limit the simple rigid-rod approximation (5.36) holds, there is no dependence on K and the agreement between the jump rates of M1 and of system (5.27) is excellent. As the polymer becomes softer, even if a significant improvement on Eq. (5.36) can be observed, the relative error between M1 and

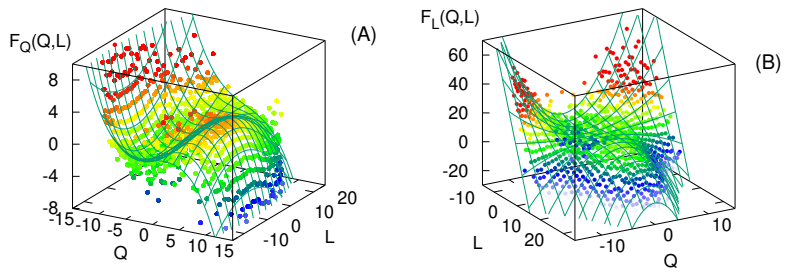

Figure 5.7. Reconstructed drift terms of Q and L in the model (M2), case $K = 4$. Points are extrapolated from data, the surface is obtained by fitting the polynomial (5.39). Other parameters are as in Fig. 5.5.

the true dynamics exceeds 30%: this is a clear hint that a 1-variable description, even if inferred directly from data, cannot reproduce all the relevant features of the dynamics. This is due to the fact that our implicit assumption on the Markovianity of the process is wrong.

5.4.3 2-variables model

The failure of model (M1) for small values of K, revealed by the discrepancies between the reconstructed and the original jump rate, suggests the necessity to go beyond a single variable description in order to achieve satisfactory results. As discussed in Section 5.4.1, a reasonable attempt to recover a Markovian dynamics is to consider the elongation of the polymer, L, as a second RC for our model, and we postulate the validity of an evolution equation of the form (M2).

Following again the strategy discussed in Section 5.3, we provide numerical values for F_Q, D_Q, F_L and D_L in the (Q, L) space, which have to be fitted using suitable functional forms. Due to the symmetries of the system, $F_Q(Q, L)$ has to be odd with respect to the variable Q, while $F_L(Q, L)$ should be even. Fig. 5.7 shows the results obtained by fitting the following polynomial form:

$$\begin{aligned} F_Q(Q,L) &= Q\left[c_{10}^{(Q)} + c_{12}^{(Q)}L^2 + c_{13}^{(Q)}L^3\right] \\ &\quad + Q^3\left[c_{30}^{(Q)} + c_{32}^{(Q)}L^2 + c_{33}^{(Q)}L^3\right] \\ F_L(Q,L) &= c_{00}^{(L)} + c_{01}^{(L)}L + c_{03}^{(L)}L^3 + c_{21}^{(L)}Q^2L\,. \end{aligned} \tag{5.39}$$

The agreement between the actual data and the proposed functional form is good enough to hope that the guessed model catches the most relevant features of the dynamics. The diffusivity terms D_Q and D_L are again fitted by constant functions. Once model (M2) is determined, we can check the reliability of its stochastic evolution by a direct comparison with the original dynamics.

A first, important benchmark is given by the ability of the model to reproduce the static properties of the system, namely the joint probability distribution in the (Q, L) space. This test is reported in Fig. 5.8 (left) for different values of K, showing a reasonable qualitative agreement even in the non-trivial case of low bond stiffness: in particular, the stretching occurring when the polymer crosses the barrier is clearly reproduced.

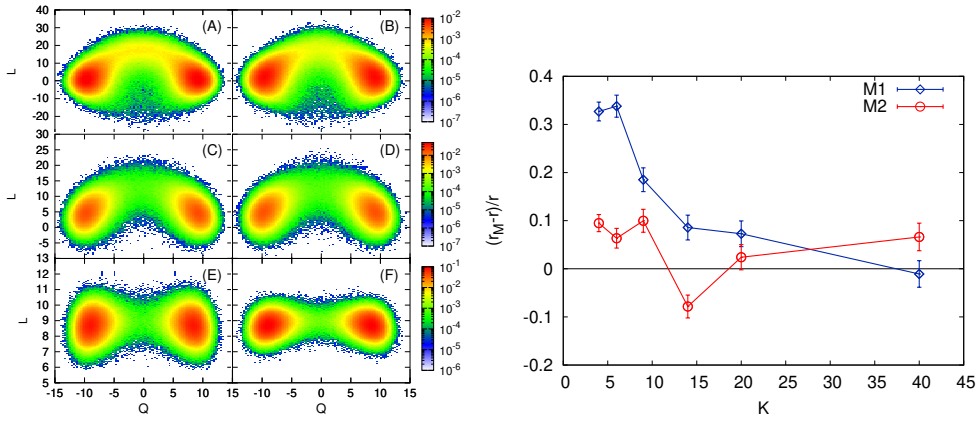

Figure 5.8. Left: p.d.f. in the two-variables phase space of the original system, first column, and in the reconstructed 2-variables model (M2), second column. Stiffness: $K = 4$ (top), $K = 20$ (center), $K = 600$ (bottom). Right: relative errors of the jump rates r in the two reconstructed models, varying K. For other parameters, see caption of Fig. 5.5.

The requirement of a variable accounting for the elongation of the polymer can be easily understood by looking at such figure. When K is high, and the system is well approximated by the rigid-rod model, the region of the phase space explored by the dynamics is a thin strip around the equilibrium value $L \simeq (N-1)\sigma$. As soon as the rigidity condition is relaxed, and the system is allowed to vary its length in a significant way, a two-lobe distribution takes place: L tends to be smaller than the rest length of the chain when the polymer occupies one of the two minima of the double-well potential, while it significantly increases during the transition across the barrier. This particular shape of the scatter plot indicates that the typical pathways in the space (Q, L) include a non-negligible deformation in L, which can be straightforwardly interpreted as follows: when the rigidity K is low, the transition across the barriers of the polymer occurs with a concomitant stretching of the bonds, presumably those that instantaneously lay on top the barrier. As a consequence, any Markovian effective description involving only the center of mass is completely insufficient to fairly approximate the dynamics of the system.

The improvement of our effective description when also L is taken into account can be fully appreciated by looking at dynamical observables as the jump rate r. Fig. 5.8 (rigth) displays the relative errors between the values of r obtained in the reconstructed models M1, M2 and in the original dynamics. As already discussed, the 1-variable model fails when the polymer is soft, while the accuracy of M2 does not seem to be affected in this limit. Let us notice, on the other hand, that for $K \gg A^2B^2/\sigma$ the reconstructed model (M2) is less reliable than the 1-variable version: this is likely a consequence of the larger number of parameters involved, which leads to a lower degree of precision on their determination with the discussed method.

5.5 Application to an experimental case: rotational diffusion in granular material

We conclude this Chapter with an example in which the method discussed in Section 5.3 is exploited in a real experimental situation. The procedure has been applied to the study of rotational diffusion in granular medium: from long time-series of measures of the angular velocity, the algorithm is able to infer the LE which approximates the dynamics to the best extent. Two cases are discussed: in the low-density limit, the application is straightforward; in the high-density regime, the introduction of a second variable is necessary (and not always sufficient) to recover Markovianity. The results presented here are discussed in Ref. [13].

5.5.1 Experiment

At first glance, granular materials share many properties with condensed "molecular" matter [94, 8], but such similitudes hide a crucial difference: grains, being macroscopic, dissipate energy through friction (in enduring contacts or rapid collisions). For this reason equilibrium statistical physics may only suggest qualitative ideas for fluidized steady states and dramatically fails in the extreme case of static or quasi-static regimes. The liquid state of granular matter, which is in the middle between fast "granular gases" and slow "granular glasses", feels stronger the need for a coherent theoretical framework. An important insight is provided by experiments, where such a liquid state is obtained through some mild shaking of the container [49, 196, 168]. In the setup described below our focus is on regimes where the longest relaxation time is reasonably smaller than the total experimental time, so that the system can be said to be in a *steady state*. In a word we are not interested, here, in the solid or glassy states [53, 81, 113].

A recent experimental study [168] has offered a new picture for dense granular flows in a wide range of time-scales, from 10^{-3} s up to 10^3 s and more, revealing an unexpectedly rich scenario. In the experimental setup, sketched in Fig 5.9A the "impurity" was constituted by an immersed blade who could rotate around a fixed vertical axis under the kicks from the grain of a vibrofluidized granular medium. The dynamics of the angular velocity $\omega(t)$ of the blade and its absolute angular position $\theta(t) = \int_0^t ds\omega(s)$, was studied in different regimes of density and intensity of vibration. In Fig 5.9B, the velocity power density spectrum (VPDS),

$$S(f) = \frac{1}{2\pi t_{TOT}} |\int_0^{t_{TOT}} \omega(t) e^{i(2\pi f)t} dt|^2, \tag{5.40}$$

is presented and its salient features are highlighted in two opposite limits, which are the gas and the cold liquid. We remind that the VPDS is the Fourier transform of the velocity autocorrelation function and that its $f \to 0^+$ limit is the self-diffusion coefficient, i.e. $D_\infty = \pi \lim_{f\to 0^+} S(f)$. We also recall that relations exist, under certain approximations, between the VPDS and the intermediate scattering function which - in liquids - is typically accessed through neutron scattering experiments [154].

In the gas limit (low packing fraction and high energy per grain) the probe velocity autocorrelation is close to a simple exponential decay $\sim e^{-t/\tau_{gas}}$, ruled by

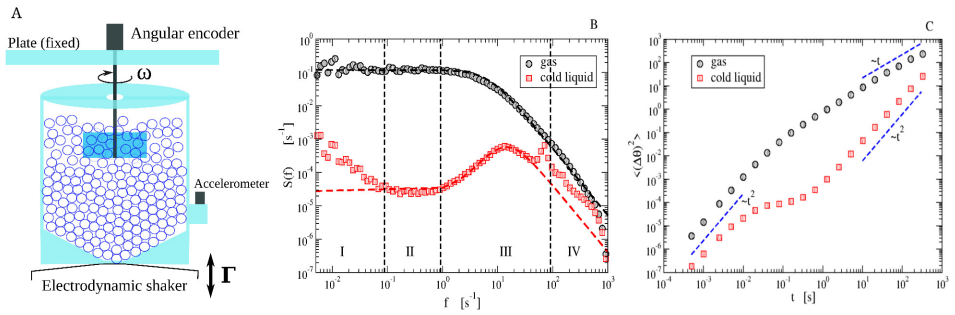

Figure 5.9. Experimental results A: Sketch of the experiment reported in Ref. [168]. B: Experimental data of the VPDS for the gas case and the "cold liquid" case, together with predictions (dashed lines) from the incomplete model discussed in Ref. [168]. C: Experimental data of the MSD for both cases, together with dashed lines useful as guides for the eye. Figure from Ref. [13].

a single relaxation time τ_{gas}: in this limit the VPDS takes the form of a Lorentzian

$$S(f) = \frac{T}{\pi\gamma} \frac{1}{1 + (2\pi I f/\gamma)^2}. \tag{5.41}$$

In the - roughly speaking - opposite limit, that of a "cold liquid" (high packing fraction $\simeq 30-35\%$ and low energy per grain), the observed VPDS strongly deviates from the Lorentzian. Ignoring a mechanical resonance due to the mounting plate at $\sim 10^2 Hz$, it displays four different regions: at high frequency (region IV) $S(f)$ decays with a negative power law equal or smaller than 2; in region III it shows a smooth parabolic maximum (centered near $\sim 10Hz$), reminiscent of a harmonic confinement ("cage") typical of molecular and granular liquids [39, 130, 160, 57]; in region II it stabilizes on a short plateau, which suggests a loss of memory (as in the plateau of the Lorentzian which marks the onset of normal diffusion); finally region I, perhaps the most surprising one, shows a diverging $S(f)$ for $f \to 0^+$, signaling a problem with the finiteness of the self-diffusion coefficient D_∞. A few longer experiments (12 hours) were conducted, showing a slow crossover toward a new higher plateau at very low frequencies. The study of the mean squared displacement (MSD), see Fig 5.9C confirmed that the four regions of the cold liquid case correspond, respectively, to short-time ballistic (free) motion (IV), dynamical arrest due to caging (III), later relaxation of the cage (II) and "final" superdiffusive behavior (I), very rarely observed in previous works on granular systems [81, 113, 189, 153]. A universal scenario for anomalous diffusion is lacking [108], but certainly it is the signal of an enduring memory.

This rich scenario can be reproduced quite accurately by proper stochastic models [168, 112]. If the studied variable (namely, the angular velocity of the probe as a function of time) is a continuous Markov process, the procedure should be able to "automatically" find the best functional form for the corresponding Langevin Equation (provided that the sampling frequency is high enough). In the following we will examine a case, the gas limit, in which this scheme can be applied quite straightforwardly; in the cold-liquid limit, on the contrary, some additional consid-

erations from physics will be needed – and not always sufficient – in order to get a satisfactory description.

5.5.2 Gas limit

Let us consider first a "dilute gas" case: the container is filled with 350 grains, corresponding to a packing fraction of $\phi = 5\%$; the shaking intensity is $\Gamma = \ddot{z}/g = 39.8$, where $\ddot{z}$ stands for the vertical acceleration and $g = 9.81 m/s^2$ is the gravitational acceleration. The measuring set-up records the angular position $\theta(t)$ of the blade with a sampling rate of $f_s = 2000 Hz$, so that we can compute the angular velocity $\omega(t) = \dot{\theta}(t)$ with a temporal resolution of $\Delta t_{min} = 1/f = 0.5 ms$. Analyzing a long time series (1 hour) of data, we would like to infer the parameters $F(\omega)$ and $D(\omega)$ of Eq (5.17).

In Fig 5.10 we plot the average quantities that appear on the r.h.s. of Eq (5.18), for several values of the time interval Δt. As discussed in Ref. [63] and recalled in the previous section, when studying data series resulting from deterministic physical processes, the Markovian approximation can be considered true only at suitable time scales, namely for $\tau_{ME} \ll \Delta t \ll \tau$, where τ_{ME} is the Markov-Einstein time and τ is a characteristic time for the autocorrelation function of the considered process. As a consequence, the limits on the r.h.s. of Eq (5.18) should be evaluated as extrapolations of the trend presented by data in a suitable time-scale range ($\Delta t \in [0.005, 0.015] s$ in our case, shaded region in Fig 5.10). We can perform a linear extrapolation using the least-square method: the vertical intercept of the resulting graph is our guess for the limit $\Delta t \to 0$. In order to evaluate a confidence interval for such value, one could estimate the uncertainty of each point of the graph and then consider the error propagation on the vertical intercept; however, since the data are not independent, this method is expected to underestimate the uncertainty. A safer way to compute the confidence interval is the "jackknife method" [58]: here we divide our sampled data into $n = 100$ blocks, then we repeat the analysis n times, discarding one block at each turn, and we compute the confidence interval from the distribution of the resulting n different expected values.

Taking the $\Delta t \to 0$ limit of the extrapolated linear trends, we have an estimate for the drift coefficient $F(\omega)$ and for the diffusivity $D(\omega)$: as it is shown in Fig 5.11 (bottom), the former has a linear dependence $F(\omega) = -A\omega$ on the angular velocity, while the latter can be approximated as $D(\omega) = D_1 + D_2\omega^2$. Of course, our procedure gives more accurate results when the angular velocity is smaller, i.e. when a bigger volume of data is available for the averages (see Fig 5.11 (top)). Let us notice that the quadratic corrections to the diffusivity are only relevant when $|\omega|$ is quite large, i.e. when our estimate is less reliable because of the low volume of data. For this reason, in the following we neglect such corrections and apply the constant approximation $D(\omega) = D$. Model (5.17) reduces then to the well known Ornstein-Uhlenbeck process [65], so that all interesting physical observables can be computed analytically.

In Fig 5.11 (top) we observe a fair agreement between the predicted stationary probability distribution of ω and the experimental one. Table 5.1 summarizes the expected values for the parameters of the model, and the corresponding uncertainties. In Fig 5.12 we compare the experimental VPDS and MSD with the theoretical

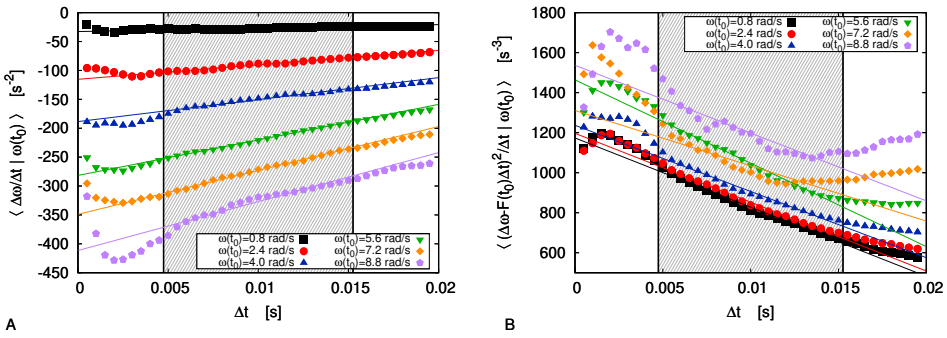

Figure 5.10. Gas limit: extrapolation Extrapolation of the limits on the r.h.s. of Eq (5.18), for several values of $\omega(t_0)$, in order to compute drift (panel A) and diffusivity (panel B) in the gas limit. Each linear fit (solid lines) has been computed - by means of a classical least-square method - considering only the data in the shaded range, within the vertical lines. Figure from Ref. [13].

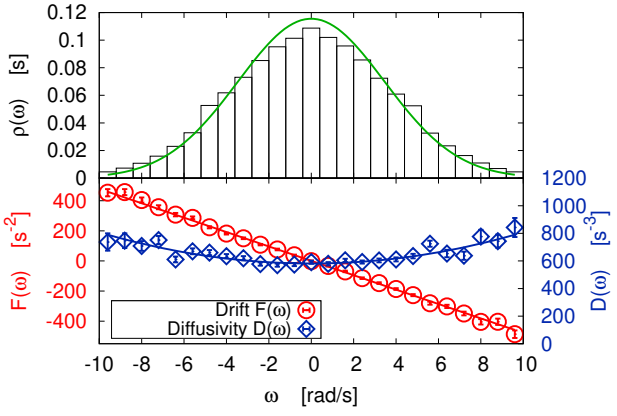

Figure 5.11. Gas limit: p.d.f., drift and diffusivity Top: p.d.f. of ω in the gas limit (the green solid line is the prediction of the derived model). Bottom: Reconstructed drift (red circles) and diffusivity (blue diamonds) in the gas limit have been respectively fitted with a linear and a parabolic function. Figure from Ref. [13].

Table 5.1. Gas limit: parameters Expected values and uncertainties for the parameters of the reconstructed model in the gas limit.

Parameter	Value
F	$(47.82 \pm 0.42)s^{-1}$
D	$(581.6 \pm 5.8)s^{-3}$

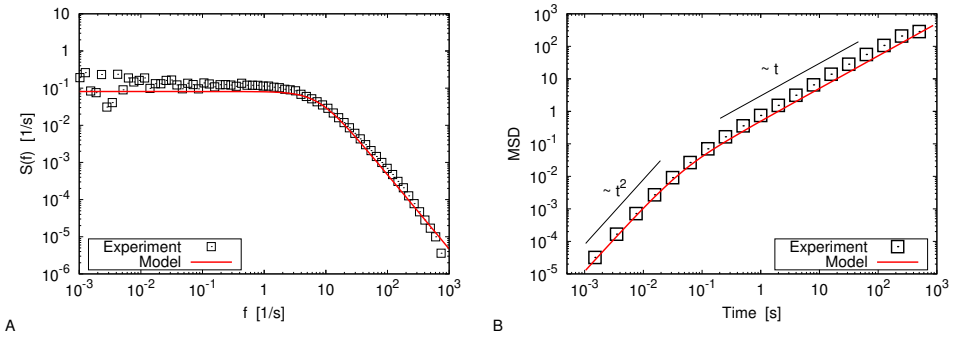

Figure 5.12. Gas limit: observables Velocity power density spectrum (panel A) and mean square displacement (panel B) in the gas limit. Experimental data (black squares) are compared with the reconstructed model (red lines). Black lines are guides for the eyes. Figure from Ref. [13].

ones for the reconstructed Ornstein-Uhlenbeck process, finding a good agreement. The gas limit can be fairly approximated by this model, as already discussed in [168]. It is useful to recall that the characteristic time of the Ornstein-Uhlenbeck process (i.e. the decay of the velocity autocorrelation) is proportional to the mean free time between particle-blade collisions and in certain conditions can be quantitatively predicted [73]. We stress that if one considers also the quadratic corrections and performs numerical simulations, the outcomes are almost identical, at least in this case.

5.5.3 Cold liquid limit

In the following we analyze a regime which is somehow "opposite" to the gas limit seen above: in this case we consider $N = 2600$ beads and a shaking intensity $\Gamma = 39.8$; the packing fraction is $\phi = 36\%$. Again, $f = 2000Hz$ and the experiment has a duration of 1 hour.

As already understood in Ref. [168, 112], in this case the rich phenomenology of the system cannot be described by a single-variable approach, since the dynamics of the granular matter involves at least two clearly separate time scales. Before enforcing the extrapolation procedure, we should be able to identify a "fast" variable and a "slow" one in order to understand how the model depends on them.

A quite straightforward way to define a variable that describes the slow behavior of the probe is to consider a running average with a Gaussian window function:

$$\theta_0(t) = \frac{1}{\sqrt{2\pi}\sigma} \int dt' \, e^{-\frac{(t'-t)^2}{\sigma^2}} \theta(t'-t) \, . \tag{5.42}$$

The fast component can be found, of course, as $\theta_1(t) = \theta(t) - \theta_0(t)$ (see Fig 5.13A). The value of the characteristic time σ (here $\sigma = 0.3s$) is suggested by the shape of $S(f)$, see Fig. 5.9: we need to filter out the features in regions III and IV, but we also demand that the interesting dynamics in region I is reproduced by the new variable; taking $2\sigma \simeq O(1)s$ seems therefore a legitimate choice. In the following we will show that varying the parameter does not affect the results of our analysis significantly, as long as σ is chosen to be of the same order of magnitude. Of course, any other choice for the kernel in Eq (5.42) could be made, provided that it canceled the fast oscillations of $\theta(t)$ (i.e. provided that it had a Fourier transform decaying fast enough).

Let us notice that, following the physical interpretation proposed in Ref. [112], θ_0 can be seen as the center of mass of the itinerant "cage" at every time, while θ_1 has the meaning of the angular distance between θ_0 and the probe itself.

First, we can use the extrapolation analysis seen before in order to determine a proper Langevin equation for the slow variable $\omega_0 = \dot{\theta}_0$. In this case the significative Δt range can be found at a much slower time scale (namely, $\Delta t \in [1.5, 6]s$): as a consequence, the volume of available data considerably shrinks, but it is still possible to estimate the dependence of the drift term on the slow angular velocity. In particular one finds (Fig 5.13B) that $F(\omega_0) = -A_0\omega_0$ is an acceptable approximation. As in the previous case, we approximate the diffusivity term with a constant, $D_0(\omega) = B_0$, neglecting the deviations for large $|\omega_0|$.

We are left with the problem of finding a model for the observed variable $\omega(t)$. In Fig 5.13C we show that the drift coefficient of ω depends significantly not only on ω itself, but also on $\theta_1 = \theta - \theta_0$. A linear function of both arguments, $F(\omega, \theta_1) = -A_1\omega - A_2\theta_1$, turns out to provide a fair description of the data. Again we consider a constant value for the diffusivity, $D(\theta_1, \omega) = B$.

The reconstructed model reads as follows:

$$\dot{\omega}(t) = -A_1\omega(t) - A_2[\theta(t) - \theta_0(t)] + \sqrt{2B}\eta(t) \tag{5.43a}$$

$$\dot{\omega_0}(t) = -A_0\omega_0(t) + \sqrt{2B_0}\eta_0(t) \tag{5.43b}$$

$$\dot{\theta}(t) = \omega(t) \tag{5.43c}$$

$$\dot{\theta}_0(t) = \omega_0(t) \tag{5.43d}$$

where $\eta(t)$ and $\eta_0(t)$ are Gaussian noises with unitary variance.

The power density spectrum of $\omega(t)$ for model (5.43) can be determined analytically:

$$S(\hat{f}) = \frac{1}{\pi} \frac{A_2^2 B_0 + A_0^2 B \hat{f}^2 + B\hat{f}^4}{A_0^2 A_2^2 + [A_2^2 + A_0^2 A_1^2 - 2A_0^2 A_2^2]\hat{f}^2 + [A_1^2 - 2A_2 + A_0^2]\hat{f}^4 + \hat{f}^6} \tag{5.44}$$

where $\hat{f} = 2\pi f$. Once $S(\hat{f})$ is known, the MSD can be found as

$$\langle [\Delta\theta(t)]^2 \rangle = \int_0^t dt' \int_0^t dt'' \langle \omega(t')\omega(t) \rangle = 2 \int_0^t dt' (t - t') C_{\omega\omega}(t') \tag{5.45}$$

where $C_{\omega\omega}(t)$, the autocorrelation function of $\omega(t)$, is the Fourier anti-transform of $S(\hat{f})$. In Fig 5.14 we compare the above analytical expressions to the experimental data.

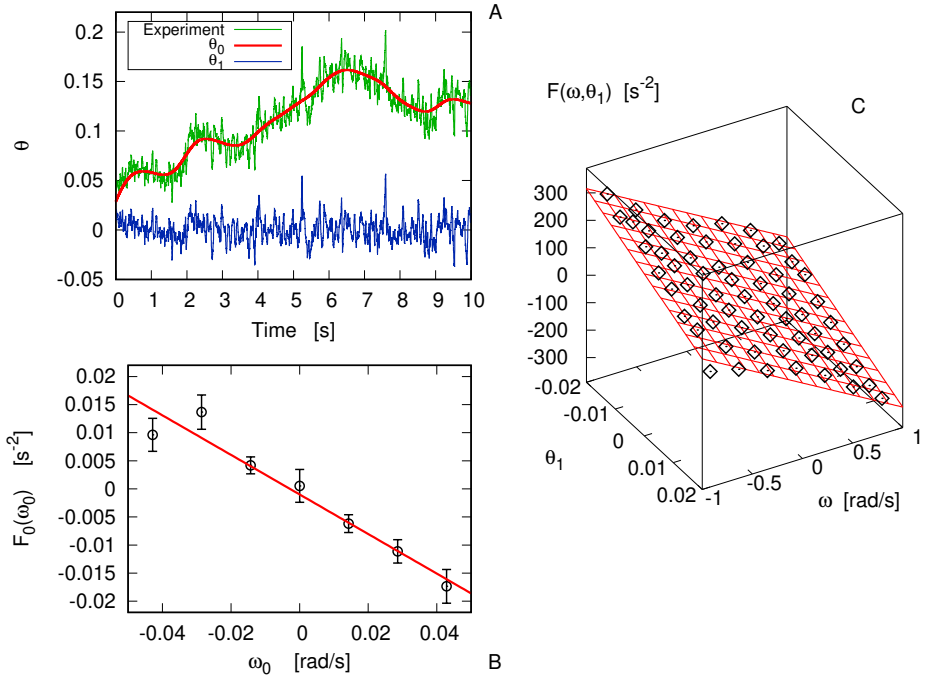

Figure 5.13. Cold liquid: slow and fast components A: Decomposing the original signal (green line) into the sum of the averaged angular position θ_0 defined by Eq (5.42) (red line) and the "fast" variable $\theta_1 = \theta - \theta_0$ (blue line). B: Drift coefficient of ω_0. C: Drift coefficient of ω, as a function of θ_1 and ω_0. Figure from Ref. [13].

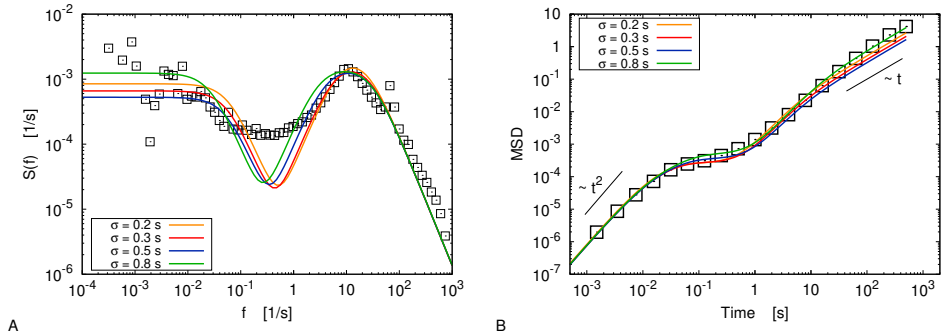

Figure 5.14. Cold liquid: observables Velocity power density spectrum (panel A) and mean square displacement (panel B) in the cold liquid case with $\Gamma = 39.8$. Experimental data (black squares) are compared with the reconstructed models (coloured lines) for several values of the smoothing parameter σ. Black lines are guides for the eyes. Figure from Ref. [13].

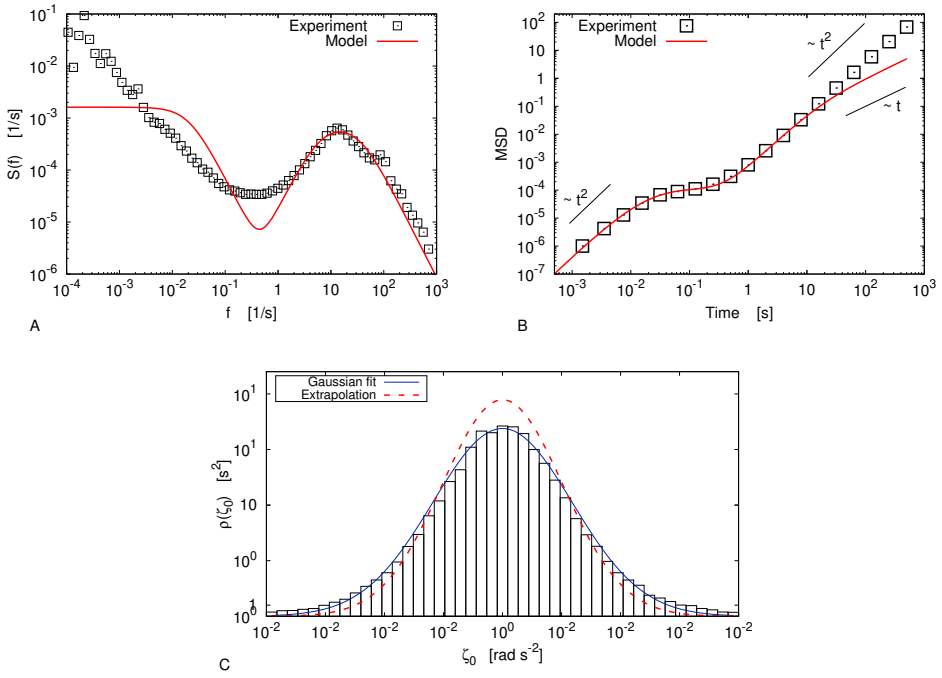

Figure 5.15. Cold liquid: limits of the method A: Velocity power density spectrum in the cold liquid limit with $\Gamma = 26.8$. B: Mean square displacement in the same case. C: Distribution of the "noise" ζ_0 defined by Eq (5.46) (with $\Delta_t = 0.6s$), Gaussian fit (blue line) and comparison with the reconstructed model (dashed red line). Figure from Ref. [13].

The VPDS shows a fair agreement in the high-frequency regime, $f \gg 1Hz$, and in the low-frequency one $f \ll 1Hz$; in the intermediate range (region II in the notation of [168]) there is a clear discrepancy between the model and the experimental data, maybe due to decorrelations of the slow variable that are not caught by the model. However, we stress that the difference concerns a frequency range which is almost inessential for the dynamical properties of the system, whose characteristic frequencies lay in regions I and III of the spectrum (see Fig 5.9B): this is completely evident when considering the MSD evolution (Fig 5.14B), that is very well reproduced by the model despite the discrepancy on $S(\hat{f})$. Let us note that changing σ by a factor 4, from $0.2s$ to $0.8s$, does not affect the results of our analysis in a significative way.

Finally, let us consider an experiment with $N = 2600$, $\Gamma = 26.8$, $\phi = 45\%$: even if the number of beads is the same as in the previous case, the lower shaking intensity entails that the accessible volume for the beads is lower, i.e. the actual packing fraction increases. The system is therefore in a "more concentrate" state. The duration of the experiment has also been raised (12 hours), and we have chosen $\sigma = 0.3s$ for the analysis.

Fig 5.15A and Fig 5.15B show the VPDS and the MSD in this case, compared to those that can be inferred through the method discussed above. Even if the

high-frequency regime is well reproduced by the model, our description fails on the long-time scale; in particular, the MSD of the reconstructed model shows a linear dependence on time for $t \simeq 50s$, while the experimental one is still quadratic on that scale.

The failure of the method could be ascribed to the choice of Gaussian noise in the equation for the slow variable: if the evolution of ω_0 was ruled by a Lévy process, an alternative analysis should be considered [173]. Let us evaluate, *a posteriori*, the noise of the slow variable as:

$$\zeta_0(t) = \frac{\omega_0(t+\Delta t) - \omega_0(t)}{\Delta t} - F_0(\omega_0(t))\,. \tag{5.46}$$

Fig 5.15C shows that the distribution of ζ_0 can be fairly approximated with a Gaussian; furthermore, the amplitude of the noise is very close to that of the reconstructed model. Hence, we can guess that the hypothesis of Gaussian noise is quite reasonable, and the discrepancy between the experimental data and the inferred model could need a different explanation.

Table 5.2 summarizes the expected values for the parameters of model (5.43), and the corresponding uncertainties, for the two considered cases in the cold liquid limit. Also in this case the confidence intervals have been computed using the jackknife method on n blocks of sampled data: we have chosen $n = 100$ for the fast variables, $n = 10$ for the slow ones.

Table 5.2. Cold liquid: parameters Expected values and uncertainties for the parameters of model (5.43) in the cold liquid limit.

Parameter	$\Gamma = 39.8$	$\Gamma = 26.8$
$A_1\ [s^{-1}]$	200.3 ± 4.4	252.0 ± 6.3
$A_2\ [s^{-2}]$	$5.76 \cdot 10^3 \pm 2.4 \cdot 10^2$	$8.55 \cdot 10^3 \pm 4.5 \cdot 10^2$
$B\ [s^{-3}]$	161.1 ± 3.9	107.3 ± 3.1
$A_0\ [s^{-1}]$	0.352 ± 0.034	$0.1317 \pm 4.9 \cdot 10^{-3}$
$B_0\ [s^{-3}]$	$2.43 \cdot 10^{-4} \pm 2.1 \cdot 10^{-5}$	$8.82 \cdot 10^{-5} \pm 2.7 \cdot 10^{-6}$

Conclusions

As discussed in Chapter 1, there are many examples of physical systems showing negative temperatures, whose level of order increases when the internal energy is incremented. Nonetheless, a certain feeling of skepticism persists among many physicists when equilibrium states with $\beta < 0$ are considered. In this Thesis we tried to show that NAT states naturally emerge in models with suitable properties, and they must be taken into account to get a full description of the thermostatistical properties of such systems.

First, we have faced the study of negative temperature starting from the framework of classical Hamiltonian systems. We have discussed some properties that allow NAT states in mechanical models, and we have identified a class of systems, characterized by bounded kinetic terms, which is particularly suitable for analytical and numerical studies on negative temperature.

We have shown that it is possible to treat negative temperature also in the sense of Thermodynamics: we can design a device (a "thermometer") which is able to classify the equilibrium states of Hamiltonian systems living in bounded phase spaces, even when their equilibrium states correspond to negative values of β. Our numerical experiments also reproduce the behavior that is expected when a system with negative temperature is coupled to a thermometer made of ordinary matter. We have also discussed a non-trivial case in which the presence of mean-field interactions leads to ensemble inequivalence at negative temperature. This example shows that in some models the descending branch of the entropy is characterized by properties that are qualitatively different from the positive-temperature ones, and such phenomenology can be only appreciated by including the study of the NAT regime.

The possibility of negative temperatures also needs to be taken into account when one considers the mesoscopic fluctuations of a single degree of freedom subjected to the action of a thermal bath. We have discussed the possibility to introduce effective stochastic equations in the form of a generalized LE also in cases with non-quadratic kinetic terms. Consistency arguments have been exploited to find out the form of a Langevin-like equation; we have checked its validity by numerically simulating the action of thermal baths on slow particles.

We focused in particular on two kinds of thermal baths. First, we modeled the action of the reservoir through a Hamiltonian systems with bounded kinetic terms, belonging to the class discussed before, which admits negative temperatures. When the energy of such bath is large enough, a mechanism of negative dissipation for the particle interacting with the bath is observed; such behavior is correctly described by the introduction of negative values of β into a generalized Einstein equation.

Then, we obtained similar results considering a thermal bath composed by Ising spins, ruled by a stochastic dynamics which fixes their temperature.

Our results, just like other studies conduced in the context of two-dimensional hydrodynamics, show that coarse-grained descriptions of systems living in bounded phase-spaces require the introduction of negative temperature; far from leading to inconsistencies or paradoxes, NATs provide a natural and handy interpretation of the effective motion observed at high energy for such kind of systems.

Finally, we have discussed two typical non-equilibrium topics: the response of a system to an external perturbation and the heat transport along a unidimensional chain. We have shown that the usual results from linear response theory can be applied to cases with negative temperature. This is particularly relevant since the FDR can be used, in general, to give an operative definition of the inverse temperature β of the system, through the measure of responses and autocorrelation functions: the presence of negative temperature does not hinder this possibility (even in absence of ensemble equivalence). About Fourier transport at negative temperature, the numerical simulations of simply tractable models (an exclusion process for a stochastic spin dynamics along a unidimensional lattice and the dynamics of a Hamiltonian chain with thermal baths at the extremes) has revealed important conceptual aspects on negative temperature out of equilibrium: in particular, the possibility of heat transport between baths at negative and positive β seems relevant to us, as it clearly shows that negative and positive temperatures can coexist in a non-equilibrium situation, being connected through a locally vanishing value of β.

In his comment to a paper by Berdichevsky, Kunin and Hussain [18], where the adoption of Gibbs' entropy was proposed for the description of Onsager's vortices, so to avoid negative temperature, Montgomery wrote that *the appropriate question for statistical mechanics would appear to be not how quantities can be formally redefined to make this novel region as similar looking as possible to spatially uniform thermodynamics, but rather how to characterize the strikingly different behavior of the high-energy regime* [137]. We completely agree with this point of view: since negative temperatures properly describe observable states of some physical systems, accounting for their peculiar properties, one should not avoid their introduction unless severe inconsistencies arise; and the results of this Thesis seem to suggest that, at least for the Hamiltonian models considered here, a statistical description in terms of negative temperatures is consistent and quite robust.

In this Thesis we have limited our attention to a particular class of Hamiltonian systems. We are aware, of course, that definitive answers on the consistency of Statistical Mechanics at negative temperatures may only come from the study of more realistic models, a potentially much more challenging task. Much work has still to be done to understand the non-trivial properties that emerge in their high-energy regimes. We hope however that the results presented here can provide some intuition about the fundamental mechanisms which rule negative temperature; such insight could reveal useful to the comprehension of more realistic systems as well.

Bibliography

[1] A. Abragam and W. G. Proctor "Spin Temperature". *Phys. Rev.* **109** (1958), pp. 1441–1458.

[2] E. Abraham and O. Penrose "Physics of negative absolute temperatures". *Phys. Rev. E* **95** (2017), p. 012125.

[3] A. Ammenti, F. Cecconi, U. Marini Bettolo Marconi, and A. Vulpiani "A Statistical Model for Translocation of Structured Polypeptide Chains through Nanopores". *J. Phys. Chem. B* **113** (2009), pp. 10348–10356.

[4] P. Ansalone, M. Chinappi, L. Rondoni, and F. Cecconi "Driven diffusion against electrostatic or effective energy barrier across α-hemolysin". *J. Chem. Phys.* **143** (2015), p. 154109.

[5] M. Antoni and S. Ruffo "Clustering and relaxation in Hamiltonian long-range dynamics". *Phys. Rev. E* **52** (1995), pp. 2361–2374.

[6] A. Ashkin "Acceleration and Trapping of Particles by Radiation Pressure". *Phys. Rev. Lett.* **24** (1970), pp. 156–159.

[7] R. J. de Assis, T. M. de Mendonça, C. J. Villas-Boas, A. M. de Souza, R. S. Sarthour, I. S. Oliveira, and N. G. de Almeida "Efficiency of a Quantum Otto Heat Engine Operating under a Reservoir at Effective Negative Temperatures". *Phys. Rev. Lett.* **122** (2019), p. 240602.

[8] A. Baldassarri, A. Puglisi, and A. Sarracino "Coarsening in granular systems". *C. R. Physique* **16** (2015), p. 291.

[9] M. Baldovin, F. Cecconi, and A. Vulpiani "Effective equations for reaction coordinates in polymer transport". *J. Stat. Mech. (accepted for publication)* (2019).

[10] M. Baldovin, A. Puglisi, A. Sarracino, and A. Vulpiani "About thermometers and temperature". *J. Stat. Mech.* **2017** (2017), p. 113202.

[11] M. Baldovin "Physical interpretation of the canonical ensemble for long-range interacting systems in the absence of ensemble equivalence". *Phys. Rev. E* **98** (2018), p. 012121.

[12] M. Baldovin, A. Puglisi, and A. Vulpiani "Langevin equation in systems with also negative temperatures". *J. Stat. Mech.* **2018** (2018), p. 043207.

[13] M. Baldovin, A. Puglisi, and A. Vulpiani "Langevin equations from experimental data: The case of rotational diffusion in granular media". *PLOS ONE* **14** (2019), pp. 1–16.

[14] M. Baldovin, F. Cecconi, M. Cencini, A. Puglisi, and A. Vulpiani "The role of data in model building and prediction: A survey through examples". *Entropy* **20** (2018), p. 807.

[15] M. Baldovin, A. Vulpiani, A. Puglisi, and A. Prados "Derivation of a Langevin equation in a system with multiple scales: The case of negative temperatures". *Phys. Rev. E* **99** (2019), 060101(R).

[16] G. Basile, L. Delfini, S. Lepri, R. Livi, S. Olla, and A. Politi "Anomalous transport and relaxation in classical one-dimensional models". *Eur. Phys. J. Special Topics* **151** (2007), pp. 85–93.

[17] G. Benettin and A. Giorgilli "On the Hamiltonian interpolation of near-to-the identity symplectic mappings with application to symplectic integration algorithms". *J. Stat. Phys.* **74** (1994), pp. 1117–1143.

[18] V. Berdichevsky, I. Kunin, and F. Hussain "Negative temperature of vortex motion". *Phys. Rev. A* **43** (1991), pp. 2050–2051.

[19] S. M. Bezrukov, I. Vodyanoy, and V. A. Parsegian "Counting polymers moving through a single ion channel". *Nature* **370** (1994), p. 279.

[20] L. L. Bonilla, A. Carpio, and A. Prados "Theory of force-extension curves for modular proteins and DNA hairpins". *Phys. Rev. E* **91** (2015), p. 052712.

[21] L. L. Bonilla, A. Prados, and A. Carpio "Nonequilibrium dynamics of a fast oscillator coupled to Glauber spins". *J. Stat. Mech.* **2010** (2010), p. 09019.

[22] F. Bouchet, T. Dauxois, D. Mukamel, and S. Ruffo "Phase space gaps and ergodicity breaking in systems with long-range interactions". *Phys. Rev. E* **77** (2008), p. 011125.

[23] S. Braun, J. P. Ronzheimer, M. Schreiber, S. S. Hodgman, T. Rom, I. Bloch, and U. Schneider "Negative Absolute Temperature for Motional Degrees of Freedom". *Science* **339** (2013), pp. 52–55.

[24] S. L. Brunton, J. L. Proctor, and J. N. Kutz "Discovering governing equations from data by sparse identification of nonlinear dynamical systems". *Proc. Natl. Acad. Sci. U.S.A.* **113** (2016), pp. 3932–3937.

[25] P. Buonsante, R. Franzosi, and A. Smerzi "Phase transitions at high energy vindicate negative microcanonical temperature". *Phys. Rev. E* **95** (2017), p. 052135.

[26] P. Buonsante, R. Franzosi, and A. Smerzi "On the dispute between Boltzmann and Gibbs entropy". *Ann. Phys. (N. Y.)* **375** (2016), pp. 414–434.

[27] P. de Buyl, D. Mukamel, and S. Ruffo "Ensemble Inequivalence In A XY Model With Long-Range Interactions". *AIP Conf. Proc.* **800** (2005), pp. 533–538.

[28] E. Caglioti, P. L. Lions, C. Marchioro, and M. Pulvirenti "A special class of stationary flows for two-dimensional Euler equations: A statistical mechanics description". *Commun. Math. Phys.* **143** (1992), pp. 501–525.

[29] E. Caglioti, P. L. Lions, C. Marchioro, and M. Pulvirenti "A special class of stationary flows for two-dimensional Euler equations: A statistical mechanics description. Part II". *Commun. Math. Phys.* **174** (1995), pp. 229–260.

[30] S. Calabrese and A. Porporato "Origin of negative temperatures in systems interacting with external fields". *Phys. Lett. A* **383**. (2019), pp. 2153–2158.

[31] H. B. Callen and T. A. Welton "Irreversibility and Generalized Noise". *Phys. Rev.* **83** (1951), pp. 34–40.

[32] A. Campa, T. Dauxois, and S. Ruffo "Statistical mechanics and dynamics of solvable models with long-range interactions". *Phys. Rep.* **480** (2009), pp. 57–159.

[33] A. Campa, A. Giansanti, D. Mukamel, and S. Ruffo "Dynamics and thermodynamics of rotators interacting with both long- and short-range couplings". *Physica A* **365** (2006), pp. 120–127.

[34] D. K. Campbell, S. Flach, and Y. S. Kivshar "Localizing Energy Through Nonlinearity and Discreteness". *Physics Today* **57** (2004), pp. 43–49.

[35] M. Campisi "On the mechanical foundations of thermodynamics: The generalized Helmholtz theorem". *Stud. Hist. Philos. Sci. B* **36** (2005), pp. 275–290.

[36] M. Campisi "Construction of microcanonical entropy on thermodynamic pillars". *Phys. Rev. E* **91** (2015), p. 052147.

[37] M. Campisi "Notes on heat engines and negative temperatures". *Preprint arXiv:1606.05244* (2016).

[38] H. Casimir and F. du Pré "Note on the thermodynamic interpretation of paramagnetic relaxation phenomena". *Physica* **5** (1938), pp. 507 –511.

[39] A. Cavagna "Supercooled liquids for pedestrians". *Phys. Rep.* **476** (2009), p. 51.

[40] F. Cecconi, M. Cencini, and A. Vulpiani "Transport properties of chaotic and non-chaotic many particle systems". *J. Stat. Mech.* **2007** (2007), p. 12001.

[41] L. Cerino, A. Puglisi, and A. Vulpiani "A consistent description of fluctuations requires negative temperatures". *J. Stat. Mech.* **2015** (2015), P12002.

[42] S. Chapman, T. G. Cowling, and D. Burnett. *The mathematical theory of non-uniform gases: an account of the kinetic theory of viscosity, thermal conduction and diffusion in gases.* Cambridge University Press, 1990.

[43] H. P. Chavanis. "Statistical Mechanics of Two-Dimensional Vortices and Stellar Systems". In: *Dynamics and Thermodynamics of Systems with Long Range Interactions*. Ed. by T. Dauxois, S. Ruffo, E. Arimondo, and M. Wilkens. Berlin Heidelberg: Springer-Verlag, 2002, pp. 208–289.

[44] P. H. Chavanis "Phase transitions in self-gravitating systems". *Int. J. Mod. Phys. B* **20** (2006), pp. 3113–3198.

[45] P. H. Chavanis and M. Lemou "Kinetic theory of point vortices in two dimensions: analytical results and numerical simulations". *Eur. Phys. J. B* **59** (2007), pp. 217–247.

[46] P.-H. Chavanis "Systematic drift experienced by a point vortex in two-dimensional turbulence". *Phys. Rev. E* **58** (1998), R1199–R1202.

[47] S. Chu, L. Hollberg, J. E. Bjorkholm, A. Cable, and A. Ashkin "Three-dimensional viscous confinement and cooling of atoms by resonance radiation pressure". *Phys. Rev. Lett.* **55** (1985), pp. 48–51.

[48] B. Cressiot, A. Oukhaled, G. Patriarche, M. Pastoriza-Gallego, J.-M. Betton, L. Auvray, M. Muthukumar, L. Bacri, and J. Pelta "Protein transport through a narrow solid-state nanopore at high voltage: experiments and theory". *ACS nano* **6** (2012), pp. 6236–6243.

[49] G. D'Anna, P. Mayor, A. Barrat, V. Loreto, and F. Nori "Observing Brownian motion in vibration-fluidized granular matter". *Nature* **424** (2003), p. 909.

[50] T. Dauxois, S. Ruffo, E. Arimondo, and M. Wilkens, eds. *Dynamics and Thermodynamics of Systems with Long Range Interactions*. Berlin Heidelberg: Springer-Verlag, 2002.

[51] A. Dhar "Heat transport in low-dimensional systems". *Advances in Physics* **57** (2008), pp. 457–537.

[52] J. Dunkel and S. Hilbert "Consistent thermostatistics forbids negative absolute temperatures". *Nature Physics* **10** (2014), pp. 67–72.

[53] J. C. Dyre "The glass transition and elastic models of glass-forming liquids". *Rev. Mod. Phys.* **78** (2006), p. 953.

[54] A. Einstein "Zur Theorie der Brownschen Bewegung". *Ann. Phys. (Berl.)* **324** (1906), pp. 371–381.

[55] H. S. Eisenberg, Y. Silberberg, R. Morandotti, A. R. Boyd, and J. S. Aitchison "Discrete Spatial Optical Solitons in Waveguide Arrays". *Phys. Rev. Lett.* **81** (1998), pp. 3383–3386.

[56] M. Falcioni, S. Isola, and A. Vulpiani "Correlation functions and relaxation properties in chaotic dynamics and statistical mechanics". *Phys. Lett. A* **144** (1990), pp. 341–346.

[57] A. Fiege, T. Aspelmeier, and A. Zippelius "Long-Time Tails and Cage Effect in Driven Granular Fluids". *Phys. Rev. Lett.* **102** (2009), p. 098001.

[58] H. Flyvbjerg. "Error estimates on averages of correlated data". In: *Advances in Computer Simulation*. Ed. by J. Kertész and I. Kondor. Berlin, Heidelberg: Springer Berlin Heidelberg, 1998, pp. 88–103.

[59] G. W. Ford, M. Kac, and P. Mazur "Statistical Mechanics of Assemblies of Coupled Oscillators". *J. Math. Phys.* **6** (1965), pp. 504–515.

[60] R. Franzosi, R. Livi, G.-L. Oppo, and A. Politi "Discrete breathers in Bose–Einstein condensates". *Nonlinearity* **24** (2011), R89–R122.

[61] D. Frenkel and B. Smit. *Understanding molecular simulation: from algorithms to applications*. Vol. 1. Elsevier, 2001.

[62] D. Frenkel and P. B. Warren "Gibbs, Boltzmann, and negative temperatures". *Am. J. Phys.* **83** (2015), pp. 163–170.

[63] R. Friedrich, J. Peinke, M. Sahimi, and M. Reza Rahimi Tabar "Approaching complexity by stochastic methods: From biological systems to turbulence". *Phys. Rep.* **506** (2011), pp. 87–162.

[64] G. Gallavotti. *Statistical mechanics: A short treatise*. Springer Science & Business Media, 2013.

[65] C. W. Gardiner. *Handbook of stochastic methods*. Springer Berlin, 1985.

[66] G. Gauthier, M. T. Reeves, X. Yu, A. S. Bradley, M. A. Baker, T. A. Bell, H. Rubinsztein-Dunlop, M. J. Davis, and T. W. Neely "Giant vortex clusters in a two-dimensional quantum fluid". *Science* **364** (2019), pp. 1264–1267.

[67] O. V. Gendelman and A. V. Savin "Normal Heat Conductivity of the One-Dimensional Lattice with Periodic Potential of Nearest-Neighbor Interaction". *Phys. Rev. Lett.* **84** (2000), pp. 2381–2384.

[68] H. A. Gersch and G. C. Knollman "Quantum Cell Model for Bosons". *Phys. Rev.* **129** (1963), pp. 959–967.

[69] C. Giardinà, R. Livi, A. Politi, and M. Vassalli "Finite Thermal Conductivity in 1D Lattices". *Phys. Rev. Lett.* **84** (2000), pp. 2144–2147.

[70] J. W. Gibbs. *Elementary Principles in Statistical Mechanics*. Yale University Press, 1902.

[71] D. Givon, R. Kupferman, and A. Stuart "Extracting macroscopic dynamics: model problems and algorithms". *Nonlinearity* **17** (2004), R55.

[72] R. J. Glauber "Time-dependent statistics of the Ising model". *J. Math. Phys.* **4** (1963), p. 294.

[73] A. Gnoli, A. Puglisi, and H. Touchette "Granular Brownian motion with dry friction". *Europhys. Lett.* **102** (2013), p. 14002.

[74] H. Grabert, P. Hänggi, and P. Talkner "Microdynamics and nonlinear stochastic processes of gross variables". *J. Stat. Phys.* **22** (1980), pp. 537–552.

[75] S. de Groot and P. Mazur. *Non-equilibrium Thermodynamics*. Dover Books on Physics. Dover Publications, 1984.

[76] A. J. Groszek, D. M. Paganin, K. Helmerson, and T. P. Simula "Motion of vortices in inhomogeneous Bose-Einstein condensates". *Phys. Rev. A* **97** (2018), p. 023617.

[77] E. Hairer, C. Lubich, and G. Wanner. *Geometric numerical integration: structure-preserving algorithms for ordinary differential equations*. Vol. 31. Springer Science & Business Media, 2006.

[78] P. J. Hakonen, K. K. Nummila, R. T. Vuorinen, and O. V. Lounasmaa "Observation of nuclear ferromagnetic ordering in silver at negative nanokelvin temperatures". *Phys. Rev. Lett.* **68** (1992), pp. 365–368.

[79] P. Hänggi, S. Hilbert, and J. Dunkel "Meaning of temperature in different thermostatistical ensembles". *Philos. Trans. Royal Soc. A* **374** (2016), p. 20150039.

[80] P. Hänggi, P. Talkner, and M. Borkovec "Reaction-rate theory: fifty years after Kramers". *Rev. Mod. Phys.* **62** (1990), pp. 251–341.

[81] C. Heussinger, L. Berthier, and J.-L. Barrat "Superdiffusive, heterogeneous, and collective particle motion near the fluid-solid transition in athermal disordered materials". *Europhys. Lett.* **90** (2010), p. 20005.

[82] S. Hilbert, P. Hänggi, and J. Dunkel "Thermodynamic laws in isolated systems". *Phys. Rev. E* **90** (2014), p. 062116.

[83] R. L. Honeycutt "Stochastic Runge-Kutta algorithms. I. White noise". *Phys. Rev. A* **45** (1992), pp. 600–603.

[84] V. V. Hovhannisyan, N. S. Ananikian, A. Campa, and S. Ruffo "Complete analysis of ensemble inequivalence in the Blume-Emery-Griffiths model". *Phys. Rev. E* **96** (2017), p. 062103.

[85] K. Huang. *Statistical Mechanics*. New York: John Wiley & Sons, 1988.

[86] I. Huopaniemi, K. Luo, T. Ala-Nissila, and S.-C. Ying "Langevin dynamics simulations of polymer translocation through nanopores". *J. Chem. Phys.* **125** (2006), p. 124901.

[87] S. Iubini, R. Franzosi, R. Livi, G.-L. Oppo, and A. Politi "Discrete breathers and negative-temperature states". *New J. Phys.* **15** (2013), p. 023032.

[88] S. Iubini, S. Lepri, R. Livi, and A. Politi "Off-equilibrium Langevin dynamics of the discrete nonlinear Schrödinger chain". *J. Stat. Mech.* **2013** (2013), p. 08017.

[89] S. Iubini, S. Lepri, R. Livi, and A. Politi "Coupled transport in rotor models". *New J. Phys.* **18** (2016), p. 083023.

[90] S. Iubini, S. Lepri, and A. Politi "Nonequilibrium discrete nonlinear Schrödinger equation". *Phys. Rev. E* **86** (2012), p. 011108.

[91] S. Iubini, A. Politi, and P. Politi "Coarsening Dynamics in a Simplified DNLS Model". *J. Stat. Phys.* **154** (2014), pp. 1057–1073.

[92] S. Iubini, A. Politi, and P. Politi "Relaxation and coarsening of weakly-interacting breathers in a simplified DNLS chain". *J. Stat. Mech.* **2017** (2017), p. 073201.

[93] S. Iubini, S. Lepri, R. Livi, G.-L. Oppo, and A. Politi "A Chain, a Bath, a Sink, and a Wall". *Entropy* **19** (2017), p. 445.

[94] H. M. Jaeger, S. R. Nagel, and R. P. Behringer "The physics of granular materials". *Physics Today* **49** (1996), p. 32.

[95] D. Jaksch, C. Bruder, J. I. Cirac, C. W. Gardiner, and P. Zoller "Cold Bosonic Atoms in Optical Lattices". *Phys. Rev. Lett.* **81** (1998), pp. 3108–3111.

[96] A. Jalalinejad, H. Bassereh, V. Salari, T. Ala-Nissila, and A. Giacometti "Excitation energy transport with noise and disorder in a model of the selectivity filter of an ion channel". *J. Phys. Condens. Matter* **30** (2018), p. 415101.

[97] S. P. Johnstone, A. J. Groszek, P. T. Starkey, C. J. Billington, T. P. Simula, and K. Helmerson "Evolution of large-scale flow from turbulence in a two-dimensional superfluid". *Science* **364** (2019), pp. 1267–1271.

[98] I. T. Jolliffe and J. Cadima "Principal component analysis: a review and recent developments". *Philos. Trans. Royal Soc. A* **374** (2016), p. 20150202.

[99] P. Jun Park and W. Sung "Dynamics of a polymer surmounting a potential barrier: The Kramers problem for polymers". *J. Chem. Phys.* **111** (1999), pp. 5259–5266.

[100] M. Kardar. *Statistical physics of particles*. Cambridge University Press, 2007.

[101] J. J. Kasianowicz, E. Brandin, D. Branton, and D. W. Deamer "Characterization of individual polynucleotide molecules using a membrane channel". *Proc. Natl. Acad. Sci. U.S.A.* **93** (1996), pp. 13770–13773.

[102] T. Kasuga "On the adiabatic theorem for the Hamiltonian system of differential equations in the classical mechanics". *Proc. Japan Acad.* **37** (1961), pp. 366–382.

[103] P. G. Kevrekidis. *The discrete nonlinear Schrödinger equation: mathematical analysis, numerical computations and physical perspectives*. Vol. 232. Springer Science & Business Media, 2009.

[104] A. I. Khinchin. *Mathematical Foundations of Statistical Mechanics*. Dover Publications, 1949.

[105] M. K.-H. Kiessling "Statistical mechanics of classical particles with logarithmic interactions". *Commun. Pure Appl. Math.* **46** (1993), pp. 27–56.

[106] M. K.-H. Kiessling and Y. Wang "Onsager's ensemble for point vortices with random circulations on the sphere". *J. Stat. Phys.* **148** (2012), pp. 896–932.

[107] Y. Kifer "Some recent advances in averaging". *Modern dynamical systems and applications* (2004), pp. 385–403.

[108] R. Klages, G. Radons, and I. M. Sokolov, eds. *Anomalous transport*. Wiley&Sons, 2008.

[109] S. Klus, F. Nüske, P. Koltai, H. Wu, I. Kevrekidis, C. Schütte, and F. Noé "Data-Driven Model Reduction and Transfer Operator Approximation". *Journal of Nonlinear Science* **28** (2018), pp. 985–1010.

[110] P. T. Landsberg "Heat engines and heat pumps at positive and negative absolute temperatures". *Journal of Physics A: Mathematical and General* **10** (1977), pp. 1773–1770.

[111] P. T. Landsberg, R. J. Tykodi, and A. M. Tremblay "Systematics of Carnot cycles at positive and negative Kelvin temperatures". *J. Phys. A* **13** (1980), pp. 1063–1074.

[112] A. Lasanta and A. Puglisi "An itinerant oscillator model with cage inertia for mesorheological granular experiments". *J. Chem. Phys.* **143** (2015), p. 064511.

[113] F. Lechenault, O. Dauchot, G. Biroli, and J. P. Bouchaud "Critical scaling and hetherogeneous superdiffusion across the jamming/rigidity transition of a granular gas". *Europhys. Lett.* **83** (2008), p. 46003.

[114] D. S. Lemons and A. Gythiel "Paul Langevin's 1908 paper 'On the Theory of Brownian Motion' ['Sur la théorie du mouvement brownien', C. R. Acad. Sci. (Paris) 146, 530–533 (1908)]". *Am. J. Phys.* **65** (1997), pp. 1079–1081.

[115] S. Lepri. *Thermal transport in low dimensions: from statistical physics to nanoscale heat transfer*. Vol. 921. Springer, 2016.

[116] S. Lepri, R. Livi, and A. Politi "Heat conduction in chains of nonlinear oscillators". *Phys. Rev. Lett.* **78** (1997), p. 1896.

[117] S. Lepri, R. Livi, and A. Politi "Thermal conduction in classical low-dimensional lattices". *Phys. Rep.* **377** (2003), pp. 1 –80.

[118] B. Li and J. Wang "Anomalous Heat Conduction and Anomalous Diffusion in One-Dimensional Systems". *Phys. Rev. Lett.* **91** (2003), p. 044301.

[119] C. C. Lin "On the Motion of Vortices in Two Dimensions". *Proc. Natl. Acad. Sci. U.S.A.* **27** (1941), pp. 570–575.

[120] R. Livi, R. Franzosi, and G.-L. Oppo "Self-Localization of Bose-Einstein Condensates in Optical Lattices via Boundary Dissipation". *Phys. Rev. Lett.* **97** (2006), p. 060401.

[121] R. Livi, M. Pettini, S. Ruffo, and A. Vulpiani "Chaotic behavior in nonlinear Hamiltonian systems and equilibrium statistical mechanics". *J. Stat. Phys.* **48** (1987), pp. 539–559.

[122] D. K. Lubensky and D. R. Nelson "Driven polymer translocation through a narrow pore". *Biophys. J.* **77** (1999), pp. 1824–1838.

[123] D. Lynden-Bell "Negative specific heat in astronomy, physics and chemistry". *Physica A* **263** (1999). Proceedings of the 20th IUPAP International Conference on Statistical Physics, pp. 293 –304.

[124] D. Lynden-Bell, R. Wood, and A. Royal "The Gravo-Thermal Catastrophe in Isothermal Spheres and the Onset of Red-Giant Structure for Stellar Systems". *Mon. Notices Royal Astron. Soc.* **138** (1968), pp. 495–525.

[125] S.-K. Ma. *Statistical Mechanics*. Phyladelphia Singapore: World Scientific, 1985.

[126] S. Machlup "Negative temperatures and negative dissipation". *Am. J. Phys.* **43** (1975), pp. 991–995.

[127] R. Mannella and V. Palleschi "Fast and precise algorithm for computer simulation of stochastic differential equations". *Phys. Rev. A* **40** (1989), pp. 3381–3386.

[128] C. Marchioro and M. Pulvirenti. *Mathematical Theory of Incompressible Nonviscous Fluids*. New York: Springer-Verlag, 1994.

[129] U. Marini Bettolo Marconi, A. Puglisi, L. Rondoni, and A. Vulpiani "Fluctuation–dissipation: response theory in statistical physics". *Phys. Rep.* **461** (2008), pp. 111–195.

[130] G. Marty and O. Dauchot "Subdiffusion and Cage effect in a Sheared Granular Material". *Phys. Rev. Lett.* **94** (2005), p. 015701.

[131] P. Mazur and E. Braun "On the statistical mechanical theory of Brownian motion". *Physica* **30** (1964), pp. 1973–1988.

[132] J. Mehra. *The Golden Age of Theoretical Physics*. World Scientific, 2001.

[133] S. Melchionna "Design of quasisymplectic propagators for Langevin dynamics". *J. Chem. Phys.* **127** (2007), p. 044108.

[134] A. Meller, L. Nivon, and D. Branton "Voltage-driven DNA translocations through a nanopore". *Phys. Rev. Lett.* **86** (2001), p. 3435.

[135] F. Miceli, M. Baldovin, and A. Vulpiani "Statistical mechanics of systems with long-range interactions and negative absolute temperature". *Phys. Rev. E* **99** (2019), p. 042152.

[136] L. Molgedey and H. G. Schuster "Separation of a mixture of independent signals using time delayed correlations". *Phys. Rev. Lett.* **72** (1994), pp. 3634–3637.

[137] D. Montgomery "Comment on 'Negative temperature of vortex motion'". *Phys. Rev. A* **44** (1991), pp. 8437–8438.

[138] D. Montgomery and G. Joyce "Statistical mechanics of 'negative temperature' states". *Phys. Fluids* **17** (1974), pp. 1139–1145.

[139] A. P. Mosk "Atomic Gases at Negative Kinetic Temperature". *Phys. Rev. Lett.* **95** (2005), p. 040403.

[140] M Muthukumar "Theory of capture rate in polymer translocation". *J. Chem. Phys.* **132** (2010), 05B605.

[141] F. Noé and F. Nuske "A variational approach to modeling slow processes in stochastic dynamical systems". *Multiscale Modeling & Simulation* **11** (2013), pp. 635–655.

[142] A. Oja and O. Lounasmaa "Nuclear magnetic ordering in simple metals at positive and negative nanokelvin temperatures". *Rev. Mod. Phys.* **69** (1997), p. 1.

[143] L. Onsager and S. Machlup "Fluctuations and Irreversible Processes". *Phys. Rev.* **91** (1953), p. 1505.

[144] L. Onsager "Statistical hydrodynamics". *Il Nuovo Cimento (1943-1954)* **6** (1949), pp. 279–287.

[145] T. Padmanabhan "Statistical mechanics of gravitating systems". *Phys. Rep.* **188** (1990), p. 285.

[146] A. Patelli and S. Ruffo. "Large Deviations Techniques for Long-Range Interactions". In: *Large Deviations in Physics*. Ed. by A. Vulpiani, F. Cecconi, M. Cencini, A. Puglisi, and D. Vergni. Berlin Heidelberg: Springer-Verlag, 2014, pp. 193–220.

[147] J. Peinke, M. R. Tabar, and M. Wächter "The Fokker–Planck Approach to Complex Spatiotemporal Disordered Systems". *Annu. Rev. Condens. Matter Phys.* **10** (2019), pp. 107–132.

[148] H. Poincaré and R. Magini "Les méthodes nouvelles de la mécanique céleste". *Il Nuovo Cimento (1895-1900)* **10** (1899), pp. 128–130.

[149] J. M. Polson, M. F. Hassanabad, and A. McCaffrey "Simulation study of the polymer translocation free energy barrier". *J. Chem. Phys.* **138** (2013), p. 024906.

[150] R. V. Pound "Nuclear Spin Relaxation Times in Single Crystals of LiF". *Phys. Rev.* **81** (1951), pp. 156–156.

[151] A. Puglisi, A. Sarracino, and A. Vulpiani "Temperature in and out of equilibrium: A review of concepts, tools and attempts". *Phys. Rep.* **709-710** (2017), p. 1.

[152] E. M. Purcell and R. V. Pound "A Nuclear Spin System at Negative Temperature". *Phys. Rev.* **81** (1951), pp. 279–280.

[153] F. Radjai and S. Roux "Turbulentlike Fluctuations in Quasistatic Flow of Granular Media". *Phys. Rev. Lett.* **89** (2002), p. 064302.

[154] A. Rahman "Correlations in the motion of Atoms in Liquid Argon". *Phys. Rev.* **136** (1964), A405.

[155] A. Ramírez-Hernández, H. Larralde, and F. Leyvraz "Systems with negative specific heat in thermal contact: Violation of the zeroth law". *Phys. Rev. E* **78** (2008), p. 061133.

[156] N. F. Ramsey "Thermodynamics and Statistical Mechanics at Negative Absolute Temperatures". *Phys. Rev.* **103** (1956), pp. 20–28.

[157] A. Rapp "Mean-field dynamics to negative absolute temperatures in the Bose-Hubbard model". *Phys. Rev. A* **87** (2013), p. 043611.

[158] A. Rapp, S. Mandt, and A. Rosch "Equilibration Rates and Negative Absolute Temperatures for Ultracold Atoms in Optical Lattices". *Phys. Rev. Lett.* **105** (2010), p. 220405.

[159] K. O. Rasmussen, T. Cretegny, P. G. Kevrekidis, and N. Grønbech-Jensen "Statistical Mechanics of a Discrete Nonlinear System". *Phys. Rev. Lett.* **84** (2000), pp. 3740–3743.

[160] P. M. Reis, R. A. Ingale, and M. D. Shattuck "Caging Dynamics in a Granular Fluid". *Phys. Rev. Lett.* **98** (2007), p. 188301.

[161] V. Romero-Rochín "Nonexistence of equilibrium states at absolute negative temperatures". *Phys. Rev. E* **88** (2013), p. 022144.

[162] R. J. Rubin "Statistical dynamics of simple cubic lattices. Model for the study of Brownian motion". *Journal of Mathematical Physics* **1** (1960), p. 309.

[163] M. A. Ruderman and C. Kittel "Indirect Exchange Coupling of Nuclear Magnetic Moments by Conduction Electrons". *Phys. Rev.* **96** (1954), pp. 99–102.

[164] H. Rugh "Dynamical approach to temperature". *Phys. Rev. Lett.* **78** (1997), p. 772.

[165] H. Rugh "A geometric dynamical approach to thermodynamics". *J. Phys. A: Math. Gen.* **31** (1998), p. 7761.

[166] M. Ruiz-Garcia, L. L. Bonilla, and A. Prados "Bifurcation analysis and phase diagram of a spin-string model with buckled states". *Phys. Rev. E* **96** (2017).

[167] B. Rumpf "Stable and metastable states and the formation and destruction of breathers in the discrete nonlinear SchrÃűdinger equation". *Physica D* **238** (2009), pp. 2067 –2077.

[168] C. Scalliet, A. Gnoli, A. Puglisi, and A. Vulpiani "Cages and Anomalous Diffusion in Vibrated Dense Granular Media". *Phys. Rev. Lett.* **114** (2015), p. 198001.

[169] U. Schneider, S. Mandt, A. Rapp, S. Braun, H. Weimer, I. Bloch, and A. Rosch "Comment on 'Consistent thermostatistics forbids negative absolute temperatures'". *Preprint arXiv:1407.4127* (2014).

[170] H.-G. Schöpf "Zur Thermodynamik negativer absoluter Temperaturen". *Ann. Phys. (Berl.)* **464** (1962), pp. 107–123.

[171] K. L. Sebastian and A. Debnath "Polymer in a double well: dynamics of translocation of short chains over a barrier". *Journal of Physics: Condensed Matter* **18** (2006), S283–S296.

[172] K. Sebastian and A. K. Paul "Kramers problem for a polymer in a double well". *Phys. Rev. E* **62** (2000), pp. 927–939.

[173] S. Siegert and R. Friedrich "Modeling of nonlinear Lévy processes by data analysis". *Phys. Rev. E* **64** (2001), p. 041107.

[174] T. Simula, M. J. Davis, and K. Helmerson "Emergence of order from turbulence in an isolated planar superfluid". *Phys. Rev. Lett.* **113** (2014), p. 165302.

[175] R. A. Smith "Phase-transition behavior in a negative-temperature guiding-center plasma". *Phys. Rev. Lett.* **63** (1989), pp. 1479–1482.

[176] R. A. Smith and T. M. O'Neil "Nonaxisymmetric thermal equilibria of a cylindrically bounded guiding-center plasma or discrete vortex system". *Phys. Fluids B* **2** (1990), pp. 2961–2975.

[177] H. Struchtrup "Work Storage in States of Apparent Negative Thermodynamic Temperature". *Phys. Rev. Lett.* **120** (2018), p. 250602.

[178] R. H. Swendsen "Thermodynamics of finite systems: a key issues review". *Rep. Prog. Phys.* **81** (2018), p. 072001.

[179] R. H. Swendsen and J.-S. Wang "Negative temperatures and the definition of entropy". *Physica A* **453** (2016), pp. 24 –34.

[180] S. Takeno and J. Hori "Continuum Approximation for the Motion of a Heavy Particle in One- and Three-Dimensional Lattices". *Progress of Theoretical Physics Supplement* **23** (1962), pp. 177–184.

[181] J. Taylor "Negative temperatures in two dimensional vortex motion". *Physics Letters A* **40** (1972), pp. 1–2.

[182] H. Touchette "The large deviation approach to statistical mechanics". *Phys. Rep.* **478** (2009), pp. 1–69.

[183] A. Tremblay "Comment on 'Negative Kelvin temperatures: Some anomalies and a speculation'". *Am. J. Phys.* **44** (1976), pp. 994–995.

[184] A. Trombettoni and A. Smerzi "Discrete Solitons and Breathers with Dilute Bose-Einstein Condensates". *Phys. Rev. Lett.* **86** (2001), pp. 2353–2356.

[185] J. H. Tu, C. W. Rowley, D. M. Luchtenburg, S. L. Brunton, and J. N. Kutz "On dynamic mode decomposition: Theory and applications". *J. Comput. Nonlinear Dyn.* **1** (2014), p. 391.

[186] R. Turner "Motion of a heavy particle in a one dimensional chain". *Physica* **26** (1960), pp. 269 –273.

[187] R. J. Tykodi "Negative Kelvin temperatures: Some anomalies and a speculation". *Am. J. Phys.* **43** (1975), pp. 271–273.

[188] R. J. Tykodi "Quasi-Carnot cycles, negative Kelvin temperatures, and the laws of thermodynamics". *Am. J. Phys.* **46** (1978), pp. 354–359.

[189] B. Utter and R. P. Behringer "Self-diffusion in dense granular shear flows". *Phys. Rev. E* **69** (2004), p. 031308.

[190] R. N. Valani, A. J. Groszek, and T. P. Simula "Einstein–Bose condensation of Onsager vortices". *New J. Phys.* **20** (2018), p. 053038.

[191] L. Verlet "Computer "Experiments" on Classical Fluids. I. Thermodynamical Properties of Lennard-Jones Molecules". *Phys. Rev.* **159** (1967), pp. 98–103.

[192] J. M. G. Vilar and J. M. Rubi "Communication: System-size scaling of Boltzmann and alternate Gibbs entropies". *J. Chem. Phys.* **140** (2014), p. 201101.

[193] M. Vladimirova, S. Cronenberger, D. Scalbert, I. I. Ryzhov, V. S. Zapasskii, G. G. Kozlov, A. Lemaître, and K. V. Kavokin "Spin temperature concept verified by optical magnetometry of nuclear spins". *Phys. Rev. B* **97** (2018), p. 041301.

[194] M. Von Smoluchowski "Zur kinetischen theorie der brownschen molekularbewegung und der suspensionen". *Ann. Phys. (Berl.)* **326** (1906), pp. 756–780.

[195] C. Wehmeyer and F. Noé "Time-lagged autoencoders: Deep learning of slow collective variables for molecular kinetics". *J. Chem. Phys.* **148** (2018), p. 241703.

[196] G. H. Wortel, J. A. Dijksman, and M. van Hecke "Rheology of weakly vibrated granular media". *Phys. Rev. E* **89** (2014), p. 012202.

[197] Y. Yatsuyanagi and T. Hatori "Self-organization mechanism in two-dimensional point vortex system". *AIP Conf. Proc.* **1668** (2015), p. 050003.

[198] Y. Yatsuyanagi, Y. Kiwamoto, H. Tomita, M. M. Sano, T. Yoshida, and T. Ebisuzaki "Dynamics of Two-Sign Point Vortices in Positive and Negative Temperature States". *Phys. Rev. Lett.* **94** (2005), p. 054502.

[199] R. Zwanzig "Memory Effects in Irreversible Thermodynamics". *Phys. Rev.* **124** (1961), pp. 983–992.

[200] R. Zwanzig "Nonlinear generalized Langevin equations". *J. Stat. Phys.* **9**. (1973), pp. 215–220.